

**FOUNDATION FOR RESEARCH
& TECHNOLOGY HELLAS
INSTITUTE OF ELECTRONIC
STRUCTURE AND LASER (IESL)**

**UNIVERSITY OF CRETE
DEPARTMENT OF
MATERIALS SCIENCE AND
TECHNOLOGY**

**Fabrication and characterization of micro-
structured silicon substrates and
hierarchical micro-nano-structured silicon
substrates with gold nanoparticles**

BSc Thesis

By Christina Lanara

Supervisor : Dr. Emmanuel Stratakis

Heraklion, Crete, February 2017

**ΙΔΡΥΜΑ ΤΕΧΝΟΛΟΓΙΑΣ ΚΑΙ
ΕΡΕΥΝΑΣ**

**ΙΝΣΤΙΤΟΥΤΟ ΗΛΕΚΤΡΟΝΙΚΗΣ
ΔΟΜΗΣ ΚΑΙ ΛΕΪΖΕΡ**

ΠΑΝΕΠΙΣΤΗΜΙΟ ΚΡΗΤΗΣ

**ΤΜΗΜΑ ΕΠΙΣΤΗΜΗΣ ΚΑΙ
ΤΕΧΝΟΛΟΓΙΑΣ ΥΛΙΚΩΝ**

**Κατασκευή και χαρακτηρισμός μικρο-
δομημένων υποστρωμάτων πυριτίου και
ιεραρχικών μικρο-νανο-δομημένων
υποστρωμάτων πυριτίου με νανοσωματίδια
χρυσού**

Διπλωματική εργασία

Χριστίνα Λαναρά

Επιβλέπων : Δρ. Εμμανουήλ Στρατάκης

Ηράκλειο, Κρήτη, Φεβρουάριος 2017

Acknowledgments

First of all, I would like to thank my supervisor Dr. Emmanuel Stratakis who gave me the opportunity to work on a very interesting project, for me, and to work in a great group. Also for the confidence he showed me and his advice on both project part and my further course. Also, I appreciate the fact that he never raised “experimental limits” to me.

Also, I would like to thank Prof. Geroge Kioseoglou, who conceded to be in the examination committee of my thesis. I didn't have the opportunity to work with him on th present thesis, but it would be a pleasure for me to work with him in the future. I would also like to thank him for the understanding and the grace he showed to me as for the time limits.

Now, it's time to express my full appreciation, to the person who is responsible for everything you will read in my thesis, but also for many things that you will not read. This person is none other than Chara Simitzi. I would like to thank her for her endless help and support, both in experimental and personal part. Her help was invaluable, since the first time she showed me how to cut a silicon substrate, until three days ago that she found a little time to rest, somewhere in “bright Brighton”, and nevertheless she devoted her time to my thesis. Also I would like to thank her for the confidence she showed me. I could write many words about this person, but it is not the time.

Also, I would like to thank Evangelos Skoulas who was the first person that I met at the laser laboratory. I would like to thank him for his unlimited patience and for all the things he taught me, as for my "irradiation" questions. Also, he told me a very wise phrase, since the first day that I met him, until today, but won't elaborate further because the words are a little bit inappropriate. Finally, I would like to thank him for his support all this time, and because he is Evangelos Skoulas, no more description.

Also, I would like to thank the SEM girl, Aleka Manousaki , for the infinite SEM images and for the unlimited discussions we had each time. The only times I do not remember what we were discussing about, were when she was telling me to go to the SEM at nine o'clock in the morning, because coffee was not allowed.

Also I would like to thank Dr. Antonios Kanaras from School of Physics and Astronomy at Southampton University, for the synthesis of gold nanoparticles and their immediate sent.

Also, I would like to thank Antonios Papadopoulos and Ioannis Paradisanos for their help on both theoretical and experimental part respectively.

Also, I would like to thank Andreas Lemonis, who is responsible for anything that moves electronically at the laboratory, as well as because he was always the happy note of the day.

Also, I would like to thank Kanelina Karali for our cooperation in the cellular process, and all the group members who helped me and "embrace" me.

Finally, I would like to thank my family and my friends for their support all these 23 years of my life, and even more, for the last five years.

Thank you all,

Christina Lanara

Heraklion Crete 2017

Abstract

Biomimetics offer the possibility of biological systems simulation on artificial surfaces, with desired properties. There are many attempts to fabricate artificially these surfaces.

The present thesis comprises two parts. The first one is the fabrication of micropatterned silicon substrates via ultra-short pulsed laser irradiation under different experimental parameters, including laser fluence and irradiation environment. The second part is the fabrication of hierarchical micro-nano-patterned substrates. These comprise micro-patterned silicon substrates which have been nano-decorated with spherical gold nanoparticles of various functionalities and sizes. Gold nanoparticles have been attached via silane chemistry. Both types of substrates have been characterized with respect to their morphological, wetting and optical properties.

Regarding the micropatterned substrates, the morphological characterization showed that as the laser fluence increased the roughness of the surface increased as well. Micropatterned substrates comprised microcones of varying height and density. Specifically, the density and the height of the micro-features (i.e. microcones) decreased and increased respectively, with increasing laser fluence. The study of the contact angle showed that as the surface roughness increased, the substrates became more hydrophobic. Optical characterization showed that as the surface roughness increases, the reflectivity decreased, across the range of wavelength (250-2500nm). The layer of silicon oxide on flat silicon substrates lead to reduction of the reflectance, in contrast with the case of micro-structured substrates, where silicon oxide layer increased the reflectivity, in near infrared spectrum.

Regarding the hierarchical micro-nano substrates, SEM analysis confirmed the successful deposition of the gold nanoparticles on the micropatterned silicon substrates. Deposition gave a homogenous distribution of single nanoparticles and some regions of small clusters. All types of the gold nanoparticles (NPs) being tested, which carried diverse functionalities (e.g. oligopeptides, including the CALNN and CALNN-RGD and organic moieties, including the stabilizer citrate and DMAP) have been successfully attached on the surfaces of the micropatterned silicon substrates. Remarkably, the NPs covered the whole 3D surface of the micropatterned substrates giving a distribution that was comparable to that on the flat silicon substrates. The study

of the contact angle showed that the initially hydrophobic micropatterned silicon substrates became more hydrophilic with the addition of gold nanoparticles . Optical characterization showed that gold nanoparticles caused a reduction of the reflectivity of the oxidized micro-patterned silicon substrates.

Finally, both the micropatterned and the hierarchical micro-nano substrates have been characterized for their use as cell culture platforms for the growth of neural stem cells. In the case of the micro-patterned substrates it was shown that the greater majority of the cells attached preferentially on the medium roughness surfaces. Remarkably, cells aligned along the major axis of the microcones. This cellular response was more pronounced in the respective hierarchical substrates which had been decorated with the RGD cell binding motif.

Περίληψη

Η Βιομημική προσφέρει τη δυνατότητα της προσομοίωσης βιολογικών συστημάτων σε τεχνητές επιφάνειες, με επιθυμητές ιδιότητες. Έχουν γίνει πολλές προσπάθειες για την τεχνητή κατασκευή αυτών των επιφανειών.

Η παρούσα διατριβή αποτελείται από δύο μέρη. Το πρώτο είναι η κατασκευή μικροδομημένων υποστρωμάτων πυριτίου μέσω ακτινοβολήσης με λέιζερ υπέρ-στενων παλμών, υπό διαφορετικές πειραματικές παραμέτρους, συμπεριλαμβανομένης της πυκνότητας ενέργειας και το περιβάλλον ακτινοβολίας. Το δεύτερο μέρος είναι η κατασκευή των ιεραρχικών μικρο-νανο-δομημένων υποστρωμάτων. Αυτές περιλαμβάνουν μικρο-δομημένα υποστρώματα πυριτίου που είναι νανο-διακοσμημένα με σφαιρικά νανοσωματίδια χρυσού διαφόρων λειτουργικών ομάδων και μεγεθών. Τα νανοσωματίδια χρυσού έχουν συνδεθεί μέσω της χημείας σιλανίου. Και οι δύο τύποι υποστρωμάτων έχουν χαρακτηρίζονται σε σχέση με τη μορφολογία τους ,τις διαβροχικές και οπτικές τους ιδιότητες.

Όσον αφορά τις μικρο-δομημένες επιφάνειες, ο μορφολογικός χαρακτηρισμός έδειξε ότι καθώς η πυκνότητα ενέργειας λέιζερ αυξάνει, αυξάνει και η τραχύτητα της επιφάνειας. Τα μικροδομημένα υποστρώματα εμφάνισαν δομές μικροκόνων ποικίλου ύψους και πυκνότητας. Πιο συγκεκριμένα, η πυκνότητα και το ύψος των μικρο-δομών (δηλαδή των μικρο-κόνων) μειωνόταν και αυξανόταν αντίστοιχα, με την αύξηση της πυκνότητας ενέργειας του λέιζερ. Η μελέτη της γωνίας επαφής κατέδειξε ότι καθώς η τραχύτητα της επιφάνειας αυξάνεται, τα υποστρώματα έγιναν πιο υδρόφοβα. Ο οπτικός χαρακτηρισμός έδειξε ότι καθώς η επιφανειακή τραχύτητα αυξάνει, η ανακλαστικότητα μειώνεται, σε όλο το εύρος του μήκους κύματος (250-2500nm). Το στρώμα οξειδίου του πυριτίου σε επίπεδες επιφάνειες πυριτίου οδηγεί σε μείωση του συντελεστή ανάκλασης, σε αντίθεση με την περίπτωση των μικρο-δομημένων υποστρωμάτων, όπου το στρώμα οξειδίου του πυριτίου αύξησε την ανακλαστικότητα, στο εγγύς υπέρυθρο φάσμα.

Όσον αφορά τις ιεραρχικά δομημένα υποστρώματα, η ανάλυση SEM επιβεβαίωσε την επιτυχή εναπόθεση των νανοσωματιδίων χρυσού στις μικρο-δομημένες επιφάνειες πυριτίου. Η εναπόθεση απέδωσε μια ομοιογενή κατανομή νανοσωματιδίων με ορισμένες περιοχές μικρών συστάδων. Όλοι οι τύποι των νανοσωματιδίων χρυσού που δοκιμάστηκαν, και τα οποία φέρουν ποικίλες λειτουργικότητες (π.χ. ολιγοπεπτίδια,

συμπεριλαμβανομένων των CALNN και CALNN-RGD και οργανικές ενώσεις, συμπεριλαμβανομένου του κιτρικού σταθεροποιητή και DMAP) έχουν επιτυχώς συνδεθεί επί των μικροδομημένων επιφανειών των υποστρώματων πυριτίου. Είναι αξιοσημείωτο ότι τα νανοσωματίδια χρυσού μπόρεσαν να καλύψουν όλη την επιφάνεια των τριασδιάστατων μικροδομημένων υποστρώματων δίνοντας μια κατανομή η οποία ήταν συγκρίσιμη με εκείνη για τα επίπεδα υποστρώματα πυριτίου. Η μελέτη της γωνίας επαφής κατέδειξε ότι τα αρχικά υδρόφοβα μικροδομημένα υποστρώματα πυριτίου έγιναν πιο υδρόφιλα με την προσθήκη νανοσωματιδίων χρυσού. Ο οπτικός χαρακτηρισμός έδειξε ότι τα νανοσωματίδια χρυσού έχουν την τάση να μειώνουν την ανακλαστικότητα του οξειδωμένου μικρο-δομημένου υποστρώματος πυριτίου.

Τέλος, τόσο οι μικροδομημένες όσο και οι ιεραρχικές επιφάνειες μικρο-νανο-τραχύτητας έχουν χαρακτηριστεί ως υποστρώματα κυτταρικής καλλιέργειας για την ανάπτυξη των νευρικών βλαστικών κυττάρων. Στην περίπτωση των μικρο-δομημένων υποστρώματων, δείχθηκε ότι η μεγαλύτερη πλειοψηφία των κυττάρων συνδέονται κατά προτίμηση στα υποστρώματα μεσαίας τραχύτητας. Αξιοσημείωτα, τα κύτταρα ευθυγραμμίζονται κατά μήκος του κύριου άξονα των μικροκόνων. Αυτή η κυτταρική αντίδραση ήταν πιο έντονη στα αντίστοιχα ιεραρχικά υποστρώματα που είχαν διακοσμηθεί με το μοτίβο RGD.

TABLE OF CONTENTS

Acknowledgments	3
Abstract	5
Table of contents	9
1. General overview	12
1.1 Biomimetic micro/nano functional surfaces.....	12
1.1.1 Biomimetics.....	12
1.1.2 Biomimetic fabrication of hierarchical surfaces.....	12
1.1.3 Biomimetic micro/nano functional surfaces for microfluidic applications.....	15
1.1.4 Biomimetic micro/nano functional surfaces for tailoring the optical properties.....	17
1.1.5 Biomimetic micro/nano functional surfaces for cell biology applications.....	18
1.2 Laser induced periodic surface structures (LIPSS).....	20
1.2.2 Silicon.....	20
1.2.1 Laser – solid interactions : Fundamental aspects.....	29
1.2.1.1 Primary process.....	29
1.2.1.2 Secondary process.....	30
1.2.3 Surface structuring of silicon via ultrashort – pulsed laser processing.....	33
1.3 Gold nanoparticles.....	36
1.3.1 Synthesis of gold nanoparticles.....	37
1.3.2 Properties of gold nanoparticles.....	39
2. Aim of the thesis	42
2.1 Problem statement & aim of thesis.....	42
2.2 Flow sheet.....	43
3. Experimental part : Materials & methods	44
3.1 Fabrication of micropatterned silicon surfaces via ultrashort – pulsed laser.....	44
3.1.1 Laser system.....	44
3.1.2 Experimental setprocedure.....	44
3.1.3 Sample preparation.....	45
3.1.4 Thermal oxidation of the substrates.....	45
3.2 Gold nanoparticles used.....	45
3.3 Deposition of gold nanoparticles onto the microstructured silicon surfaces.....	46
3.4 Characterization of the micro/nano patterned silicon surfaces.....	49

3.4.1 Scanning electron microscopy (SEM).....	49
3.4.1.1 Technique.....	49
3.4.1.2 Experimental process.....	49
3.4.2 Energy-dispersive X-ray spectroscopy (EDS)	49
3.4.2.1 Technique.....	49
3.4.2.2 Experimental process.....	50
3.4.3 Wetting response by static contact angle.....	50
3.4.3.1 Technique.....	50
3.4.3.2 Experimental process.....	51
3.4.4 Ellipsometry	51
3.4.4.1 Technique.....	51
3.4.4.2 Experimental process.....	52
3.4.5 Optical reflectance measurements	53
3.4.5.1 Technique.....	53
3.4.5.2 Experimental process.....	53
3.5 <i>In vitro</i> experiments with NSCs on the micro-nano patterned substrates.....	53
3.5.1 Substrate preparation.....	53
3.5.2 Cell culture.....	54
3.5.3 Characterization of cellular response.....	54
3.5.3.1 Fluorescence microscopy.....	54
3.5.3.1.1 Technique.....	54
3.5.3.1.2 Experimental process.....	55
4. Experimental part : Results.....	56
4.1 Morphological characterization of artificially structured silicon surfaces.....	56
4.1.1 Micropatterned silicon surfaces.....	56
4.1.1.1 The effect of roughness.....	56
4.1.1.2 The effect of SF ₆ gas.....	59
4.1.2 Hierarchical micro/nano patterned surfaces.....	62
4.2 Wetting response of the micro-nanopatterned substrates.....	63
4.2.1 The effect of roughness	63
4.2.2 The effect of irradiation environment.....	64
4.2.3 The effect of SiO ₂ thickness layer.....	66
4.2.4 The effect of silane.....	68
4.2.5 The effect of gold nanoparticles.....	69

4.3 Optical properties of micro/nano - patterned substrates.....	71
4.3.1 The effect of roughness.....	71
4.3.2 The effect of SiO ₂ layer.....	72
4.3.3 The effect of gold nanoparticles.....	73
4.4 NSCs growth and differentiation on the micro/nano patterned surfaces.....	75
5. Discussion & Conclusions.....	76
5.1 Micropatterned Si substratesfabricated via ultrashort-pulsed laser processing as artificial biomimetic surfaces.....	76
5.2 Irradiation parameters influence the surface micro-topography.....	76
5.3 The influence of surface micro-topography on its wetting properties.....	77
5.4 The influence of chemistry on the wetting properties of silane micropatterned surface....	79
5.5 The influence of a homogeneous gold nanoparticle layer on the wetting properties of micropatterned silicon.....	80
5.6 The influence of functionalized gold nanoparticles on NSCs growth.....	81
5.7 The influence of surphase roughness and AuNPs size on surface reflectivity.....	82
6. References.....	83

1 General overview

1.1 Biomimetic micro/nano functional surfaces

What has wings like a butterfly, skin like a shark, and eyes like a moth? The future of science...

1.1.1 Biomimetics

Biomimetics (word coined by Otto Schmitt in 1957), or biomimicry (word coined in 1960 by Jack Steele), based on the effort of people to listen to the nature. The driving force is the restless perfection of nature, where everything is "tuned" to work perfectly. Nature is a source of inspiration, since it presents a unique and distinct ways to solve complex problems. The study and simulation of biological systems with desired properties is popularly known as *biomimetics* [Stratakis, E. I. and Zorba, V., 2010¹]. Although biomimetics exists from Daedalus and Icarus, who imitated the birds, biomimetics has evolved in recent years because of the development of nanotechnology, which takes impulses from biological systems (both flora as and fauna) which have surfaces composed of micro- and nano- structures with a special role , and in general there is a great diversity of surface structures in different sizes. Currently, a large area of biomimetic research deals with functional micro- and nanostructures for nanoscale devices, water repellence, self-cleaning, drag reduction in fluid flow, energy conversion and conservation, high adhesion, aerodynamic lift, materials and fibers with high mechanical strength, antireflection, structural coloration, thermal insulation, self-healing, responsiveness, and sensory aid mechanisms¹ . All the above applications are based on biological systems and the excellent functional properties they have, so leading us to continually attempt to construct operably optimum surfaces such as those found in nature.

1.1.2 Biomimetic fabrication of hierarchical surfaces

The greater range of biomimetic research relates to the construction of functional micro- and nanostructures on respective surfaces. Since surfaces incorporating structures of different size scales (micro- and nano-scale) are characterized as *hierarchical* . Nature develops biological objects by means of growth or biologically controlled selfassembly adapting to the environmental condition. Such adaptive and

optimization of the biological material at each level of hierarchy, so as to yield outstanding performance [Xia, F., and Jiang, L., 2008²]. Biological materials are highly organized from the molecular to the nano-, micro-, and macroscales, often in a hierarchical manner with intricate nanoarchitecture that ultimately makes up a myriad of different functional elements [Alberts B. et al., 2008³]. Similar to all natural materials, biological surfaces exhibit hierarchical morphology at the micro- and the nanoscales while the desired functionality is achieved through a tailored synergy of surface roughness and chemistry [Stratakis E. et al., 2011⁴]. The hierarchical structure of biological surfaces, attains considerable interest for the development of nanotechnology, both in the understanding of such multifunctional systems, and to the effort to implement, some interesting examples of which are shown in Figure 1.1.

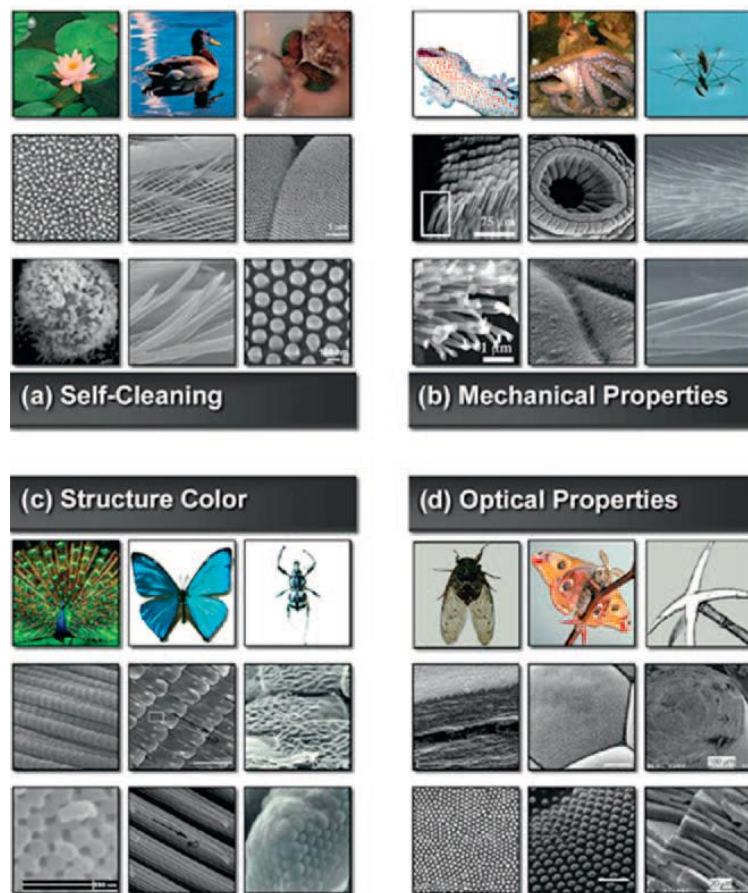


Figure 1.1

Multiscale structure in biology. Four types of interesting biological properties can be found in nature: a) self-cleaning properties: lotus leaf, duck feather, and mosquito eye (from left to right), b) mechanical properties: gecko feet, octopus suckers, and water strider, c) color through structure: peacock feather, butterfly wings, and beetle shells, and d) optical properties: cicada wings, moth compound eyes, and sponge spur. In each case the first row shows a photograph of the biological feature, while the second and third row show scanning electron microscopy (SEM) images of corresponding micro- and nanometer-scale structures¹.

The two basic manufacturing methods techniques for nanostructures is “bottom up” and “top down”. In the first one the desired features are constructed from fundamental building blocks (e.g., self-assembly, sol–gel methods, layer-by-layer deposition), without the need for patterning. In the contrary in the top down approach material is produced in bulk which is then shaped into a finished part through a variety of processes (e.g., casting, molding, rolling). Often the complex hierarchical structures are fabricated by the combination of the above two methods¹.

Various methods have been developed for structuring surfaces and fabrication of hierarchical surfaces. Specifically, by techniques such as electron – beam lithography [E. Martines et al., 2008⁵] , photolithography [J.-Y. Shiu et al., 2004⁶] , plasma treatments [I. Woodward et al., 2003⁷] , it is possible to integrate, onto the surface topographical features with specific geometry, roughness and orientation in a controlled manner. Figure 1.2 shows SEM micrographs, where the morphological difference is obvious between the flat surface (a), micro- (c), nano- (b) and hierarchical (d) structures.

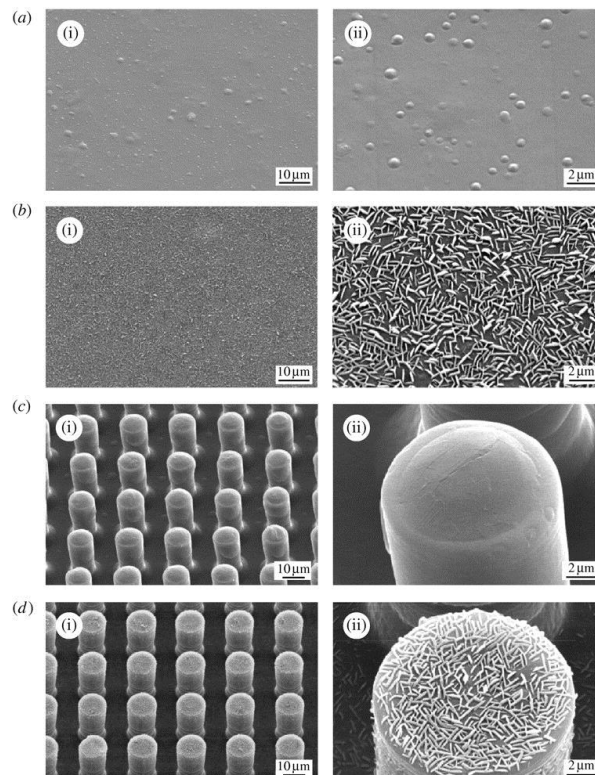


Figure 1.2

SEM images of (a)the flat surface, (b) nanostructure, (c) microstructure and (d) hierarchical structure measured at 45° tilt angle (shown using two magnifications (i)(ii)). All samples are fabricated with epoxy resin coated with 0.2 mg mm⁻² mass of n-hexatriacontane [Bhushan, B. et al., 2009⁸] .

A promising technique for fabrication of micro / nano structures with hierarchical surfaces is irradiation using pulsed laser, with pulse duration lower than a second, i.e. short and ultra-short pulse. Microstructuring using pulsed laser with pulse duration in the range of femtosecond (fs) [Her, T et al., 1998¹⁰], picosecond (ps) [Zorba, V. et al, 2008⁹], or nanosecond (ns) [Zorba, V et al., 2006¹¹] in a special environment irradiation is particularly attractive because it leads to the formation of microconical structures with high aspect ratio on surfaces⁵. The properties that can be tailored with surface structuring via ultra-short fs laser include electrical, mechanical, chemical [Stratakis, E., 2012], tribology [Bonse, J. et al, 2014²²], wetting [Zorba V. et al., 2008¹³, Hermens, U., 2016³⁰] and optical [Rudenko, A et al., 2016¹⁵]. Biomedical applications of artificial hierarchical surfaces include reduction or enhancement of cell adhesion, proliferation or differentiation depending on the types of cells [Simitzi, C. et al, 2015^{14, 13}]. With proper setting of the laser parameters (e.g. fluence) and the environment (reactive gas), it is possible the formation of surfaces with different morphologies.

This thesis focuses on the technique of micro / nano structuring surfaces by using ultra-short laser pulses with a pulse duration in the range of fs. Specifically it refers to irradiation of crystal silicon (Si) surface, in the presence of reactive gas. Choosing the experimental parameters (such as laser energy, number of pulses, irradiation environment, etc.), (section 3.1), the final morphology of the surface consists of 3D arrays semi-periodical microconical structures (spikes). In high laser fluence values, these structures are decorated with ledges size of nanometer scale (hierarchical surfaces).

1.1.3 Biomimetic micro/nano functional surfaces for microfluidic applications

What is microfluidics? It is the science and technology of systems that process or manipulate small (10^{-9} to 10^{-18} litres) amounts of fluids, using channels with dimensions of tens to hundreds of micrometres. The field of microfluidics has four parents: molecular analysis, biodefence, molecular biology and microelectronics [Whitesides, G. M., 2006¹⁷]. Microfluidic devices were developed through the study of controlled manipulation of liquids. The most common approach for liquid actuation in microfluidics, is the manipulation of liquid via surface energy gradients⁴. In parallel with the morphology of a surface, we can tune the chemistry of it. Thus, by depositing

chemicals / materials onto structured surfaces, the resulting surfaces can exhibit both stable morphology, and wettability changes of the surfaces. This is very important for the analysis of the characteristics of micro / nano-structured surfaces, for applications in microfluidics and tissue engineering.

The most widely known plant of nature for its special wetting properties, which is a surface model for many scientists [^{3,13}, Koch, K. et al, 1943¹⁸, Guo, Z. et al, 2011¹⁹], who have found ways to represent it artificially, is superhydrophobic Lotus (*Nelumbo nucifera*) leaves, which patented for first time from Wilhelm Barthlott in 1980 [Karthick, B., & Maheshwari, R., 2008²¹]. According to this model, we can study the wetting properties of surfaces, via static contact angle measurements (section 4.2), and associate them for their potential use to microfluidics applications. Figure 1.3 shows the Lotus leaf (a), a magnification of a water drop on Lotus leaf (b), SEM images of the surface of the Lotus leaf, which comprises randomly distributed bell-shaped papillae with sizes 5–10 μm (c) decorated with branch like protrusions with sizes of about 150 nm (d).

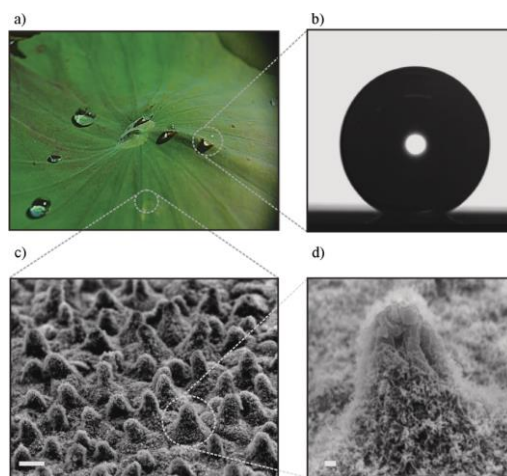


Figure 1.3

a) Picture of water droplets on a *Nelumbo nucifera* (Lotus) leaf. b) Static contact angle measurement of a water droplet of 0.78 mm radius on the Lotus leaf surface; the contact angle is $153^{\circ} \pm 1^{\circ}$ c) SEM image of the leaf surface comprising almost-hemispherically-topped papillae with sizes 5–10 μm with surface density of $4.2 \times 10^5 \text{ cm}^{-2}$ (scale bar 10 μm). d) High magnification SEM image of a single papillae depicting branch-like protrusions with sizes of about 150 nm (scale bar 1 μm) ¹³.

The present thesis studies the wetting properties of artificial hierarchical surfaces, with specific micro/nano topography (spikes) fabricated via ultra- short fs laser under

reactive gas pressure, by altering surface chemistry with different experimental processes each time, based on the lotus effect. The ultimate goal is to correlate of the surface wetting response, with the cellular response, which has already studied for some types of cells [14, Ranella, A. et al, 2010²⁰] for tissue engineering applications.

1.1.4 Biomimetic micro/nano functional surfaces for tailoring the optical properties

Since millions of years ago biological systems were using nanometre-scale architectures to produce striking optical effects [Vukusic, P., & Sambles, J. R.,2003²³]. Nature, apart from surfaces with excellent wetting properties, offers surfaces with excellent optical properties (e.g. moth eye [Stuart A. Boden and Darren M. Bagnall,2015²⁶] and wings [Boden, Stuart A, and Darren M Bagnall,2009²⁷], wings of Morpho [Watanabe et al., 2005²⁹] and Greta Oto [Siddique et al.,2015²⁸] butterflies) which are a source of inspiration for scientific research field. Animals such as fish and cephalopods which have chromomorphic (colour-changing) and controllable goniochromic (iridescent-changing) properties, can control the optical properties of their skins for camouflage [Rossiter, J. et al., 2012²⁴]. Also antireflective surfaces composed of biomimetic sub-wavelength structures that employ the ‘moth eye principle’ for reflectance reduction are highly desirable in many optical applications such as solar cells, photodetectors and laser optics [Morhard, C. et al.,2010²⁵]. Some

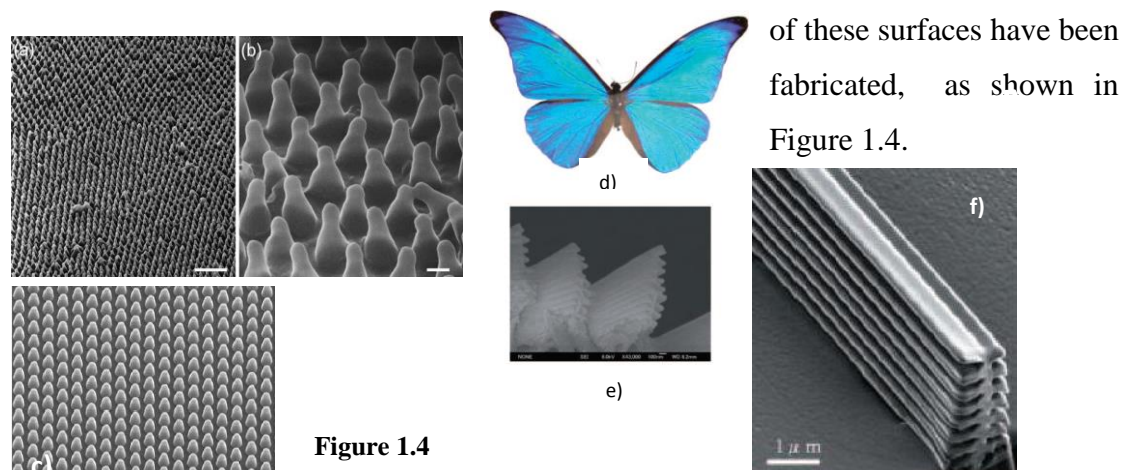


Figure 1.4

Moth-Eye antireflective structures. (left-up): Scanning helium ion microscope images of natural moth-eye structures found on the transparent wing of *Cephonodes hylas* (scale bars: (a) 1 mm and (b) 100 nm), (left-down): scanning helium ion micrograph of silicon moth-eye structure fabricated using electron-beam lithography and dry etching (c)²⁶.

Morpho-butterfly structures. (right): (d) Top view optical microscope image, (e) Cross-sectional view SEM image, (f) SIM images of Morpho-butterfly-scale quasi-structure fabricated by FIB-CDV²⁹.

The optical phenomena (e.g. structural coloration, broad-range coloration, antireflectivity, strong flicker contrast¹) of these surfaces, stem from their unique and remarkable structure of both micro- and the nano-scale. Fabrication of such surfaces has been performed by various methods and materials [23-29]. In our case, the fabrication of hierarchical surfaces, regards to silicon (Si) surfaces which are irradiated with ultra – short fs laser, in the presence of reactive gas. In particular, in this thesis we study the optical properties of ultra – short fs laser structured Si. *We study the effect of different laser irradiation parameters (e.g. laser fluence) and surface chemistry on the optical reflectance of the fabricated structures, compared with flat silicon, as well as their response to the effect of different sizes gold nanoparticles (AuNPs).*

1.1.5 Biomimetic micro/nano functional surfaces for cell biology applications

Until now we referred to physical organisms, which are visible to the naked eye, and our attempt to imitate them, lies in the fact that we can see their behavior. But the invisible is more creepy. All living organisms (animals, plants, humans) are composed of the basic structural, functional and biological unit that exhibits the phenomenon of life, which is none other than the cell, or else “building block of life”. But how can we connect the concept of the cell with the artificial hierarchical surfaces? All tissues and organs contain an ensemble of cells and non-cellular components, which form well-organized networks called extracellular matrix (ECM). ECM provides not only physical scaffolding into which cells are embedded, but also regulate many cellular processes including growth, migration, differentiation, survival, homeostasis, and morphogenesis [C. Frantz et al.,2010³³, K.C. Clause and T.H. Barker 2013³⁴, A.D. Theocharis et al.,2012³⁵]. ECM is a non-cellular three-dimensional macromolecular network whose components bind each other as well as cell adhesion receptors forming a complex network into which cells reside in all tissues and organs. Variations in the composition and structure of ECMs' components affect both the overall structure and biomechanical properties of the formed network. All cell types (e.g. epithelial, fibroblasts, immune cells, endothelial cells) synthesize and secrete matrix macromolecules under the control of multiple signals thus participating in the formation of ECMs [Theocharis et al.,2016³⁶].

Therefore, the connection between biomimetic surfaces and cells, is the fabrication of surfaces, which mimic the natural extracellular environment, in order to decipher the cellular mechanisms, but also the cell-material interaction for the creation of compatible biomaterials for tissue engineering application. Material properties such as surface chemistry, energy, and morphology are recognized as key factors in controlling cell assembly into 3D features [Liu et al.,2007³⁷].

Micro-and nanofabrication techniques provide the opportunity to develop new types of cell culture platform, where the effect of various topographical cues on cellular functions such as proliferation and differentiation can be studied¹⁴. In particular, microscale surface roughness can affect cell morphology, cytoskeletal structure, and differentiation, while nanoscale roughness and cellular activities remain unclear [Lee et al.,2015³⁸]. In our case, surfaces which were fabricated via ultra – short fs laser in the presence of reactive gas, exhibit areas of semi-periodic elliptical micro-conic shape (spikes) exhibiting different geometrical characteristics and surface chemistries. It is a surface pattern which has already been studied regarding the cellular response of various cell types (i.e.fibroblasts²⁰, PC12 pheocromocytoma cells¹⁴, Schwann cells (neuroglial cells)¹² and neurons⁴). Thus, the conclusion is that microconical-patterned surfaces could be used as cell culture platforms for the systematic exploitation of microconical morphology on neuron cell adhesion and growth [¹⁴, Papadopoulou EL et al.,2010³⁹]. Also both micro/nano topography of the surface and surface chemistry (wetting properties) influence to a large extent adhesion, directivity, proliferation of each cell type. *The present thesis studies the cellular response of primary neural stem cells (NSCs) on micro/nano structured silicon surfaces with different functionalized gold nanoparticles.*

1.2 Laser induced periodic surface structures (LIPSS)

Since the development of the first lasers, the interaction of laser irradiation with materials has been of scientific and technological interest [Janzen, E et al.,1984⁴¹]. Absorption of laser irradiation by a solid can lead to a permanent modification of its surface, causing melting and resolidification, vaporization, or ablation of the material. Laser processing of solids, using both continuous and pulsed lasers, has been studied over the years for different classes of materials including metals [Nolte, S et al.,1997⁴²], semiconductors [Jost, D. et al.,1986⁴³] and dielectrics [Henryk, M et al.,1999⁴⁴]. Laser light-material interaction mechanisms depend strongly on i) the laser beam parameters (e.g. wavelength, pulse duration, intensity, spatial and temporal coherence, polarization etc.), ii) the physical and chemical properties of the material employed (absorption coefficient, thermal diffusion etc.), iii) as well as on the environmental conditions (vacuum, reactive or non-reactive surrounding medium) [^{9,15}, Barberoglou M. et al.,2013⁴⁵, Jing-tao⁴⁶]. In this section we focus on the fundamental primary and secondary processes that take place upon the interaction of laser pulses with semiconductors, and more specifically with Silicon (Si) and we refer to the proposed mechanisms underlying the spontaneous formation of periodic structures (LIPSS) [J.F.Young et al., 1983⁷⁰] on the surfaces of materials upon laser irradiation in reactive gas ambient. But before dealing with the creation of periodic micro-structures, the basic properties of silicon (Si) are mentioned.

1.2.1 Silicon

Silicon (Si) is the second most abundant element (Clarke number ~26%) on Earth and exists mainly in the oxidized silicate (SiO₂) form. Si sources are neither localized in very specific regions nor are they noble. However, crystalline (c-Si) and amorphous (a-Si) silicons remain the most fundamental, purely inorganic materials used for microelectronics, optoelectronics, integrated-circuit (IC) fabrication and photonics because the lithographic and p-n doping processes are already well-established in industry [Sukumar Basu 2011⁴⁷]. Nowadays the use of silicon has been established in the commercial fabrication of many mechanical components, such as switches, filters, oscillators, fluidistic devices, medical and biochips, microphones,

accelerometers, gyroscopes, flow detectors, micromirrors, and cantilever sensors [J. Voldman et al., 1999⁴⁸, P. Sievila, 2013⁴⁹]. Furthermore silicon is widely used for material microfabrication and silicon-based microfabricated substrates with well-defined topographies have been extensively developed for a variety of applications [14,20,29,30,38, T. Pearce and J. Williams, 2007⁵⁰, Stratakis E. 2012⁵¹].

- **Silicon lattice form**

Silicon is used either as bulk material (polycrystalline silicon) or as a thin film (including epitaxial, amorphous, and polysilicon layers) [Hunt LP, 1990⁵²]. The different properties of single crystal, polycrystalline and amorphous silicon, which dictate their respective application, are mainly interrelated with the different crystal structure. Two-dimensional representations of the amorphous, polycrystalline, and single-crystal materials are shown in Figure 1.5.

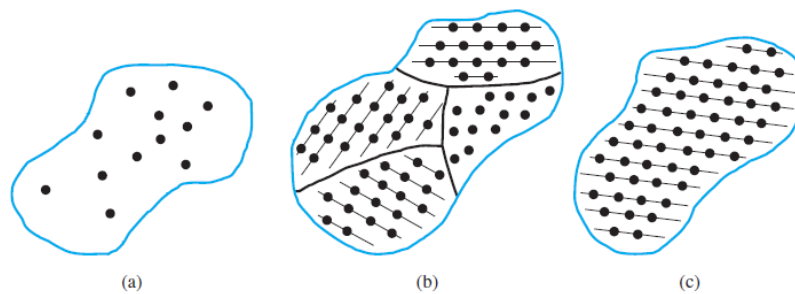


Figure 1.5: Schematics of three general types of forms based on crystal structures: (a) amorphous, (b) polycrystalline, (c) single. [Brown P, 1974⁵⁴]

Two fundamental parameters characterizing Si substrates are the crystallographic orientation of the wafer surface, and the crystallographic direction perpendicular to the wafer flat. Single-crystal Si is one of the simplest three-dimensional lattice system, referred to as the cubic lattice system. Bulk Si is an ideal lattice comprised of an infinite number of repetitive unit cells and an infinite number of cross-sectional planes and lattice directions. Figure 1.6 shows the unit cell of Si crystal, diamond structure, lattice constant (a), and the four nearest neighbor atoms bonding the Si lattice.

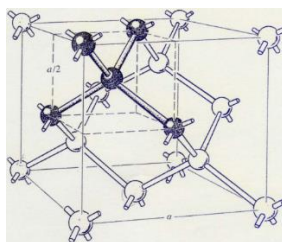


Figure 1.6: Unit cell of the silicon crystal (diamond lattice), is actually two interpenetrating face-centered cubic (fcc) lattices separated by $a/4$ along each axis of the cell

All lattice planes and lattice directions are described by a mathematical description known as the Miller Index. For the cubic lattice system, the direction $[hkl]$ defines a

vector direction normal to surface of a particular plane or facet [B.G. Streetman, 1990⁵³].

Figure 1.7 shows three common planes, i.e. (100), (110), (111). Monocrystalline is opposed to amorphous silicon, in which the atomic order is limited to a short range order only.

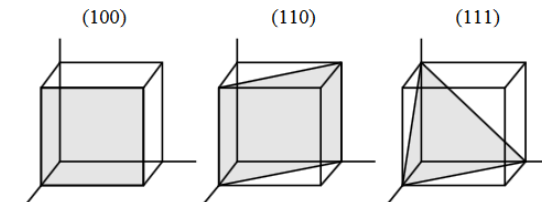


Figure 1.7: Three different crystal orientation (high symmetry) of single-crystal silicon (cubic system): (100), (110) and (111)

Polycrystalline silicon is composed of a large number of single crystals (grains or crystallite). The granules usually have a diameter 100nm-100µm. The boundary separating two small grains or crystals with different crystallographic orientations imposes an interfacial defect. This leads to higher chemical reactivity in these regions. Some important physical and chemical properties of silicon are shown in Table 1.1.

Table 1.1: Physical and chemical properties of silicon (Si).

<i>Physical properties</i>		<i>Chemical properties</i>	
<i>Color</i>	Pure silicon is a hard, dark gray solid	<i>Chemical formula</i>	Si
<i>Phase</i>	Solid	<i>Compounds</i>	Silicon forms compounds with metals (silicides) and with non-metals
<i>Luster</i>	Metallic shine or glow	<i>Oxidation</i>	Combined with oxygen as silica (silicon dioxide, SiO ₂) or with oxygen and metals as silicate minerals. It is stable in air even at elevated temperatures owing to the formation of a protective oxide film
<i>Allotropic*</i>	Silicon has two allotropic forms, a brown amorphous form, and a dark crystalline form	<i>Flammability</i>	Dark-brown crystals that burn in air when ignited
<i>Solubility</i>	Soluble in hydrofluoric acid and alkalis	<i>Reactivity with acids</i>	Dissolves only in a mixture of nitric acid and hydrofluoric acid
<i>Melting point</i>	Melts at 1417°C	Is transparent to long-wavelength infra-red radiation	
<i>Boiling point</i>	Boils at 2600°C		
<i>Conductivity</i>	Semi-conductor		

*Allotropic – Allotropes: Forms of an element with different physical and chemical properties occurring in two or more crystalline forms in the same physical state

- **Energy bands of Si**

A crystalline solid (e.g. silicon) consists of atoms arranged in a repetitive structure. Specifically, each silicon atom is surrounded by four nearest neighbors as illustrated by the shaded cluster in Figure 1.6. Recall that electrons in an atom occupy discrete energy levels as shown in Figure 1.8(a). If two atoms are in close proximity, each energy level will split into two due to the Pauli exclusion principle, that states that each quantum state can be occupied by no more than one electron in an electron system such as an atom molecule, or crystal. When many atoms are brought into close proximity as in a crystal, the discrete energy levels are replaced with bands of energy states separated by gaps between the bands as shown in Figure 1.8(b). Naturally, the electrons tend to fill up the low energy bands first. Between the (basically) totally filled and totally empty bands lie two bands that are only nearly filled and nearly empty as shown in Fig. 1.8(b). These energy bands are the valence band (top nearly filled band with electrons) and the conduction band (the lowest nearly empty band). These bands are separated by a region which designates energies that the electrons in the solid cannot possess. This region is called the forbidden gap, or bandgap E_g . This is the energy difference between the maximum valence band energy E_v and the minimum conduction band energy E_c , as shown in Figure 1.9. The concept of E_g , is very important for the laser-solid interactions (section 1.2.2).

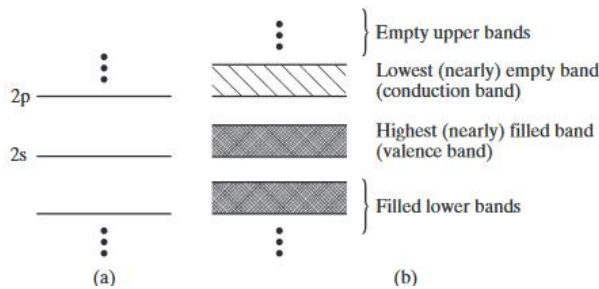


Figure 1.8

The discrete energy states of a Si atom (a) are replaced by the energy bands in a Si crystal (b).

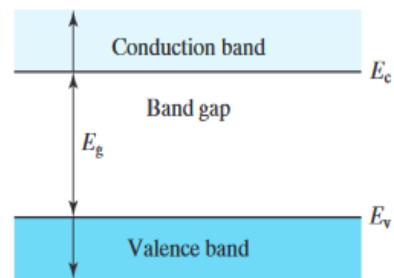


Figure 1.9

The energy band diagram of a semiconductor

- **Silicon oxide layer (SiO₂)**

Semiconductor surfaces have been investigated for many years. Due to its dominant role in silicon devices technologies (e.g. IC industry) [F. J. Himpsel et al., 1988⁵⁶, M. Razeghi, 2010⁵⁷] and because of its good electronic properties, as well as Si/ SiO₂ interface, the above SiO₂ properties has been intensively studied in the last decades. In contrast to other materials which suffer from one or more problems, SiO₂ offers a lot of desired characteristics and advantages [A.Hierlemann⁶³]:

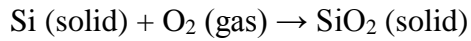
1. Excellent electrical insulator with a high dielectric strength and wide band gap (Resistivity > 1×10²⁰ Ωcm , Energy Gap ~ 9 eV)
2. High breakdown electric field (> 10MV/cm)
3. Dielectric constant SiO₂: 3.9 (whereas Si₃N₄ : 7; Si: 11.9)
4. Stable and reproducible SiO₂ interface
5. Conformal oxide growth on exposed Si surface
6. SiO₂ good diffusion mask for common dopants: B, P, As, Sb
7. Very good etching selectivity between Si and SiO₂
8. SiO₂ has a high-temperature stability (up to 1600°C)

According to these properties of SiO₂ and Si/SiO₂ interface, the silicon oxide layer (SiO₂) is a high quality electrically insulating layer on the silicon surface, serving as a dielectric in numerous devices that can also be a preferential masking layer in many steps during device fabrication [Logofatu C. et al., 2011⁵⁵].

Among all the various oxidation methods (thermal oxidation, electrochemical anodization and plasma enhanced chemical vaporization deposition), only thermal oxidation in a resistance-heated oxidation furnace can provide the highest-quality oxides having the lowest interface trap densities. Thermal oxidation of Silicon can be performed in two ways: 1. Dry and 2. Wet oxidation process. A typical oxidation growth cycle consists of dry-wet-dry oxidations, where most of the oxide is grown in the wet oxidation phase⁵⁵.

1. *Dry thermal oxidation process*

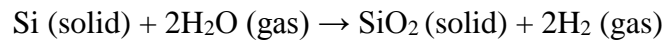
Dry oxidation uses dry oxygen. Oxidation process is slow e.g., 50 nm/h at 1000°C and results in more dense and high-precision thin oxide layers. The chemical reaction describing thermal oxidation of silicon in dry oxygen is:



Dry thermal oxidation process is usually used in a device structure because of its good Si-SiO₂ interface characteristics.

2. Wet thermal oxidation process

Wet process uses (pyrogenic) water vapor. The oxidation process is fast, e.g., 400 nm/h at 1000°C and therefore is mainly used for thick oxide formation applications. The chemical reaction is the following:



In the wet oxidation method, the water vapor introduced into the furnace system is usually creating by passage a carrier gas into a container with ultra pure water and maintained at a constant temperature below its boiling point (100°C). Wet oxidation results in much more rapid growth and is used mostly for thicker masking oxide layers. In this thesis, silicon substrates have been processed via dry thermal oxidation.

For both means of oxidation, the high temperature allows the oxygen to diffuse easily through the silicon dioxide and the silicon is consumed as the oxide grows. SiO₂ layer incorporates silicon consumed from the substrate and oxygen supplied from the ambient. Thus the silicon oxide grows both down into the wafer and up out of it , so the total thickness increases [B.E.Deal and A.S.Grove, 1965⁵⁸], as shown in Figure 1.10.

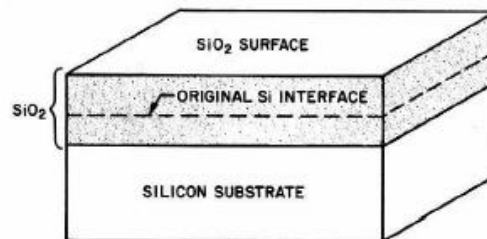


Figure 1.10 : Schematic of the thermal oxide (SiO₂) formation [S. M. Sze, 2002⁶⁴]

Kinetics of growth

A model elucidating the kinetics of oxide growth has been developed by Deal and Grove⁵⁸, where it is assumed that oxidation proceeds by an inward movement of the oxidant species rather than an outward movement of silicon. At the initial stage of oxidation, the oxidizing species (oxygen or water vapor) reacts with silicon atoms at the surface. This results in growth of a thin SiO₂ layer. Now, in order to oxidize Si, the oxidizing species has to diffuse through the SiO₂ layer of the Si-SiO₂ interface. More specifically, the transported species must go through the following stages:

1. It is transported from the bulk of the oxidizing gas to the outer surface where it reacts or is adsorbed.
2. It is transported across the oxide film towards the silicon
3. It reacts at the silicon surface to form a new layer of SiO₂

The model is generally valid for temperatures between 700 and 1300°C, partial pressure between 0.2 and 1.0 atmosphere, and oxide thickness between 30 nm and 2000 nm for oxygen and water ambient. The model is valid for (111), (100) single crystal silicon, and polysilicon. According to the equations of this model, which are analyzed by B. Deal and A. Grove, 1965.⁵⁸, oxidation rate charts (different for dry and wet oxidation) have been developed based on which, oxide thickness layer for the optimum oxidation parameters can be predicted. However, the most reliable technique, to measure the SiO₂ thickness layer is ellipsometry (section 3.5.4).

SiO₂ layer structure

Regarding its structure, SiO₂ can be described as a three-dimensional network constructed from tetrahedral entities which are centered on a silicon atom. The four corners of the tetrahedral structure could be either silicon or oxygen atoms. It is accepted that an oxygen atom is bonded by two silicon atoms and never with another oxygen atom. The length of the Si-O bond is 1.62 Å while the distance of the bond between oxygen ions is 2.26 Å (Figure 1.11(a)) and Si-Si bond distance depends on the particular form of SiO₂ and is about 3.1 Å. The angle formed by the Si-O bonds in the Si-O-Si bridge is 144° [Carrier P. et al., 2002⁶¹], and the angle between two oxygen atoms is 109.5°. Taking into account the fact that the silicon atom is four-coordinated and the oxygen is two-coordinated, concludes that, oxygen atoms are involved in Si-

O–Si bridges, which means two Si-O bonds and Si atoms will contribute to Si–Si and Si–O–Si bonds.

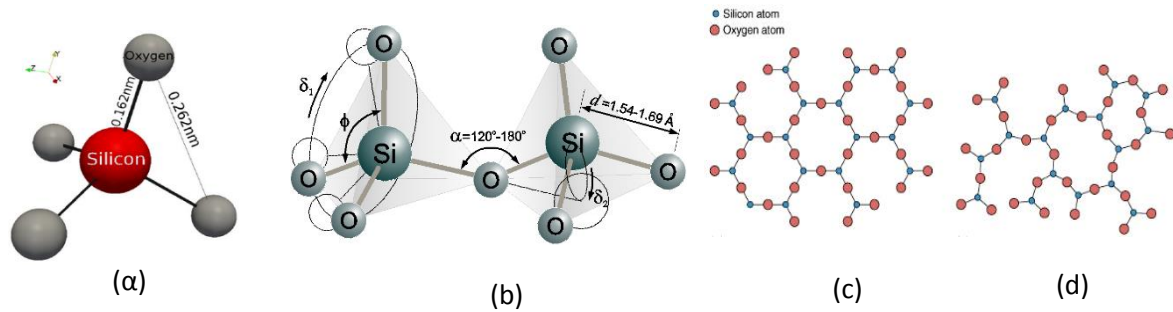


Figure 1.11 : (a)Structural unit of SiO_2 , (b)Regular silica structure: Si-O bond length (d), tetrahedral angle (ϕ), the Si-O-Si bridge bond angle (α), bond torsion angles (δ_1 , δ_2), [Henderson and Baker, 2002⁶⁰], (c) Quartz crystal lattice (2D), (d) Amorphous SiO_2 (2D)

The six-membered ring structure of SiO_2 is presented in Figure 1.11(d). In an ideal network the vertices of the tetrahedra are joined by a common oxygen atom called bridging oxygen (i.e. O atoms that bond to two silicon atoms). In the amorphous forms of SiO_2 (Figure 1.11(d)), some non-bridging oxygen atoms can also exist. These phases are often named, fused silica. Crystalline forms of SiO_2 , such as quartz contain only bridging oxygen bonds. The various crystalline and amorphous forms of SiO_2 arise due to the ability of the bridging oxygen bonds to rotate, allowing the position of one tetrahedron to move with respect to its neighbors. This same rotation allows the material to lose long-range order and hence become amorphous. The rotation and the ability to vary the angle of the Si-O-Si bond from 120° to 180° (Figure 1.11(b)) with only a little change in energy play an important role in matching amorphous SiO_2 with crystalline silicon without breaking bonds. Dry oxides having larger ratio of bridging to non-bridging sites as compared to wet oxides, are thus “more stable”. The chemical bonding configurations are important basis for understanding the electronic states of the fabricated silicon oxides. In order to understand the chemical and electronic structures of the Si-SiO₂ interface, the Si-SiO₂ interface has been studied by various techniques such as X-ray photoelectron spectroscopy (XPS)⁵⁵. The conclusion was that, while the oxide layer grows, it is progressively less and less influenced by the properties of the interface.

Native oxide layer

Another important issue when dealing with silicon is the so called native oxide layer, which is built up on the surface when a clean Si surface is exposed to atmosphere at room temperature. It is of great importance, because it may influence the thermal oxidation kinetics. Native oxide films on Si surfaces prevent the low-temperature growth of high-quality epitaxial Si films and precise control of the thickness and electrical properties of very thin gate oxide films, plus give an increase of the contact resistance for via-holes of a small area. Native oxides serve as source of impurities to diffuse into the silicon and produce defects in succeeding high-temperature processes. The presence of native oxide film on silicon surfaces degrades the ability to control the quality of device fabrication processing and the performance and reliability of semiconductor devices themselves. The detection of the native oxide layer takes place through X-ray Photoelectron Spectroscopy (XPS). The oxidation mechanism of Si in air at room temperature (RT) is entirely different from the thermal oxidation mechanism. The following model [M. Morita et al., 1990⁶²] is proposed for the oxidation of Si at room temperature (Figure 1.12):

1. Si atoms at a cleaned wafer surface are terminated by hydrogen (Fig. 1.12(a)). In our case, the Si wafers were cleaned by aqueous hydrofluoric acid (HF).
2. The oxygen species (O) are expected to break preferentially the $\text{Si}_{\text{bulk}}=\text{Si}(\text{H})_2$ backbonds rather than the Si-H bonds on the surface at the initial stage. ($\text{Si}_{\text{bulk}}-\text{O}-\text{Si}(\text{H})_2$ bonds are formed- Fig. 1.12b).
3. After all Si atoms of the top layer are oxidized, the chemical structure of the second monolayer are broken by subsequent insertion of O_2 (Fig. 1.12d).
4. In this way, a layer-by layer growth of the native oxide film takes place on Si surfaces exposed to air at RT.
5. The overlayer structure converts to the amorphous phase.
6. The remaining $\text{O}-\text{Si}(\text{H})_2$ bonds on top layer cause hydrophobic behavior of the surface, which can be observed during the initial phase of native oxidation in air.

7. The Si-H bonds on the surface are oxidized only after completion of the backbond oxidation, and silanol groups SiOH are respectively formed, which introduce polarity (and the surface becomes less hydrophobic).

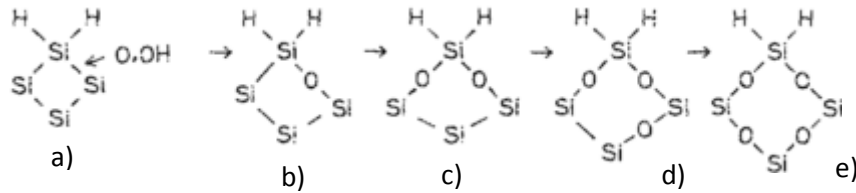


Figure 1.12 : A model of native oxide growth in air ⁶²

1.2.2 Laser – solid interactions: Fundamental aspects

The interpretation of the basic interaction mechanisms between the intense light of a laser beam and matter, is an aspect of increasing interest⁴². Controlling the light-matter interactions is crucial for the success and scalability of materials-processing applications¹⁶. In our case, this is achieved by surface irradiation with ultra-short laser pulses because pulse duration is a critical parameter for material processing. In order to understand and control the material response after/upon laser irradiation, the laser-matter interactions have to be taken into consideration.

1.2.2.1 Primary process

The initial interaction of laser pulses with a semiconducting material is the excitation of electrons; upon photon absorption electrons are excited from their equilibrium states into higher-lying unoccupied states. More specifically, the energy band gap of silicon ($E_{g(Si)}$: 1 to 1.5 eV) is less than 3.0 eV, which means that Si absorbs energy through photoionization when irradiating in Vis-IR spectrum because the photon energy is bigger than the energy bandgap. Primary absorption processes involving interband transitions of electrons are: (a) single photon absorption, (b) multiphoton absorption (the electrons excite to the conduction band), (c) interband transitions by free-carrier excitation or (d) impact ionization [E. Magoulakis et al. 2010⁶⁵]. This process increases the number of free carriers in the conduction band. If the laser intensity is high enough, multi-photon absorption and impact ionization can lead to optical breakdown, which produces a plasma [A.C. Tien , 1999⁶⁶].

1.2.2.2 Secondary process

Following the primary absorption mechanisms the energy absorbed by the electron is relaxed through a variety of processes which can eventually end in modification of the material structure. Figure 1.13 [S. K. Sundaram and E. Mazur, 2002⁶⁷] summarizes the most important processes involved after the absorption of the laser energy, its redistribution and transport through the target and the resulting structural and thermal effects, together with their typical timescales.

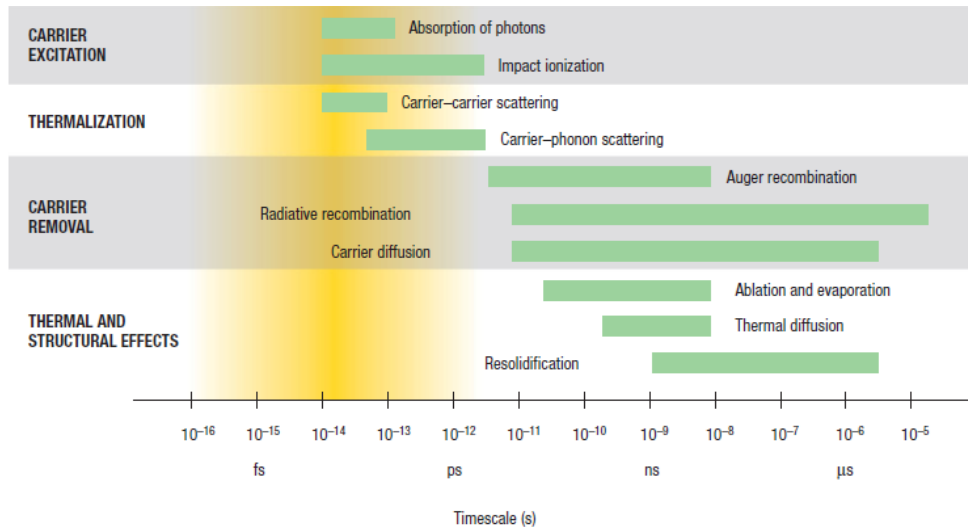


Figure 1.13 : Processes (and associated timescales) taking place in the target following the absorption of the laser pulse⁶⁷.

(i) Carrier excitation: Carrier (electrons in metals or electron-holes in semiconductors) excitation is the movement of an electron to a higher energy state due to absorption of photons by a laser beam. Single or multiphoton absorption are the dominant mechanisms for exciting electrons in the valence band provided that the energy gap is smaller or greater respectively than the photon energy. If some of the carriers are excited well above the band gap, impact ionization can generate additional excited states.

(ii) Thermalization: On a time scale of about $10^{-14} - 10^{-12}$ sec described as the electron phonon relaxation time, the initial energy distributed among the electrons is transferred to the lattice via carrier-carrier and carrier-phonon scattering.

(iii) Carrier removal: Once the carriers and the lattice are in equilibrium, the material is at a well-defined temperature. Although the carrier distribution has the same

temperature as the lattice, there is an excess of free carriers compared to that in the thermal equilibrium. These are removed by recombination or carrier diffusion processes.

(iv) Thermal and structural effects: On the time scale of 10^{-11} sec and below carriers and lattice come to an equilibrium temperature and heat is diffused from the material's surface to the bulk. If the laser pulse intensity exceeds the melting or boiling point thresholds, melting or vaporization of the material occurs. As the deposited optical energy is converted to kinetic energy of the lattice ions, material removal via ablation can occur in the form of individual atoms, ions, molecules or clusters. Finally solidification of the material occurs in timescales from nanosecond through microseconds.

So, why to use an ultra-short femto-second pulse laser?

Nanosecond laser ablation of materials occurs due to melt expulsion driven by the vapour pressure and the recoil pressure of light, so the ablated area on the surface of the material target is not precise and uniform. Furthermore, nanosecond laser ablation creates a heat-affected zone (HAZ) [Lucas, L. and J. Zhang , 2012⁶⁸].

In the case of ultra-short laser pulses (pulse duration less than a few picoseconds (10^{-12} seconds)), pulse duration is considerably shorter than the timescale required for energy transfer between the lattice and the free electrons of the material target. The laser energy is absorbed by the electrons, leaving the ions cold, and only after the laser pulse is gone thermalization take place. As a result, very high temperatures and pressures are produced at a very shallow depth in the range of microns. However, the absorbed energy heats the material very quickly past the melting point, directly to the vapor phase with its high kinetic energy. The material is removed by direct vaporization away from the surface without formation of a recast layer. This provides negligible HAZ and very fine, sharp features. Also, the intensity of a femtosecond pulse is high enough to drive highly nonlinear absorption processes in materials that do not normally absorb at the laser wavelength⁶⁸. There are two major mechanisms to explain material removal by laser ablation: thermal vaporisation, and the occurrence of a Coulomb explosion. As shown in Figure 1.14, the long-pulse lasers have more heat-affected zones and shock waves in comparison with the shorter picosecond and femtosecond lasers.

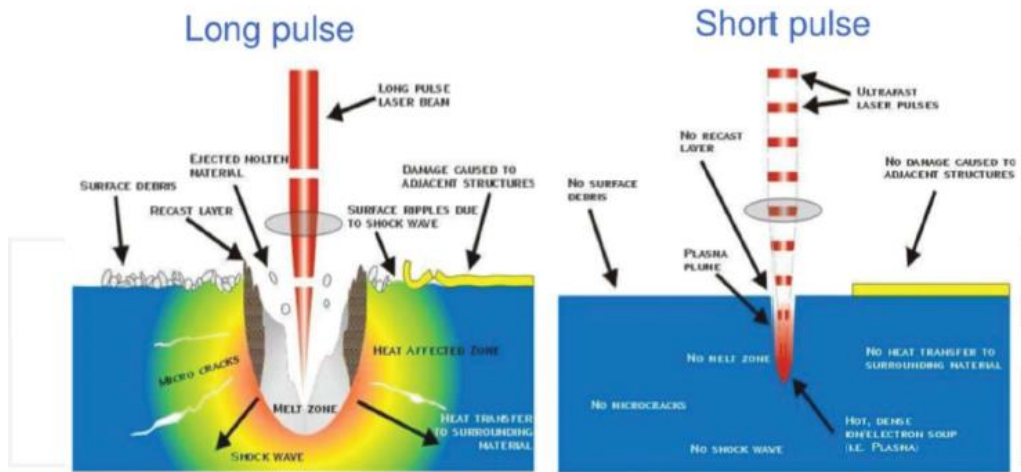


Figure 1.14: Long-pulse and ultrafast-pulse laser interaction with target material.

So by using ultrafast lasers with pulse duration less than sub-picosecond, we can limit the thermalization and thermal diffusion, caused by the relaxation process, in order to avoid the ablation of clusters and evaporation of material and to encourage the formation of controllable periodic structures in micro and nano scale [Y.C. Koji Sugioka, 2013⁶⁹].

Laser-Induced Periodic Surface Structures (LIPSS) is a form of laser induced surface modification which appears to be spatially periodic in nature, and which occurs on a wide variety of both opaque and transparent materials. The formation of LIPSS by a single laser beam is a universal phenomenon that can appear on any material absorbing radiation, regardless of its dielectric constant [J.F.Young et al., 1984⁷⁰]. The resulting structures/ morphology depend on the material (optical and thermal properties), laser source (such as laser fluence, repetition rate, wavelength, etc.) and irradiation environment (liquid, vacuum or reactive gas). In this respect, upon irradiation with laser pulses at a fluence close to the melting threshold, the surfaces of the substrates develop ripples (coherent structures) with a spacing equal to or larger than the laser wavelength⁷⁰. Focusing on silicon, ripple formation leads to low spatial frequency ripples (*LSFR*) perpendicular to the beam polarization, where the periodicity (spatial interval between the repeating structures (Λ)) is near to the laser wavelength (λ) ($\Lambda \sim \lambda$), or to high spatial frequency ripples (*HSFR*) where the periodicity is smaller than the laser wavelength ($\Lambda < \lambda$) and depends only on the frequency (electron density) of the surface plasmon wave [S. Sakabe et al., 2009⁷³]. The formation of *microgrooves* leads to structures with periodicity larger than the laser wavelength ($\Lambda > \lambda$) [Tsibidis George

D. et al., 2015⁷²]. In case of micro-conical formation (*spikes*), structures are characterized as *supra-wavelength quasi-periodic surface structures*, which means that the periodicity is markedly, even multiple times, higher than the laser wavelength ($A \gg \lambda$) [Tsibidis George D. et al., 2016⁷¹]. Figure 1.15 shows the morphological changes induced on a Si surface following fs pulse laser irradiation.

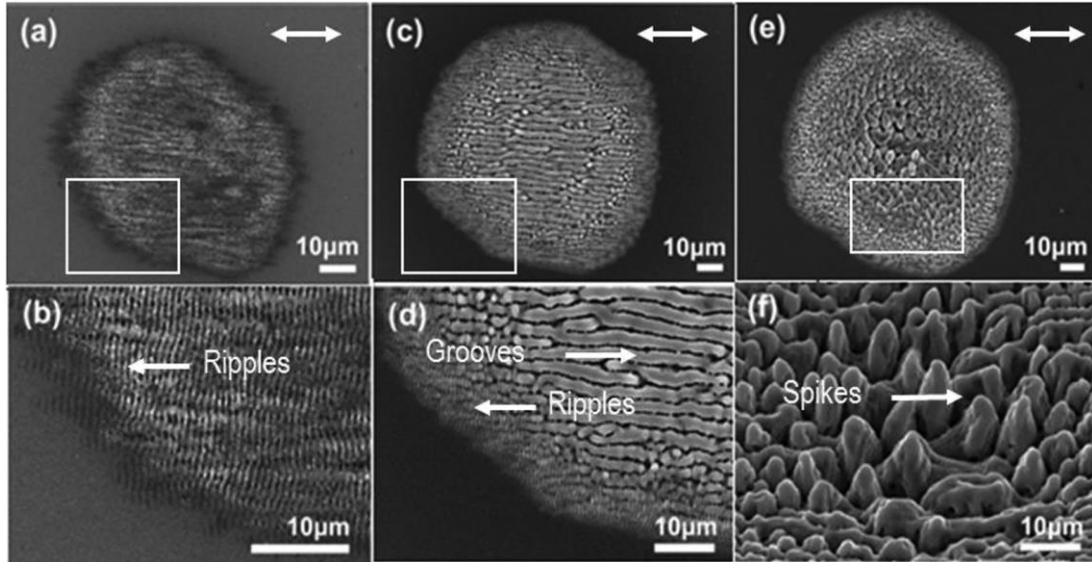


Figure 1.15: Morphological changes induced on a Si surface following irradiation with NP = 10 (a), 40 (c), and 100 (e) pulses, laser beam wavelength $\lambda = 800$ nm, where (b), (d), and (f) provide an enlarged area. Double-ended arrows indicate the laser beam polarization⁷².

1.2.3 Surface structuring of silicon via ultrashort – pulsed laser processing

The irradiation of a solid surface via ultra-short fs pulsed laser, leading to microstructures of different morphologies. The resulting structures/ morphology depend on the material (e.g. optical and thermal properties), laser source (such as laser fluence, repetition rate, wavelength, etc.) and irradiation environment (liquid, vacuum or reactive gas). By irradiating silicon surfaces with fs laser pulses above the ablation threshold in the presence of a variety of background gases, quasi-periodic sharp conical micrometer-sized spikes are formed. High-intensity nanosecond pulses can induce the formation of much larger conical microstructures [A. Pedraza et al., 1999⁷⁴, S. Dolgaev et al., 2001⁷⁵]. Microstructuring by ultra-short pulsed lasers is an especially attractive approach, because it leads to the formation of arrays of high-aspect ratio microcones (MCs) on solid surfaces. In particular, fs lasers allow patterning through non-linear

absorption processes, providing excellent control over the regularity and uniformity of 3D micron and submicron features¹⁶. This method exploits a number of phenomena taking place under the action of intense pulsed laser irradiation of crystalline Si in the presence of a reactive gas, in order to induce morphological, structural and compositional modifications on its surface. The resulting structures, apart from their unique (conical) morphology, they also exhibit improved optical, electronic and wetting response. Proper tuning of the laser (such as laser fluence, repetition rate, etc.) and reactive gas parameters (such as pressure) can lead to the formation of structures with different morphologies [Zorba V. et al., 2006⁷⁶]. One of the most useful properties of ultrafast laser induced modification is the limited size of the affected volume, resulting in perfect control of structures fabrication in micro- and submicron scales, for reasons which explained in section 1.2.2.2.

The role of reactive gas

The main objective of the present thesis was the fabrication of hierarchical silicon structures. One way to achieve the fabrication of double roughness surfaces (micro- and nano- scales), is the irradiation via ultra-short fs pulsed laser in presence of a gas which reacts with the initiate surface. More specifically, microstructuring of the flat silicon (Si) substrate surfaces by ultrafast fs lasers under reactive gas (SF_6) atmosphere chosen as a method of surface micro-structuring because it produces surface morphologies through a simple one-step process [T.-H.Her et al., 1998⁷⁷]. Pure sulfur hexafluoride (SF_6) plasmas produce large quantities of atomic fluorine (F) that is used to quickly etch silicon. When SF_6 plasma is used to etch silicon, it typically results in etch profiles that are isotropic in nature [Bates Robert L. et al., 2014⁷⁸]. At room temperature SF_6 is stable and does not chemisorb on Si. However heating at approximately 1000 °C may initiate a thermal reaction. This suggests that laser heating could cause a reaction. SF_6 can be physisorbed at 90K or for $P \geq 1\text{Torr}$ at room temperature [D. Bäuerle et al., 2000⁷⁹]. The dissociation of SF_6 leading to the formation of fluorine radicals. Etching of Si can then occur through the formation of these F radicals, which eventually react with Si to form volatile Si containing fluorine compounds. A theoretical model is developed for plasma etching of silicon with SF_6 . The three-dimensional model developed includes diffusion and convection of molecular fragments in a duct

geometry [Lii, Y.~J. et al., 1990⁸⁰]. Gaseous or physisorbed SF₆ molecules are excited into higher vibrational states and chemisorb on Si surfaces resulting to the formation of fluorine ions. Part of the chemisorbed F⁻ ions penetrate into the Si forming a fluorosilyl layer [J.D.Fowlkes et al., 2000⁸¹]. The chemical reactions describing the chemisorbtion processes are shown in Figure 1.16.

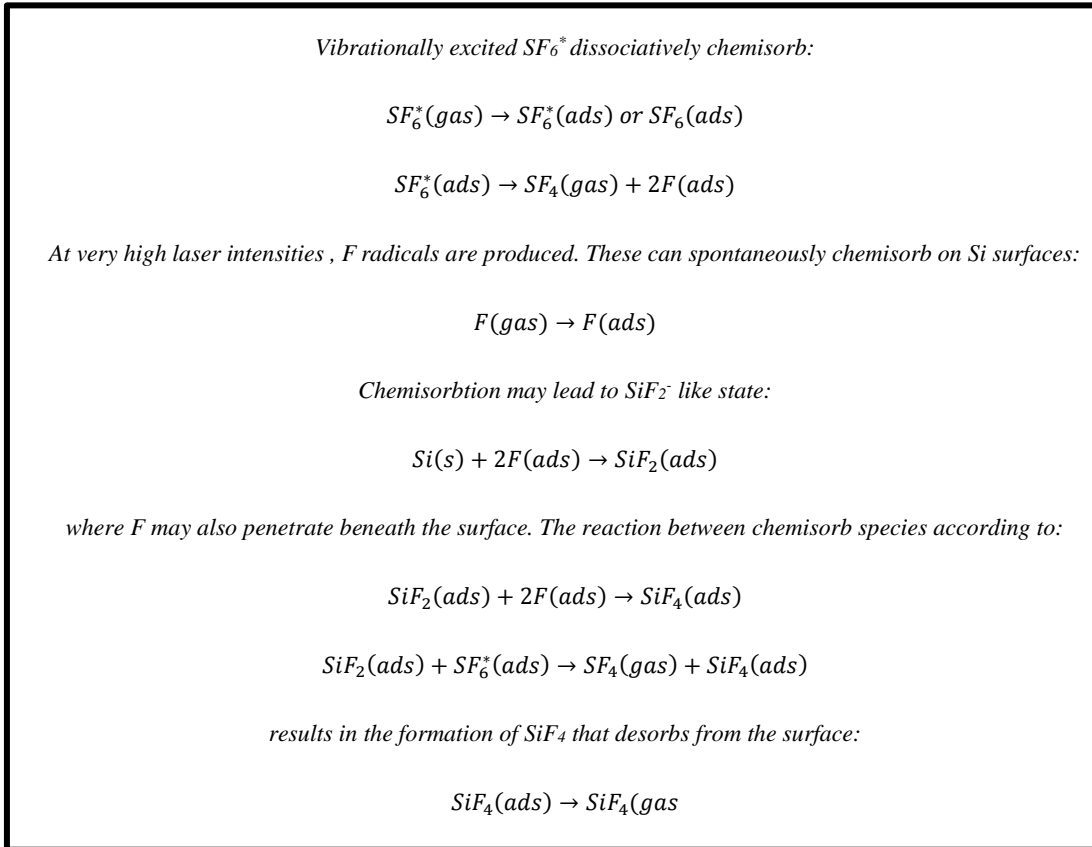


Figure 1.16: Stages of SF₆ gas chemisorption on silicon under laser irradiation [D. Bäuerle , 1986⁸²]
 As a result, the formation of the nano-roughness on the MCs structures becomes more apparent with increasing the pressure of SF₆ gas (section 4.1.1.2).

1.3 Gold nanoparticles

Nanotechnology generally refers to a field of science and engineering dedicated to materials of sizes ranging from 1 – 100 nm [Mody et al. 2010⁸⁵, Salata 2004⁸⁵]. The term ‘ nano ’ is extracted from the Greek word ‘ dwarf ’ , which means ‘ extremely small ’ . When used as a prefix, it means 10^{-9} or 0.000000001 meter [Thakkar et al. 2010⁸⁴]. Particles of sizes between 1 and 100 nm show fascinating properties with unusual characteristics that lead to the formation of unique properties in nanosystems, which are not observed in ordinary materials. These are considered as nanoparticles (NPs). Metallic nanoparticles have different physical and chemical properties from bulk metals (e.g., lower melting points, higher specific surface areas, specific optical properties, mechanical strengths, and specific magnetizations). Their unique properties might prove attractive in various industrial applications [Vollath, D.,2013⁸⁶]. Gold nanoparticles (AuNPs) and their arrays are some of the most studied nanomaterials, with promising applications in many fields such as electronics, optoelectronics, catalysis, solar cells and biology [Zhou et al., 2009⁸⁷]. These particles are also malleable in a molecular sense: groups of functional molecules (ligands) can be attached easily as shown in Figure 1.17.

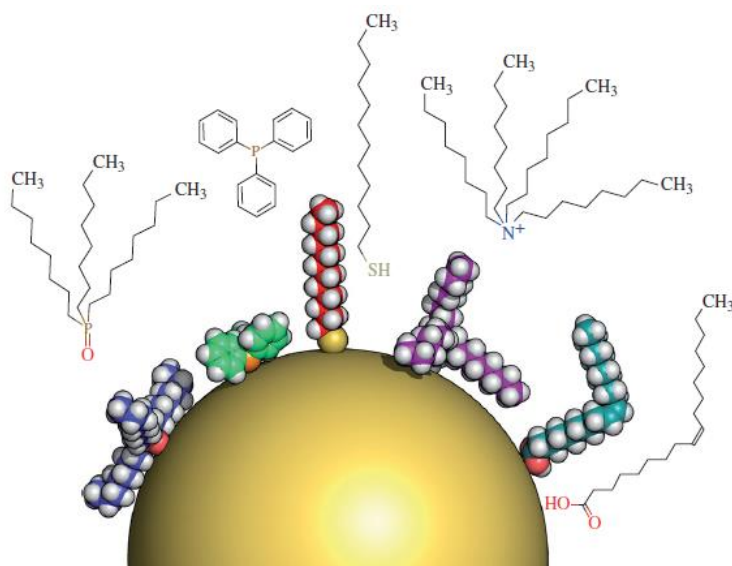


Figure 1.17 : Commonly used hydrophobic ligand molecules drawn to scale along with a particle of 5nm diameter. The particle is idealized as a smooth sphere; the schematic molecule structures above are not drawn to scale. Left to right: triethylphosphine oxide (TEPO), triphenylphosphine (TPP), dodecanethiol (DDT), tetraoctylammonium bromide (TOAB) and oleic acid (OA). The spatial conformation of the molecules is only shown schematically as derived from their chemical structure and space-filling models [Sperling R. and W. J. Parak, 2010⁸⁸].

1.3.1 Synthesis of gold nanoparticles

The most important property of nanoparticles is their size, as many applications depend on it. Size polydispersity is an undesirable characteristic. Thus, prediction of both size and size dispersity for a given system is of concern in systematizing the manufacture of nanoparticles. The methods of nanoparticle synthesis are classified as (i) gas-phase and (ii) liquid-phase [Kumar S. et al., 2007¹⁰⁰].

- (i) Gas-phase based synthesis method: Bulk material is evaporated using high energy sources such as resistive heating and lasers to obtain a supersaturated gas phase, which, under controlled conditions, produces nuclei that grow to become nanoparticles.
- (ii) Liquid-phase based synthesis method: Precursors react to form a supersaturated solution, which nucleates and gives rise to particles ranging from 1 to 100 nm in size with stability ranging from a couple of hours to years. Wet synthesis methods are attractive at least for two reasons: a) they are more energy efficient and b) they can be used to produce nanoparticles using the standard apparatus available in a laboratory.

So far, two strategies have been followed for wet synthesis. In the first strategy, two reactants, usually both of them in micellized form, are mixed and nanoparticles form inside them by precipitation. The size of particles is controlled by the rates of nucleation and growth, and stabilization is provided by adsorption of surfactant. This strategy offers scope for good control over particle size. In the second strategy, precipitation is carried out in bulk in the presence of stabilizers that adsorb on nanoparticles and prevent coagulation of particles. Three widely used bulk-precipitation-based techniques for the synthesis of gold nanoparticles are as follows: (1) citrate method of Turkevich et al.,¹⁰¹ (2) citrate-tannic acid method of Muhlfordt,¹⁰² and (3) Brust-Schiffrin method of Brust et al.¹⁰³. The first two methods yield particles which are stable against coagulation, whereas the last one produces particles which are also capped and cannot grow further.

More specifically, colloidal nanoparticles are dispersed in a solvent that can be either water-based or an organic solvent for hydrophilic or hydrophobic particles, respectively, while amphiphilic nanoparticles can be dispersed in both kinds of solvents. The synthesis of colloidal NPs involves surfactant molecules that bind to their surface, which stabilize the nuclei and larger nanoparticles against aggregation by a

repulsive force⁸⁸. The ligand molecules bound to the nanoparticle surface not only control the growth of the particles during synthesis, but also prevent the aggregation of the nanoparticles. The repulsive force between particles can, in principle, be due to electrostatic repulsion, steric exclusion or a hydration layer on the surface. Various chemical functional groups possess a certain affinity to inorganic surfaces, the most famous example being thiol to gold.

Conjugation strategies for AuNPs

The labile capping ligands on AuNPs (citrates, thiols, or other adsorbed ligands) can be displaced by thiols through a place ligand exchange reaction to synthesize mixed monolayer-protected AuNPs (Figure 1.20(A)). Place ligand exchange allows the secondary tethering of organic molecules or biomolecules to the surface of AuNPs (Figure 1.20(B)). Non-covalent conjugation is a simpler way for molecules to bind to AuNPs. Alternatively, covalent conjugation of molecules to AuNPs stabilizes the conjugates, which is more useful when stable constructs are required (e.g., amine-carboxylate coupling [U. Drechsler et al., 2004¹¹⁰]).

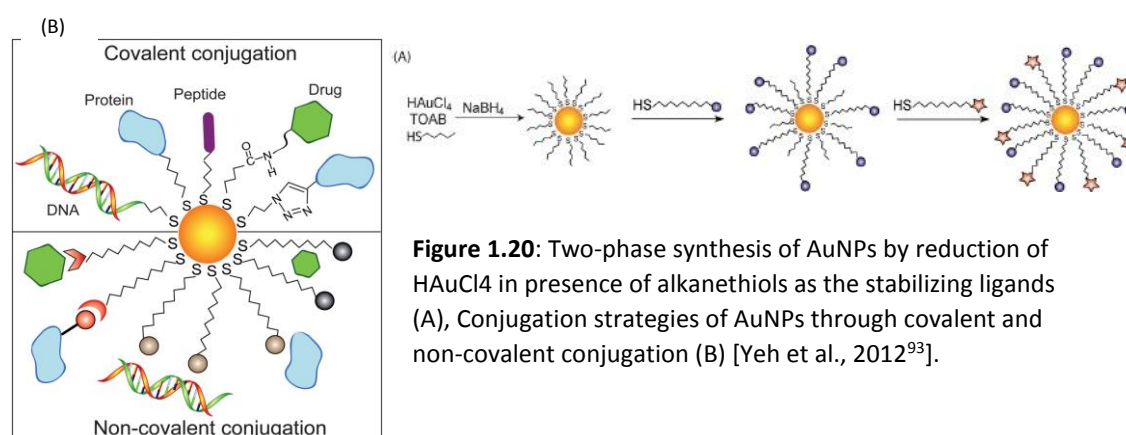


Figure 1.20: Two-phase synthesis of AuNPs by reduction of HAuCl₄ in presence of alkanethiols as the stabilizing ligands (A), Conjugation strategies of AuNPs through covalent and non-covalent conjugation (B) [Yeh et al., 2012⁹³].

Although there are several synthesizing methods for AuNPs, such as electrochemical method [Reetz and Helbig 1994¹⁰⁵, Reetz et al., 1995¹⁰⁴], seeding growth method [Jana et al., 2001¹⁰⁶], biological method [Das et al., 2011¹⁰⁸, Smitha et al., 2009¹⁰⁸], sonochemical method [Itoh et al., 2004¹⁰⁹], electron beam lithography [Eustis Susie, and Mostafa El-Sayed, 2006⁹⁶].

1.3.2 Properties of gold nanoparticles

AuNPs are being widely used in a variety of biomedical applications because of their compatibility of synthesis and functionalization, less toxicity, and facility of detection [Tiwari et al. 2011⁹⁵]. Their properties depend on their shape and size. Colloidal gold, unlike bulk gold, is considered to be highly reactive, allowing for new applications. The applications of gold are further extended by colloidal gold which are submicrometer size particles of gold [Shah M et al., 2014⁹²]. Prerequisite for every possible application, of colloidal AuNPs (range 1 nm to 1 μ m), is the proper surface functionalization of such nanoparticles, which determines their interaction with the environment. These interactions ultimately affect the colloidal stability of the particles, and may yield to a controlled assembly or to the delivery of nanoparticles to a target, e.g. by appropriate functional molecules on the particle surface [Sperling R. and W. J. Parak., 2010⁸⁷]. Their synthesis technique, makes them extremely stable for both shape and size (section 1.3.1). Also the functionalization of colloidal AuNPs can be done via bioconjugation with antibodies, proteins or oligonucleotides [Yeh et al., 2012⁹³]. This is a very promising technique for scaffold fabrication for drug and gene delivery [Majidi et al., 2016⁹⁴]. *In response to the properties of the functionalization of gold nanoparticles, we chose to work with colloidal AuNPs, which have on their surfaces functional groups such as amino acids, organic moieties.*

Of particular importance, the optical property is one of the fundamental attractions and a characteristic of a nanoparticle. AuNPs have exceptional optical properties due to surface plasmon resonance (SPR) effects. SPR is an optical phenomenon occurring from the interaction between an electromagnetic wave and the conduction of electrons in a metal. [Hu et al. 2006⁹⁰]. The SPR properties of AuNPs makes them quite useful in the fields of bioimaging and biomedical therapeutics, and as biodiagnostic tools [Verma et al. 2014⁸⁹, Jain et al. 2006⁹¹]. In particular, AuNPs present localized surface plasmon resonances (LSPRs) that lead to a strong absorption/scattering and local field enhancement near such structures [Hubert, C. et al., 2007⁹⁹]. More recent treatments have shown that the color of AuNPs is due to the collective oscillation of the electrons in the conduction band, known as the surface plasmon oscillation. The oscillation frequency is usually in the visible region for gold and silver, giving rise to the strong surface plasmon resonance absorption. When AuNPs are enlarged, their optical properties change only slightly as observed for the different samples in Figure 1.18,

whereas the absorption peak of the surface plasmon resonance shift (“red shift”). However, when an anisotropy is added to the nanoparticle, as is the case of nanorods, the optical properties of the nanoparticles change dramatically [Eustis Susie, and Mostafa El-Sayed , 2006⁹⁶]. These changes are due to the free d electrons of gold, which can oscillate in the conduction band. Figure 1.19 shows not big enough color changes for the case of gold nanospheres, with increasing size. On the contrary, in the case of the gold nanorods big color changes can be observed with increasing aspect ratio (length/width).

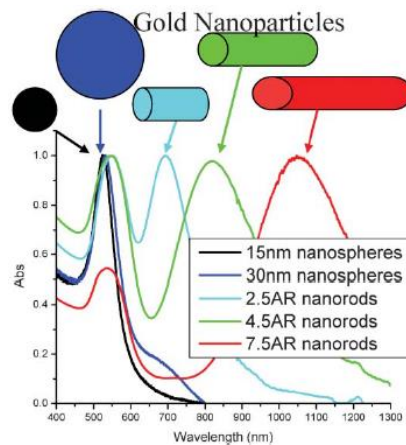
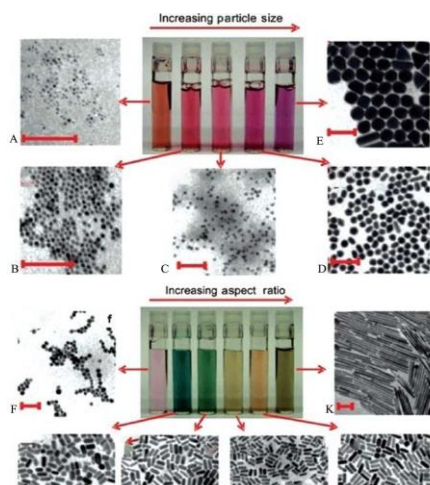


Figure 1.18: Gold nanoparticles – absorption of various sizes and shapes [Eustis Susie, and Mostafa El-Sayed , 2006⁹⁶].

The absorbance of surface plasmon resonance peak for anisotropic AuNPs can be resolved along the three main axes. The surface plasmon resonance is not only responsible for the high absorption of the AuNPs, but also causes non-linear properties. The nonlinear properties of spherical AuNPs is closely linked to the depreciation



coefficient of the absorption (higher nonlinear properties around the top SPR ~ 520nm) [Pong et al., 2007⁹⁷]. Gold nanorods (GNr) have been shown to have two plasmon resonances, one due to the transverse oscillation of the electrons at visible region (~520nm) for gold and the other due to the longitudinal plasmon resonance at near infrared (NIR) region as shown for various aspect ratios in Figure 1.18.

Figure 1.19: TEM images of gold spheres and gold nanorods in increasing order of dimensions with a scale bar of 100 nm for all. Size for gold spheres (A-E) varies from 4-40 nm whereas for gold nanorods (F-K), the aspect ratio varies from 1.5. to 20 ⁹².

In general, AuNPs have the ability to strongly scatter the electromagnetic irradiation in a specific wavelength which belongs to the visible range and it depends on the size, shape, concentration and environmental optical properties [Turkevich, John , 1985¹⁰¹].
In the present thesis, on the size of AuNPs and the effect they have on the optical properties of microstructured Si surfaces.

2 Aim of the thesis

2.1 Problem statement & aim of thesis

Nature is a source of inspiration, since it presents unique and distinct ways to solve complex problems. Many models of nature, have been studied and artificially constructed.

The attempt of the man to study and simulate artificially the biological systems with their desired properties is termed biomimetics. One of the applications of biomimetic research is the construction of surfaces with optimized properties. The most famous of all is the lotus leaf, which comprises a dual scale roughness and exhibits incredible wetting properties. These surfaces are called hierarchical micro-nano surfaces because they incorporate features of different size scales (e.g. micro- and nano-scale)

Using techniques such as photolithography, microcontact printing, microfluidic patterning, electrospinning and self-assembly, 3D topographical features of tailored geometry, roughness and orientation, complemented by the desired spatial resolution at micron and submicron scales, can be realized on material surfaces.

The approach used in the present study involves the fabrication of microconical structured silicon surfaces by ultra-short pulsed laser processing. It has been shown in previous work of the group that when flat silicon is irradiated by ultra-short pulsed laser microconical features arise. The resulting surfaces exhibit remarkable wetting and optical surfaces [Stratakis, E. I., & Zorba, V. 2010¹]. Thus, we wanted to see how these properties of the micropatterned substrates are influenced by the incorporation of a nanoparticles coating. In other words, the first aim of the present thesis was to study what are the respective properties of the hierarchical nano-micro-patterned substrates.

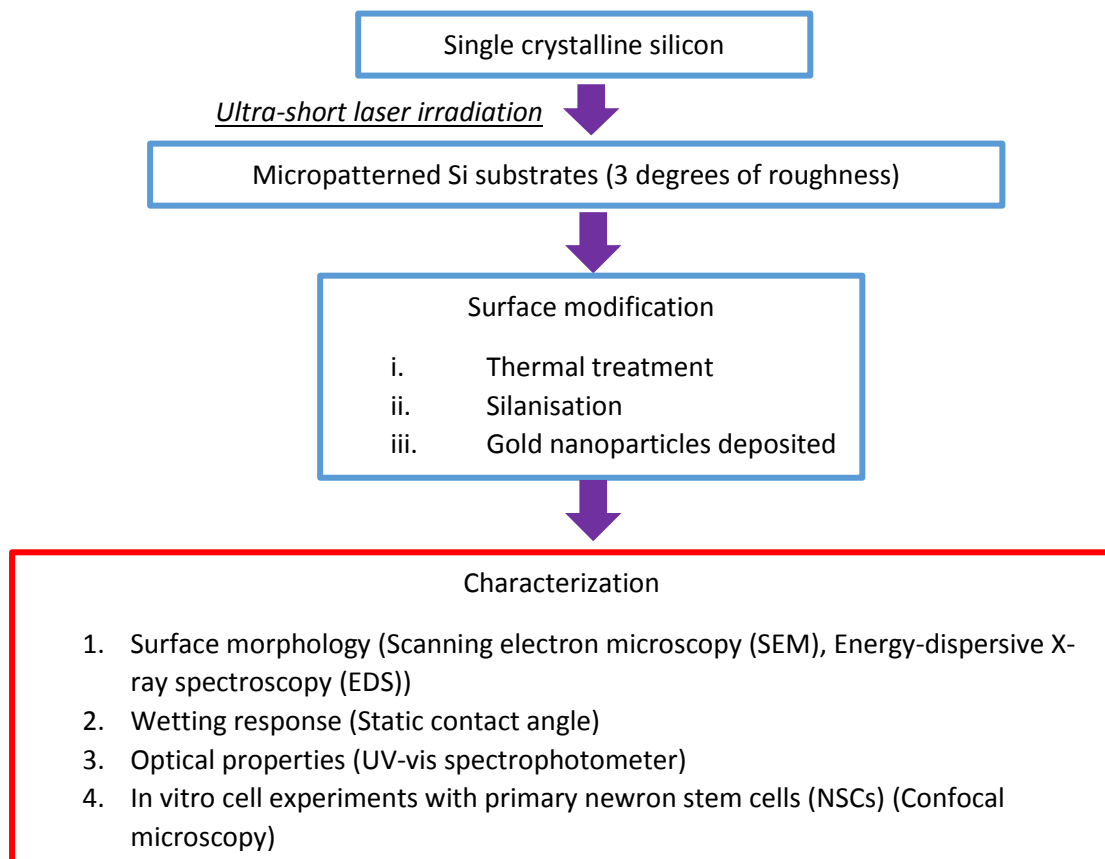
Furthermore, we wanted to see how do the cells respond to this dual scale roughness. Previous work of the group has shown that fibroblasts [A.Ranella et al.2010²⁰]and primary neurons and neuroglial cells [C. Simitzi et al.¹²] can grow on the micropatterned silicon substrates. Specifically

It was shown that controlling surface roughness and wettability of the micropatterned Si substrates, fibroblast cell adhesion could be tuned²⁰. Furthermore, it was shown that both Schwann cells and axons of sympathetic neurons could grow on the micropatterned silicon substrates exhibiting a differential orientation based on the type

of the substrate roughness [C. Simitzi 2015¹²]. To this respect, the second aim of the present thesis was to investigate how a hierarchical silicon surface could influence the cell growth. For that reason, neural stem cells have been used.

2.2 Flow sheet

Figure 2.1 illustrates the flow sheet of the experimental design of the present thesis.



3 Experimental part : Materials & methods

3.1 Fabrication of micropatterned silicon surfaces via ultrashort – pulsed laser

3.1.1 Laser system

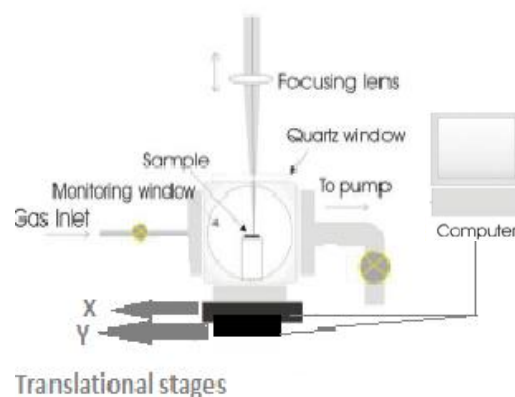
Ti:Sapphire laser system is a high repetition rate femtosecond laser system based on chirped pulse amplification (CPA) technique, which uses directly diode-pumped Yb:KGW (ytterbium doped potassium gadolinium tungstate) crystal as active medium. Automated second/third harmonic module for the Ti:Sapphire laser system offers the possibility to choose between three laser wavelengths (1030nm , 515nm and 343nm) by sending a command via computer (USB) or Remote Control Module (RCM). The switching between wavelengths in harmonics module is implemented by means of switchable mirrors which are controlled by two servo motors. The fundamental emission from the laser is directed through a periscope of two mirrors to the output of the harmonics module. The polarization of the output at 1030nm is horizontal.

3.1.2 Experimental procedure

Single crystal n-type Silicon (1 0 0) wafers microstructuring took place in a vacuum chamber evacuated down to a residual pressure of $\sim 10^{-2}$ mbar by means of a vacuum pump. A micro valve system attached to the chamber enabled a precise backfilling of an ambient gas (SF_6). The pressure of the backfilling gas was measured with a needle gauge. The laser fluence was varied by using a filter. The laser beam entered the chamber through a quartz entrance window, while the irradiation process could be monitored through a plexiglas window, which was laterally mounted on the vacuum chamber.

The processing chamber was placed on a computer driven high precision X-Y translational stage with spatial resolution of 1 μm allowing sample displacement with regard to the laser beam up to 10000 μm (Figure 3.1).

The laser fluence used in these experiments was in the range 0.17–0.78 J/cm^2 , in constant wavelength to 1030nm, repetition rate 1kHz and pulse duration 180fs.



3.1.3 Sample preparation

Single crystal n-type Silicon (1 0 0) wafers, of thickness 300-750 +/- 25 μm thickness, were cut in square shape by using a pen-diamond, in various sizes, depending on the micro-structured surface size under study, each time. Substrates were first immersed in a vial with ethanol, and left in ultrasound for 2 minutes and then dried with nitrogen gas.

3.1.4 Thermal oxidation of the substrates

Before thermal treatment, Si substrates immersed in aqueous solution of hydrofluoric acid (HF) with a concentration of 30% for 1 hour. Then dried with nitrogen gas.

Flat and micropatterned Si substrates of all types of roughness were subjected to dry thermal oxidation in a ceramic tube furnace at 1000⁰C for 90 minutes, with ramp rate 20⁰C/minute (Figure 3.2). The substrates were further processed to characterization and deposition of the gold nanoparticles.

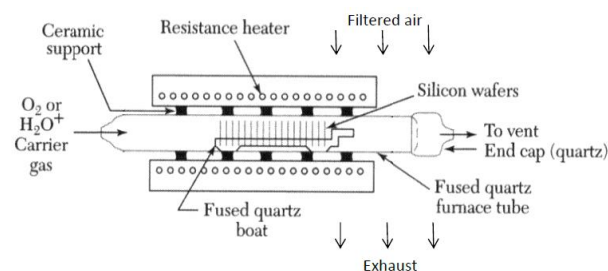


Figure 3.2: Schematic cross section of resistance-heated oxidation furnace [E.H. Nicollins and J.R. Brews, 1952¹²⁹]

3.2 Gold nanoparticles used

Colloidal gold nanoparticles (AuNPs), of spherical size and two diameters (i.e. 7 & 13 nm) have been used for the fabrication of the hierarchical micro-nano substrates. The gold nanoparticles carried the following functionalities: i) the oligopeptides CALNN or CALNN-RGD, and small organic moieties, including the stabilizer citrate and the 4-dimethylaminopyridine (DMAP) (Figure 3.1a). All four types of gold nanoparticles were in aqueous solution.

For the deposition of AuNPs on the microstructured silicon substrates, manufactured gold nanoparticle solutions, which proportionally diluted either in nanopure water or in

pure ethanol. Figure 3.1 shows the chemical composition and the nomenclatures of the functional groups of AuNPs. Table 3.1 shows the proportions of AuNPs solutions and their sizes.

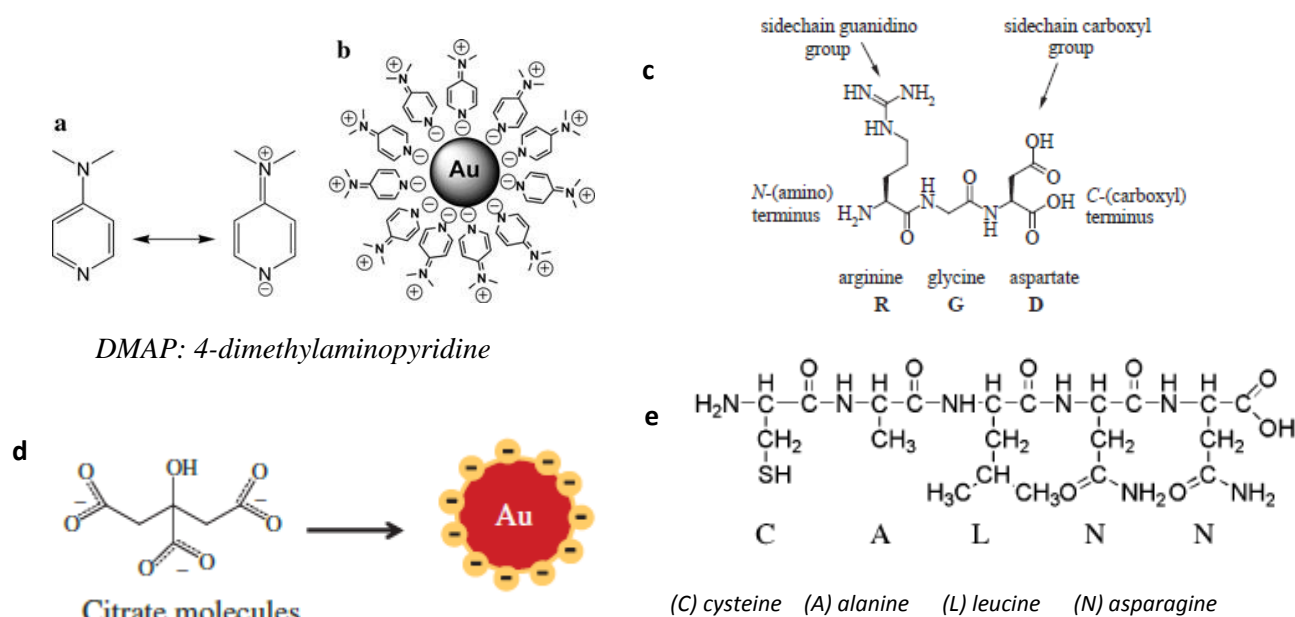


Figure 3.1: Chemical structures of functional groups of AuNPs. Resonance of the DMAP molecule (a) and schematic representation of a DMAP-Au NPs (b) [Biver, T et al., 2012¹²⁵], RGD sequence, its molecular formula and nomenclature (c) [Hersel et al., 2013¹²⁶], schematic representation of AuNP formulation by one phase system by citrate reduction (Citrate-AuNP) (d) [Remant Bahadur et al., 2014¹²⁷], pentapeptide CALNN structure [Lévy et al., 2004¹²⁸].

Table 3.1: Proportions of AuNPs solutions and AuNPs' diameters.

<i>AuNP type</i>	Diameter (nm)	Dilute solvent
<i>DMAP</i>	7	30% nanopure water
<i>Citrate</i>	13	30% pure ethanol
<i>RGD</i>	13	40% pure ethanol
<i>CALNN</i>	13	40% pure ethanol

*AuNPs synthesized from as.prof. Antonios Kanaras research group, at University of Southampton, United Kingdom, Laboratory for Inorganic Colloidal Nanocrystals and Applications.

3.3 Deposition of gold nanoparticles onto the microstructured silicon surfaces

In order to deposit the gold nanoparticles onto the microstructured silicon surfaces, the micropatterned silicon substrates had to be activated and functionalized, i.e. to

create surface functional groups, which tend to form covalent bonds with the gold nanoparticles. The activation of the surfaces has been performed via the piranha solution (i.e. a mixture of sulfuric acid and hydrogen peroxide, v/v: 3:1). Piranha solutions are strong oxidizers and used to remove organic residues from substrates. The functionalization of the surfaces was in turn performed with a Sulfur terminated silane, the (3-Mercaptopropyl)trimethoxysilane (MPTMS).

Micropatterned silicon substrates have been thermally oxidized at 1000°C for 30 min in air. This treatment results in a conformal silicon oxide layer [REF]. Substrates have been in turn functionalized with (3-Mercaptopropyl)trimethoxysilane (MPTMS). For that, substrates have been activated via immersion in Piranha solution [i.e. H₂SO₄: H₂O₂=3:1 (v/v)] for 30min at room temperature (RT), followed by thorough rinsing with nanopure water and drying with Nitrogen. Then, substrates have been immersed in MPTMS solution in dry toluene [1.85% (v/v)] for 3hrs at RT followed by rinsing in toluene and ethanol (two times), drying with nitrogen and thermal annealing at 100°C for 30min.

For the binding of the nanoparticles onto the MPTMS-functionalized surfaces, drop deposition has been followed. A drop of 20 µl has been deposited onto the MPTMS-functionalized micropatterned silicon surfaces, let be evaporated for 16hrs, followed by a thorough rinse with nanopure water to remove the nanoparticles that were not immobilized. For the *in vitro* experiments with cells the RGD-terminated gold nanoparticles have been used (RGD-NP micropatterned substrates).

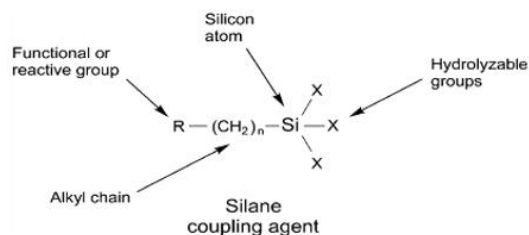


Figure 3.3: The general structure of a silane coupling agent includes a functional group or reactive group at the end of an organic spacer [Hermanson Greg T.¹³⁰].

There are several silanes which offer functionalization on surfaces. To present experiments used MPTMS (3-Mercaptopropyl)trimethoxysilane) (Figure 3.4).

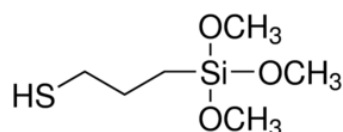


Figure 3.4: Chemical composition of MPTMS, with thiol as functional group (SH) (adopted by Sigma Aldrich)

To effect the binding of the silane, MPTMS diluted in dry toluene (organic solvent), an substrate immersed in for 2:30 hours, because the method of silanation, which uses organic solvent is suitable for highly reactive silane derivatives, such as MPTMS. Also, this method is convenient to use for the functionalization of metallic nanoparticles, having the requisite $-OH$ end groups¹³⁰. Figure 3.5 shows the final morphology of the functionalized silicon substrates.

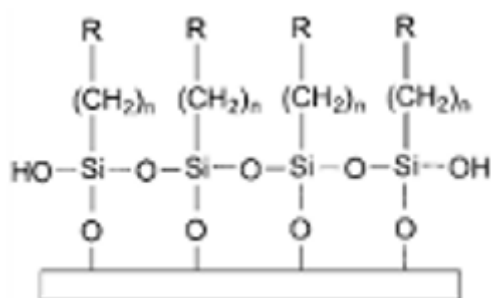


Figure 3.5: Covalent bond formation and coating of surfaces with functional silanes¹³⁰.

After this experimental step, the substrates characterized via static contact angle measurements (section 4.2.4).

3.4 Characterization of the micro/nano patterned silicon surfaces

3.4.1 Scanning electron microscopy (SEM)

3.4.1.1 Technique

Scanning electron microscope (SEM) is a type of microscope that uses an electron beam to illuminate the specimen and produce a magnified image. The beam of electrons is produced at the top of the microscope (electron gun), follows a vertical path through the column of the microscope, makes its way through electromagnetic lenses which focus and directs the beam down towards the sample. The beam passes through pairs of scanning coils or pairs of deflector plates in the electron column, typically in the final lens, which deflect the beam in the x and y axes so that it scans over a rectangular area of the sample surface. The focused beam of high-energy electrons generates a variety of signals at the surface of solid specimens. The signals that derive from electron-sample interactions reveal information about the sample, including external morphology or surface topography, chemical composition and other properties, such as electrical conductivity. The spatial resolution of SEM depends on the size of the electron spot, which in turn depends on both the wavelength of the electrons and the electron-optical system which produces the scanning beam. Depending on the instrument, the resolution ranges between 1 and 20 nm. [N. Cortadellas et al., 2012¹³¹].

3.4.1.2 Experimental process

Micro-structured surfaces were morphologically characterized by scanning electron microscopy (SEM). SEM was performed on a JEOL 7000 field emission scanning electron microscope with an acceleration voltage of 15 kV.

3.4.2 Energy-dispersive X-ray spectroscopy (EDS)

3.4.2.1 Technique

As its name suggests, X-ray microanalysis involves using X-rays to study very small scales, down to the micro or even nano- and atomic levels. In general terms, X-ray microanalysis relies on the ability to detect X-rays generated when a specimen is bombarded with high-energy electrons in an electron microscope, with the method used to detect the X-rays defining the exact form of the technique. The X-rays can be

detected using a crystal spectrometer fitted with a diffracting crystal to choose the wavelength of interest, or they can be detected with an energy-dispersive spectrometer, which can separate X-rays with different energy levels. An EDS system include: a semiconductor detector, and a main amplifier that provides further amplification and a fast pulse inspection function. All of this can be fully controlled with a computer-assisted system. When the electron beam hits the sample, there is a high probability that an X-ray will be generated. The resulting X-ray escapes the sample and hits the detector. This short-lived current is then converted into a voltage pulse with an amplitude reflecting the energy of the detected X-ray. Finally, this voltage pulse is converted to a digital signal [John Wiley & Sons ,2015¹³²]

3.4.2.2 Experimental process

In our case, EDS spectrums, ensured via SEM. So the experimental process is the same as in section 3.4.1.2.

3.4.3 Wetting response by static contact angle

3.4.3.1 Technique

Contact angle analysis involves measuring the angle of contact (θ) between a liquid and a surface. The phenomenon of contact angle can be explained as a balance between the cohesive force among the liquid molecules and the adhesive force between the surface and the liquid molecules. When a drop of liquid is placed on a surface, it will spread to reach a force equilibrium, in which the sum of the interfacial tensions in the plane of the surface is zero: $\cos\theta = (\gamma_{SV} - \gamma_{SL}) / \gamma_{LV}$, where γ_{SV} represents the solid-vapor surface tension, γ_{SL} represents the liquid-solid surface tension, and γ_{LV} represents the liquid-vapor surface tension. The energetics at each of the interfaces causes the droplet (usually water) to assume a particular shape (different degree of spreading). Calculations based on measured contact angle values yield an important parameter—the solid surface tension, which quantifies the wetting characteristics of a solid material. Depending on the contact angle value, a surface can be characterized as hydrophilic ($<90^\circ$) or hydrophobic ($>90^\circ$) (Figure 3.6). There are a number of ways to measure the contact angle including sessile drop, captive air bubble method, capillary rise method. Contact angle analysis provides a first screening of material surface and gives an insight

into how the surface will interact with the external world. It indirectly measures surface energy, roughness, contamination, etc. and directly surface wettability. Wettability (or wetting response of a surface) is very critical in the early stages of many interfacial phenomena, such as cell – biomimetic surfaces interactions^{4,12,14,20}.

3.4.3.2 Experimental process

Static contact angle measurements were performed using an automated tension meter, using the sessile drop method. A 2-3 μl distilled, deionized millipore water droplet was gently positioned on the surface, using a microsyringe, and images were captured to measure the angle formed at the liquid– solid interface. The surfaces being measured had a surface area of at least $5 \times 5 \text{ mm}^2$. All experiments were carried out under

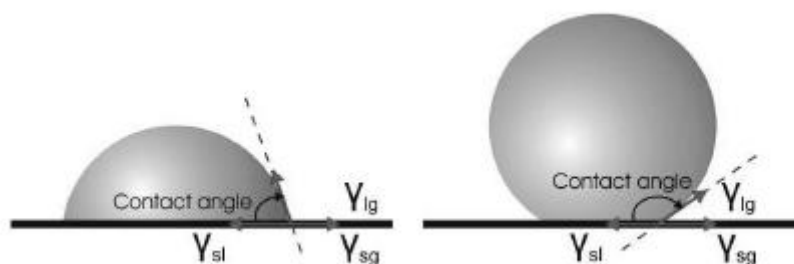


Figure 3.6: A sessile liquid drop on (a) a hydrophilic and (b) a hydrophobic surface [V. Zorba,2007¹³³] normal atmospheric conditions and at an ambient temperature of 20°C . The mean value was calculated from at least three individual measurements. Successive measurements were reproducible within $\pm 1^{\circ}$.

3.4.4 Ellipsometry

3.4.4.1 Technique

Ellipsometry is an optical measurement technique to measure the transmission and reflection properties after light is incident on some material. The name ellipsometry comes from the fact that most often light becomes elliptically polarized after passing through the medium. In ellipsometry change in polarization state is studied to infer properties of medium [Chauhan, Sourabh Singh,2014¹³⁷]. When a monochromatic, plane light wave is directed at a surface at oblique incidence, the plane of incidence is defined as a plane perpendicular to the surface and containing the vector which points in the direction of

propagation of the light wave. Figure 3.7 illustrates how a beam of linearly polarized light incident, on a film-covered surface is reflected (r).

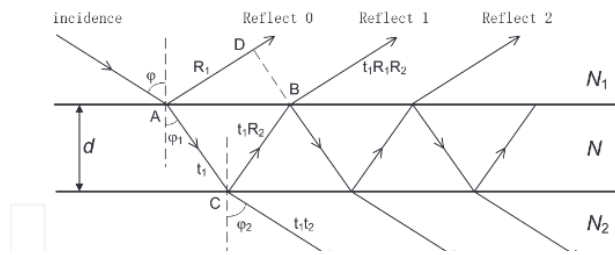


Figure 3.7: Reflection and transmission of polarized light from a transparent film covered surface, where d is the thickness of the film¹³⁴.

3.4.4.2 Experimental process

In our case, the measurements for the thickness of silicon oxide made by, the ellipsometer 439, rudolph instrments company. The arrangement of optic comprising shown in Figure 3.8.

Beam with wavelength $\lambda = 632.8$ nm produces a laser He-Ne and vertically passes initially through a linear polarizer, and subsequently, by a delay chip phase $\pi/2$ (compensator). The resulting package, incident on the sample at an angle, and regulated by turning the axle, which includes the laser, the polarizer and the compensator. The sample is placed on a regulated basis. The reflected beam passes by a diaphragm and

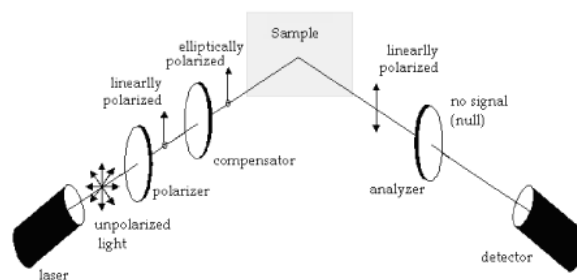


Figure 3.8: Schematic diagram of ellipsometry device [Débora Gonçalves and Eugene A. Irene, 2002¹³⁵].

then by another linear polarizer (the analyzer), resulting in the light detector (photomultiplier). The light entering the detector is limited by using an interference filter. The polarizer and the analyzer revolve around the direction of light propagation, and on the side supplied evidence (degrees) for the angle between the optical axis with the components of the passing wave. The compensator is located permanently at a 45° to produce elliptical polarized wave [R.M.A. Azzam and N.M.Bashara,1977¹³⁶].

Simultaneously adjusting the angle polarizer - analyzer achieves the minimum intensity of the beam reaching the detector, and note the angles of analyzer and polarizer. Then, measure the complementary angle rotating the polarizer, and the opposite angle of the analyzer, until reach the minimum intensity of the beam. Through a number of equations can be calculated the film thickness.

3.4.5 Optical reflectance measurements

3.4.5.1 Technique

A common way to measure reflectance and transmittance from strongly scattering materials is to use an integrating sphere; a hollow sphere coated internally with a matte finish, diffusing type material. In this way the light that enters the sphere can be scattered uniformly around its interior through multiple reflections, before it is detected. The measurements were performed using a UV/VIS/IR spectrophotometer equipped with an integrating sphere (PerkinElmer Lambda-950). An all-reflecting, double monochromator optical system was used, for the UV/Vis and NIR range. The two radiation sources, a deuterium lamp and a halogen lamp covered the working range of the spectrometer.

3.4.5.2 Experimental process

Initially, ensure that the sample is clean, and the radiation beam is incident only on the sample area we want to measure. Then, substrates placed on a black cardboard (it absorbs radiation) and fixed with a tape.

3.5 In vitro experiments with NSCs on the micro-nano patterned substrates

3.5.1 Substrate preparation

The substrates, before used for cell cultures, sterilized by precipitation in 100% ethanol for 30 minutes and then rinsed with sterile double deionized water.

3.5.2 Cell culture

NSCs isolated and expanded from the cortices of mouse embryos in the 14th embryonic day (E14) using the neurosphere assay. Tissue was isolated and mechanically chopped and then processed to a single-cell suspension. The NSCs were cultured in the presence of epidermal growth (epidermal growth factor, EGF 20mg/ml) and fibroblast growth factor-2 (FGF- 2, 20 ng/ml), heparin (5 µg/ml) and supplemented with N2 12%) which allows the formation of spherical aggregates (neurospheres) after 5-7 days consisting of multipotent stem cells. The cultures maintained at 37°C in a humidified incubator . Every 4-5 days, the spheres passaged, re-suspended into single cells and then seeded onto the surfaces and allowed to grow for 5 and/or 7 days.

3.5.3 Characterization of cellular response

3.5.3.1 Fluorescence microscopy

3.5.3.1.1 Technique

Fluorescence results when molecules called fluorophores absorb light, which briefly raises their energy level to an excited state. They emit fluorescent light as they decay from this excited state. In general, a fluorophore excited by high frequency light (wavelengths in the ultraviolet, violet, or blue region of the spectrum), and emit light at slightly lower frequencies (wavelengths in the green or red region of the spectrum). Fluorophores come in a range of colors that span the visible spectrum (traditionally red, green, and blue fluorophores are used) [Ghiran and Ionita C.,2011¹³⁸].

Fluorescence microscope uses ultra violet light that excites fluorescent molecules in the sample of interest. The microscope uses a dichroic mirror that reflects light shorter than a certain wavelength but transmits light of longer wavelength. Thus, the light from the main source is reflected and passes through the objective to the sample, while the longer-wavelength light from the fluorescing specimen passes through both the objective and the dichroic mirror [Semwogerere et al.,2005¹³⁹] (Figure 3.9).

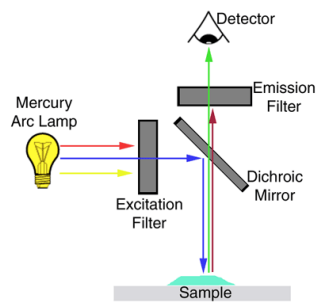


Figure 3.9: Fluorescent filter setup¹³⁸.

3.6.3.1.2 Experimental process

The morphology and proliferation of NSCs on the fabricated biomimetic substrates was investigated using immunocytochemistry (evaporation of antibodies labeled with fluorescent dyes) for the expression of Nestin, a specific cytoplasmic stemness marker and the proliferative potential was determined by the ki67 marker which was detected in the nuclei of the proliferating NSCs. The cells imaged at confocal scanning microscope Leica SP8.

4 Experimental part : Results

4.1 Morphological characterization of artificially structured silicon surfaces

In order to study the effect of platform architecture on primary neural stem cell adhesion and proliferation, ultra-short pulsed laser structuring was applied on crystalline silicon (Si) wafers. This technique offers the advantage of patterning Si surfaces with periodic arrays of topographical features of microscale size, while offering high accuracy and reproducibility¹⁶. By varying the laser energy per unit area (fluence), substrates with different roughness have been obtained. At low laser fluence values, the irradiated surfaces comprised submicron-sized ripples, while at increased laser energy, quasi-periodical arrays of conical microstructures (denoted as microcones -MCs- or spikes) were formed (Figure 4.1).

More specifically, we examined the effect of the different laser fluences in a range of 0,17 to 0,78 (J/cm²), which means different laser beam intensity, as well as the effect reactive gas pressure (SF₆). The parameters that have been kept constant was the laser wavelength (λ) at 1026 nm, the repetition rate (f) at 1kHz, the pulse duration (τ) at 180fs and the irradiation step axes (x,y).

4.1.1 Micropatterned silicon surfaces

In this section we study the formation of microstructures on the surface of Si, by using the Ti:Sapphire laser system ($\lambda=1026$ nm, $\tau=180$ fs), operating at a repetition rate of 1 kHz and SF₆ gas pressure at 650 mbar. The effect of the laser processing parameters on the morphology and geometrical characteristics of the fabricated structures was investigated via scanning electron microscopy (SEM). As shown in Figure 4.1, upon increasing laser fluence, conical microstructuring is promoted on the Si surface, with structures becoming more pronounced and spatially separated. In this case fluences varied from 0,17 J/cm² to 0,78 J/cm².

4.1.1.1 The effect of laser fluence

We chose three different topographies as low (0.17J/cm²), medium (0.35J/cm²) and high (0.57J/cm²) roughness (Figure 4.2) . As the laser fluence increased, spikes density (MCs number/cm²) and interspike distance (μm) decreased. It has to be noted that, for all fluencies the direction of MCs is the same, and it is perpendicular to the beam polarization (or else to the electric field), (Figure 4.2C).

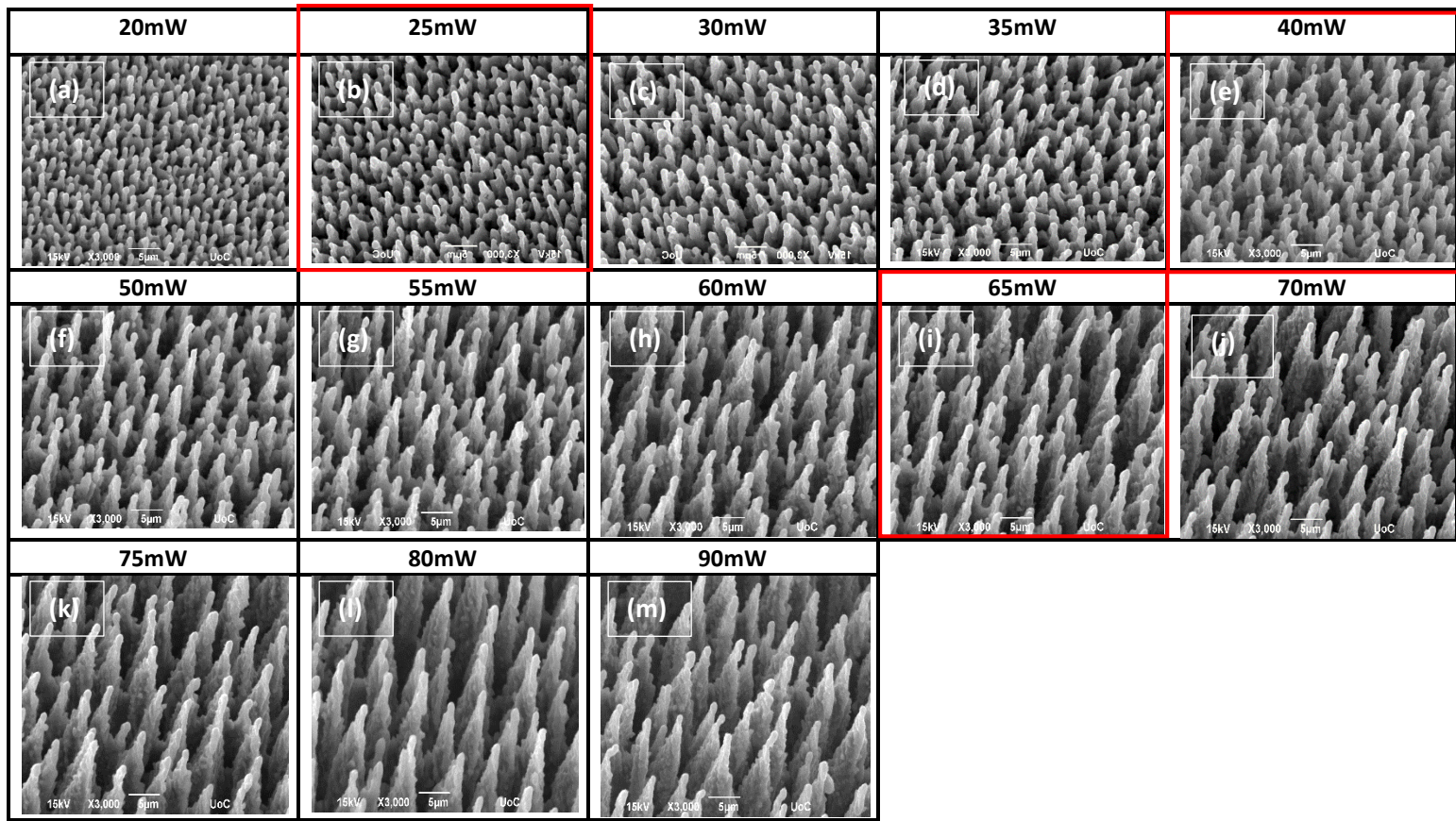


Figure 4.1 : Side SEM images of Si microstructures with increasing laser fluence (a to m). The effect of increasing laser power beam (mW) lead to fluences (a) 0.17 J/cm², (b) 0.22 J/cm², (c) 0.26 J/cm², (d) 0.30 J/cm², (e) 0.35 J/cm², (f) 0.43 J/cm², (g) 0.48 J/cm², (h) 0.52 J/cm², (i) 0.57 J/cm², (j) 0.61 J/cm², (k) 0.65 J/cm², (l) 0.70 J/cm², (m) 0.78 J/cm².

For further investigation, we chose three types of roughness (low, medium, high), as shown with red color, in Figure 4.1. As shown in Figure 4.2 for fluencies 0.22J/cm², 0.35 J/cm² and 0.57J/cm² (for low, medium, high roughness substrates respectively), MCs' density decreases with increasing laser fluence. Specifically its value ranges from 10⁶ to 10⁷/cm² (MCs density is 10.78±0.04, 6.80±0.10 and 4.69±0.04 on low, medium and high roughness substrates, respectively). While spike density was lower in the high roughness structures, the MCs height increased. More specifically, MCs height varied from 3.21 ± 0.48 µm in the low roughness structures to 13.81 ± 2.00 µm in the high roughness structures (Table 4.1). Also, the interspike distance increase, while the fluence and spikes height increase. More specifically, MCs distance varied from 3,51±0,35 µm in the low roughness structures to 7,2±1,7 µm.

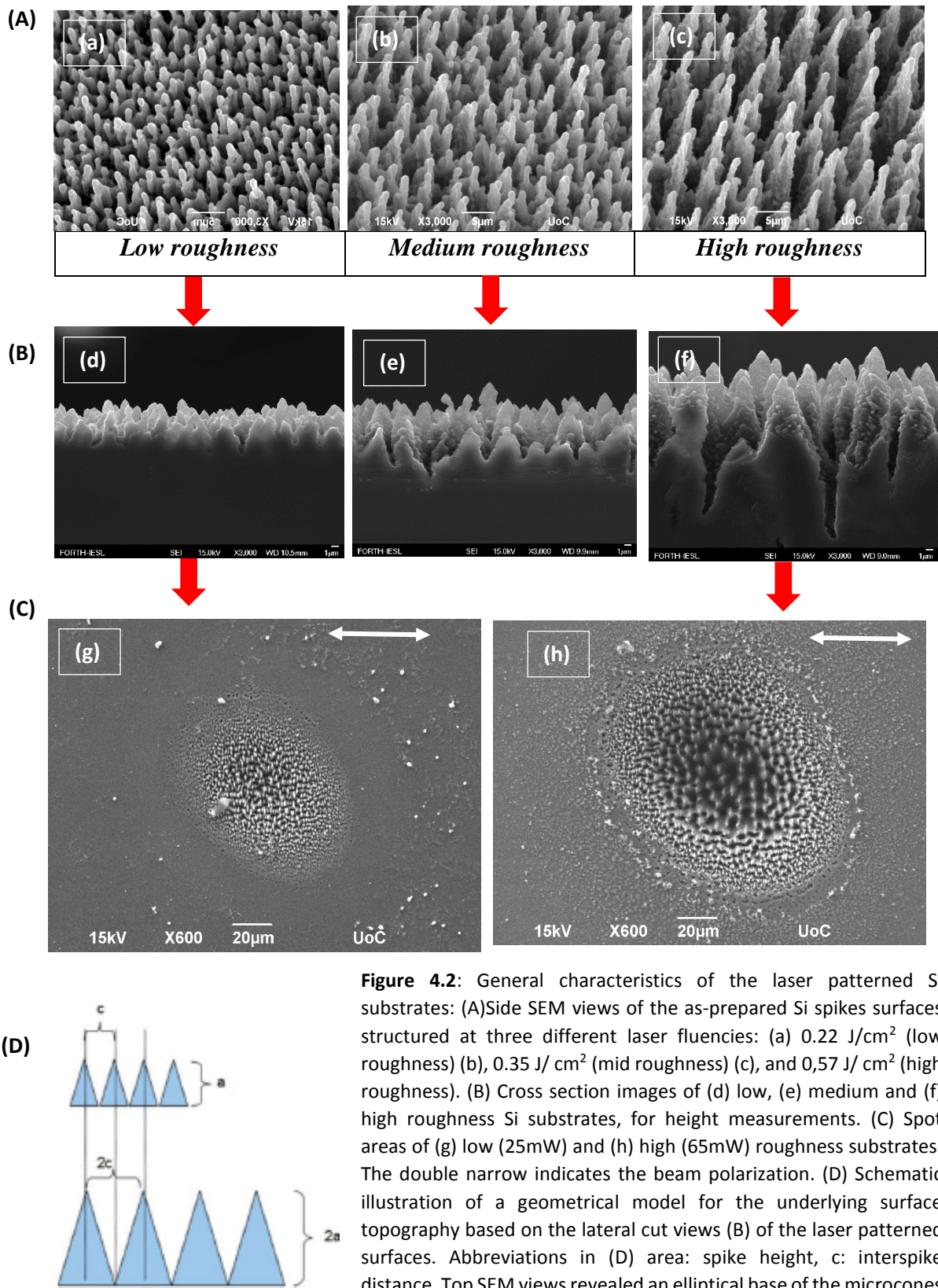


Figure 4.2: General characteristics of the laser patterned Si substrates: (A) Side SEM views of the as-prepared Si spikes surfaces structured at three different laser fluencies: (a) 0.22 J/cm² (low roughness) (b), 0.35 J/cm² (mid roughness) (c), and 0.57 J/cm² (high roughness). (B) Cross section images of (d) low, (e) medium and (f) high roughness Si substrates, for height measurements. (C) Spot areas of (g) low (25mW) and (h) high (65mW) roughness substrates. The double narrow indicates the beam polarization. (D) Schematic illustration of a geometrical model for the underlying surface topography based on the lateral cut views (B) of the laser patterned surfaces. Abbreviations in (D) area: spike height, c: interspike distance. Top SEM views revealed an elliptical base of the microcones which was more pronounced as the laser fluence/ surface roughness are increased.

Table 4.1: Geometrical characteristics of the different micropatterned Si substrates. *

Type of roughness	Density $D \pm \text{STDEV}$ (* $10^6/\text{cm}^2$)	Height, $a \pm \text{STDEV}$ (μm)	Interspike Distance, $c \pm \text{STDEV}$ (μm)	Fluence (J/cm^2)
<i>Low</i>	10.78 ± 0.04	3.21 ± 0.48	$3,51 \pm 0,35$	0.22
<i>Medium</i>	6.80 ± 0.10	4.51 ± 0.33	5.52 ± 0.80	0.35
<i>High</i>	4.69 ± 0.04	13.81 ± 2.00	$7,2 \pm 1,7$	0.57

* Geometrical characteristics of the different substrates used for this study, calculated out of the scanning electron microscopy (SEM) images with the aid of image processing software (ImageJ). The mean values were calculated from at least four individual measurements.

4.1.1.2 The effect of SF₆ gas

In this section we examine the effect of reactive gas (SF₆) on the morphology of microstructured Si substrates. The Si structures fabricated in vacuum were blunt, irregular and shorter than spikes fabricated in SF₆ environment (Figure 4.3). The reactive gas, plays a distinct role in the spikes fabrication process, since it determines the sharpness of the structures obtained (Figure 4.4). However they became more pronounced and with increasing ambient gas pressure (300-800 mbar) as shown in Figure 4.5. Increasing reactive gas pressure, with constant laser fluence and pulses number, acts favorably to the formation of second-lengthscale roughness on the surface of the cones.

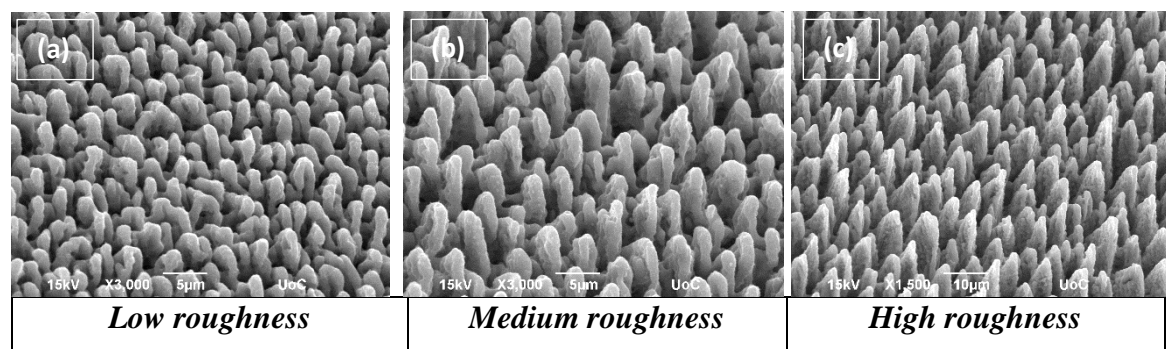


Figure 4.3: Sem images from Si micropatterend substrates for three different micro-topographies , (a)low, (b)medium and (c)high roughness (25mW, 40mW and 65mW respectively) , fabricated in vacuum environment. Comparing these structures to that of Figure 4.2A, wherein the laser parameters was the same, but the irradiation environment was in reactive gas atmosphere (SF₆) , we see that the structures prepared in vacumm are blank , opaque and irregular.

Figure 4.4 shows that the SF₆ has a dramatic effect on the height of MCs in low fluencies. More specifically, as shown in Table 4.1 height of fabricated MSCs in SF₆ gas atmosphere (650 mbar) is $3.21 \pm 0.48 \mu\text{m}$, $4.51 \pm 0.33 \mu\text{m}$ and $12.81 \pm 2.00 \mu\text{m}$ for low, medium and high roughness substrates respectively. Height measurements of MCs which fabricated in vacuum atmosphere varies from $0.31 \pm 0.5 \mu\text{m}$ in the low roughness structures to $13.01 \pm 2.00 \mu\text{m}$ in the high roughness structures.

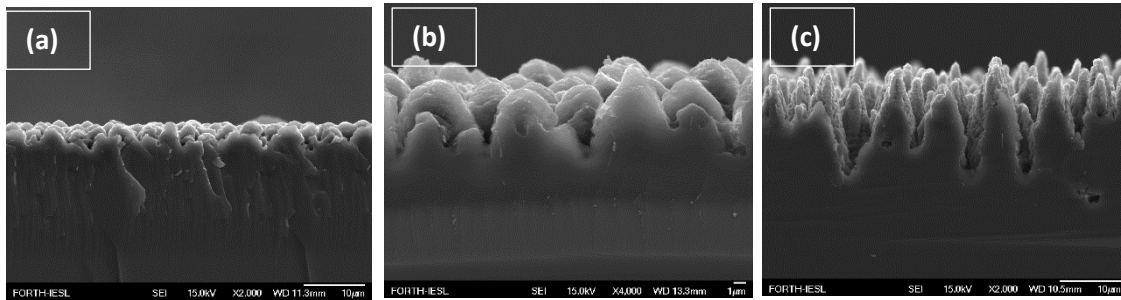


Figure 4.4: Cross section SEM images of (a) low, (b) medium and (c) high roughness Si micropatterned substrates fabricated in vacuum environment, for MCs height measurements. Respectively height is $2.10 \pm 0.5 \mu\text{m}$, $4.49 \pm 0.65 \mu\text{m}$ and $13.01 \pm 2.00 \mu\text{m}$.

Table 4.2: MCs height measurements for two different irradiation environments.

Type of roughness	Height, $a \pm \text{STDEV}$ (μm)	
	Vacuum	SF ₆ reactive gas
<i>Low</i>	$2.10 \pm 0,5$	3.21 ± 0.48
<i>Medium</i>	$4.19 \pm 0,65$	4.51 ± 0.33
<i>High</i>	13.01 ± 2.00	13.81 ± 2.00

Figure 4.5 shows cross-section SEM images from micro-structured Si surfaces irradiated in two different SF₆ gas pressures (300 & 800mbar). Double-scale roughness becomes more obvious.

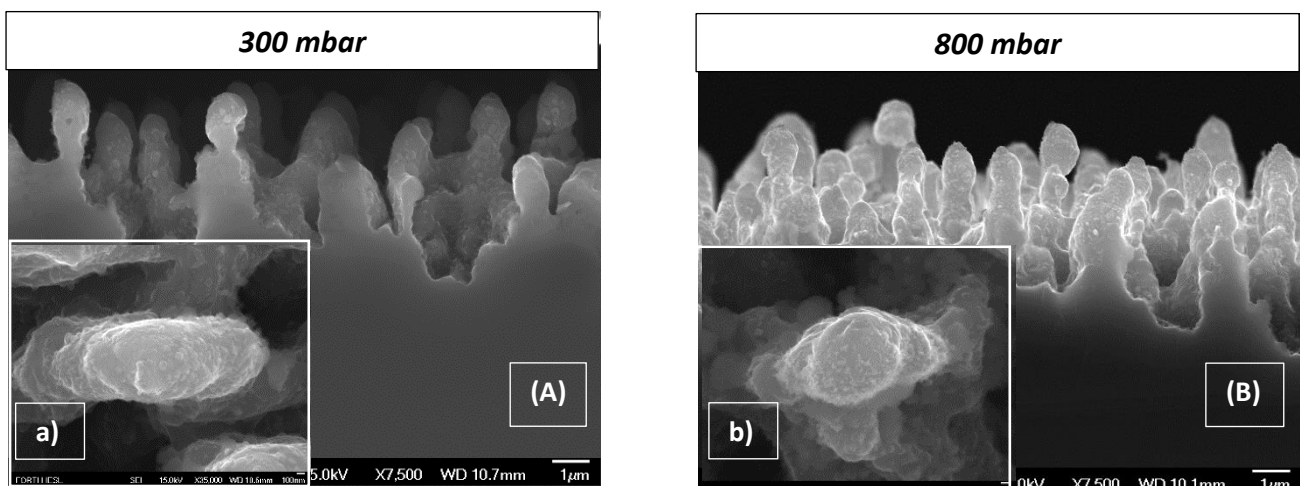


Figure 4.5: SEM images of Si low roughness micropatterned structures in (A) 300mbar SF₆ pressure and (B) 300mbar SF₆ pressure. MCs height is 2.43±0.53µm and 3.44±0.34µm respectively. a) Magnification to a single peak of (A), b) Magnification to a single peak of (B).

Table 4.3: Comparison of low roughness Si MCs height measurements for four different condition environments.

Type of roughness	Height, $a \pm \text{STDEV}$ (μm)				
	Environment condition	Vacuum	SF ₆ (300mbar)	SF ₆ (650mbar)	SF ₆ (800mbar)
Low roughness		2.10±0.5	2.43±0.53	3.21 ± 0.48	3.44±0.34

Elemental analysis with Energy-dispersive X-ray spectroscopy (EDS), showed that substrates that have been irradiated with SF₆ contained greater concentration of fluorine radicals, as shown in Figure 4.6.

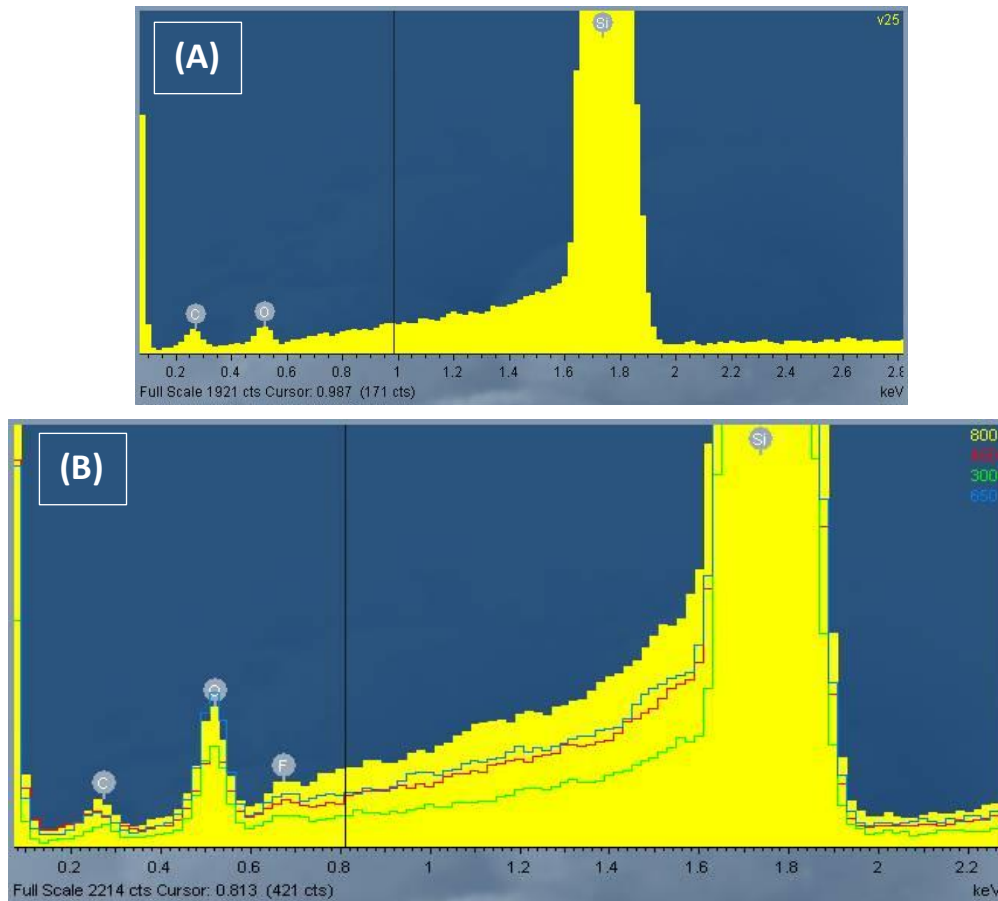


Figure 4.6: EDS spectrum of Si micropatterned substrates in different irradiation environment conditions. (A) Si substrates irradiated in vacuum, (B) Si substrates irradiated in different SF₆ gas pressures (yellow: 800mbar, blue: 650mbar, red: 450mbar, green: 300mbar). The amplification of the signal for the fluorine, reduces as the SF₆ gas pressure reduces.

4.1.2 Hierarchical micro/nano patterned surfaces

Scanning Electron Microscopy (SEM) confirmed the i) successful binding of the gold nanoparticles on the micro-structured substrates, ii) all the types of spherical gold nanoparticles, regardless of diameter and functional groups have a very nice and homogeneous distribution with single nanoparticles. This was independent of the substrates' roughness.

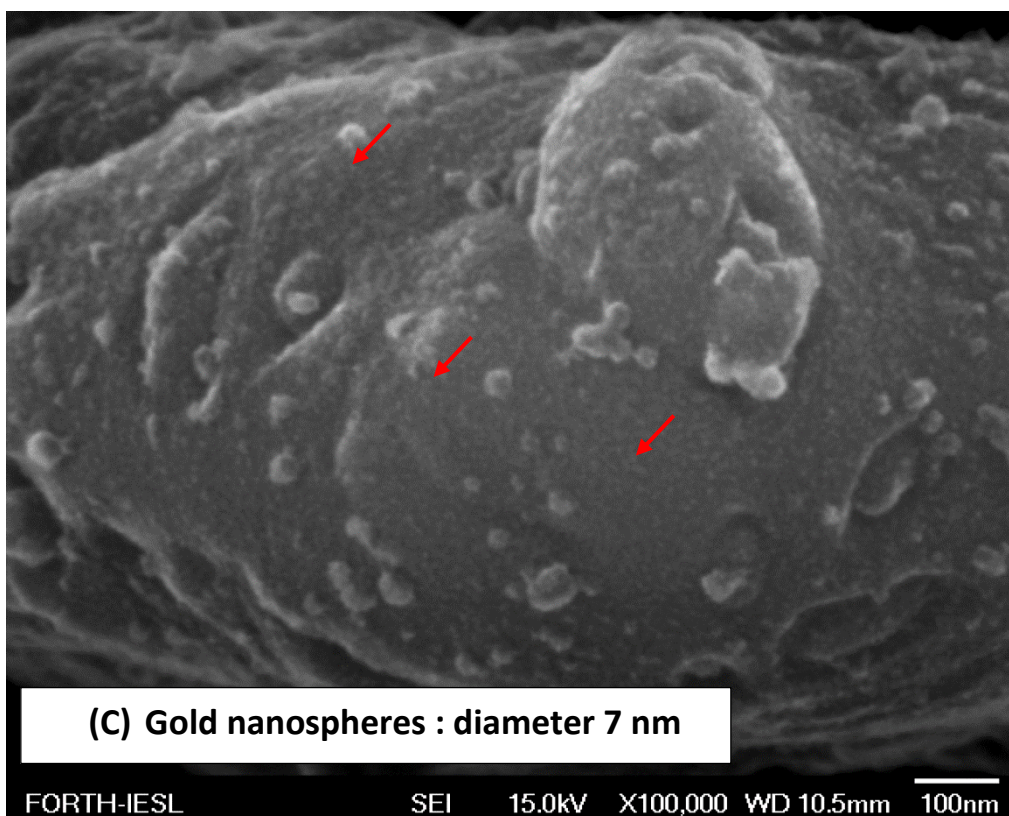
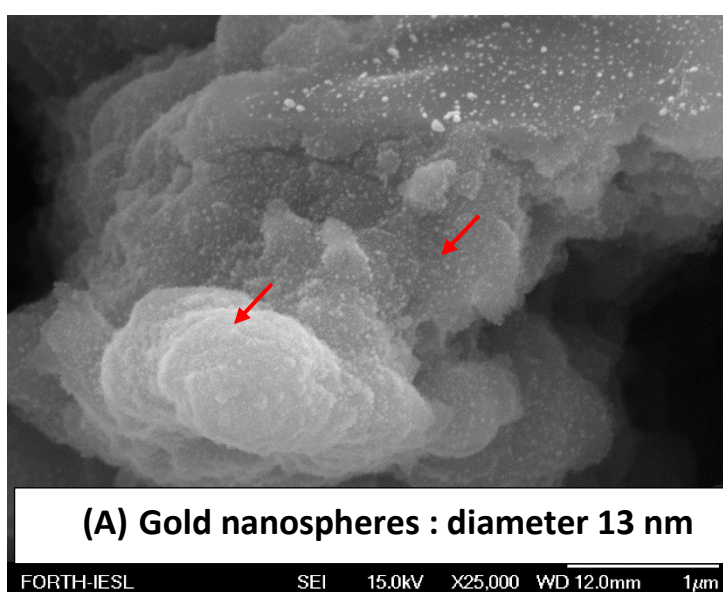
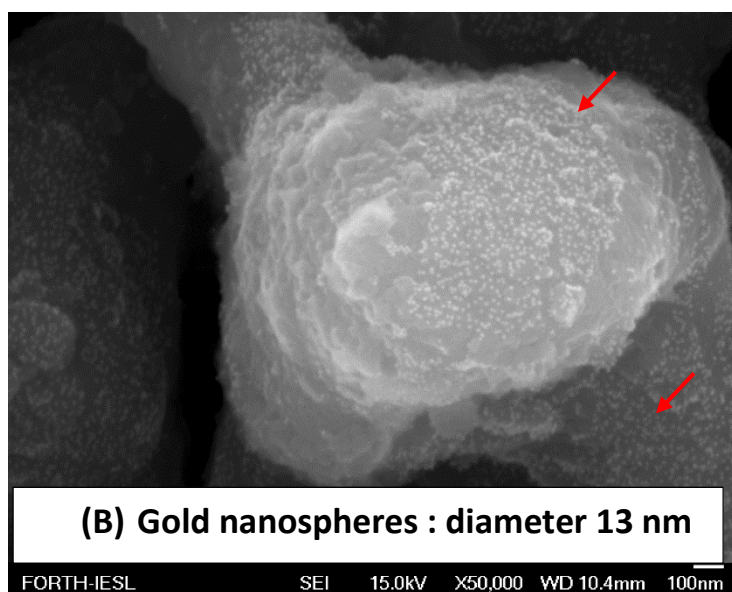


Figure 4.7: SEM images from hierarchical structured Si substrates with gold nanoparticles.

On *low roughness* (Fig 4.7B) Si substrate with evaporated gold nanospheres diameter:13nm. Magnification on a single peak.

On *high roughness* (Fig 4.7A) Si substrate with evaporated gold nanospheres diameter:13nm.

On *medium roughness* (Fig 4.7C) Si substrate with evaporated gold nanospheres diameter:7nm. High magnification on a single peak.

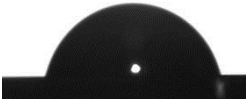
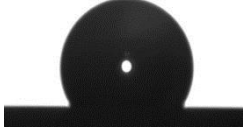
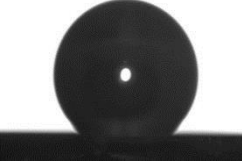
4.2 Wetting response of the micro-nanopatterned substrates

Controlling the wetting properties of artificial hierarchical surfaces, in this section we systematically study the wetting response of Si surfaces structured using the Ti:Sapphire fs laser source ($\lambda=1026$ nm, $\tau=180$ fs). In particular we examine the effect of roughness of micro-structured Si substrates, fabricated in both vacuum condition and in the presence of various SF₆ gas pressure. Also, we study: the effect of silicon oxide (SiO₂) thickness layer, the effect of silane and finally the effect of gold nanoparticles (AuNPs).

4.2.1 The effect of roughness

Laser structuring of Si in a reactive gas (SF₆) atmosphere, was shown to greatly enhance the overall roughness of its surface (section 4.1.1.2). In this section we study the effect of different surface morphologies on the wettability of processed Si. Textured Si surfaces have been fabricated by employing the same wavelength (1026 nm), with increasing the beam intensity for constant SF₆ gas pressure to 650 mbar. We chose three different topographies as low (0.22J/cm²), medium (0.35J/cm²) and high (0.57J/cm²) roughness (Figure 4.2A). Table 4.4 shows that as the fluence increases, surface become more hydrophobic (increase of static contact angle (C.A.)). The control substrates for the C.A. measurements, was the flat Si substrate. Micro-structured substrates are (5.5x5.5)mm , flat Si is (6.0x6.0)mm and water droplet's volume is stable to 3 μ l.

Table 4.4: Static contact angle measurements of increasing roughness micro-structured Si substrates.


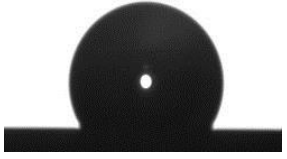

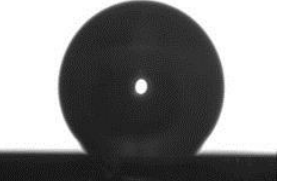
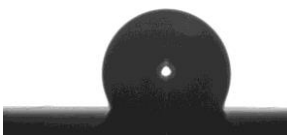
<i>Type of roughness</i>	<i>Flat Si</i>	<i>Low roughness</i>	<i>Medium roughness</i>	<i>High roughness</i>
				<i>Super-hydrophobic</i>
<i>C.A. ± STDEV (°)</i>	75±4.8	113±3.7	127±1.3	

4.2.2 The effect of irradiation environment

The role of irradiation environment is very important for surfaces' wetting properties. As we've already seen in section 4.1.1.2 , laser irradiation in vacuum environment leads to blank and irregular surface morphology of Si MCs (Figure 4.3), in contrast with the irradiation in the presence of reactive gas SF₆ which leads to more sharp surface morphology, by adding disorderly nano-roughness because of the fluorine radicals (Figure 4.2A). Also, by increasing the SF₆ gas pressure, increasing the MCs' height (Figure 4.5) and their nano-topography.

To investigate the effect of vacuum irradiation environment, have to compare the static contact angle measurements of this case, with the C.A. measurements of micro-structured Si substrates which irradiated in the presence of constant pressure SF₆ gas, with the same laser parameters (fluence, pulse duration). Micro-structured substrates' size is (5.5x5.5)mm , with stable droplet volume to 3μl. Table 4.5 shows the effect of two different environment conditions for the same laser parameters (fluence, pulse duration).

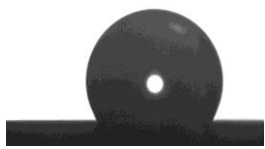
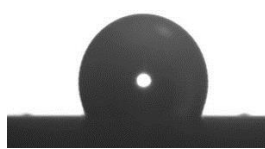


Table 4.5: Static contact angle measurements for irradiation environments.

<i>Type of roughness</i>	Irradiation environment	
	Vacuum	SF₆ (650 mbar)
<i>Low roughness</i>		
C.A. ± STDEV (°)	67±3.9	113±3.7
<i>Medium roughness</i>		
C.A. ± STDEV (°)	108±2.3	127±1.3
<i>High roughness</i>		<i>Super - hydrophobic</i>
C.A. ± STDEV (°)	110±2.1	

Note that the effect of the SF₆ gas is evident, as the difference in the C.A. measurements is pretty high. Also, low roughness substrates present even greater change, as the surface converts from hydrophilic to hydrophobic.

As was shown in section 4.1.1.2 irradiation at higher SF₆ gas pressure, leads to structures with more pronounced nano-roughness because of increased concentration of fluorine radicals on MCs' surface and to more sharp morphological surfaces. Table 4.6 shows the comparison of C.A. measurements between low roughness micro-structured substrates fabricated in constant SF₆ gas pressure (650 mbar) and low roughness micro-structured substrates fabricated in different gas pressures (300, 450 and 800 mbar).

Table 4.6: C.A. measurements of low roughness micro-structured Si substrates irradiated in different SF₆ gas pressure.

<i>Type of roughness</i>	SF₆ gas pressure			
<i>Low roughness</i>	300 mbar	450 mbar	650 mbar	800 mbar
				
C.A. ± STDEV (°)	110 ± 0.3	112 ± 2.3	113 ± 0.5	115 ± 0.3

Note that, for SF₆ gas pressure to 650 mbar, C.A. measurement identical with the corresponding C.A. measurement in Table 4.5. Also, our first morphological characterizations are confirmed. As the SF₆ gas pressure increase, thus increasing nano-roughness of the surface, so the surface becomes more hydrophobic.

4.2.3 The effect of SiO₂ thickness layer

In this section we study the effect of SiO₂ layer, fabricated via dry thermal oxidation for different thermal oxidation times. Higher oxidation time leads to thicker SiO₂ layer. Three different SiO₂ layers have been fabricated and characterized via ellipsometry technique (section 3.5.4), for three different oxidation times (Figure 4.8).

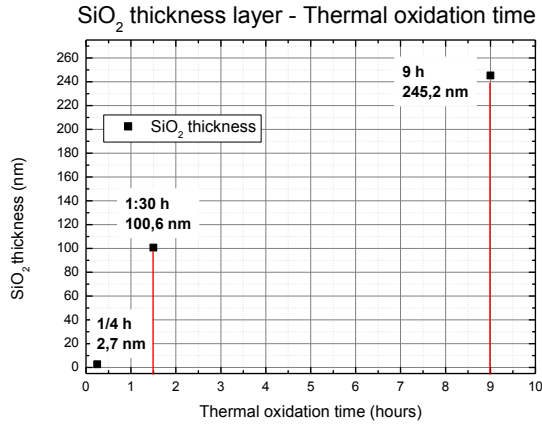
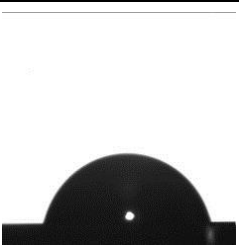
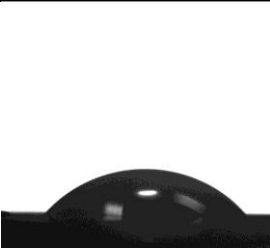
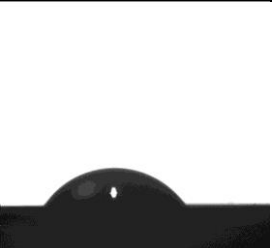
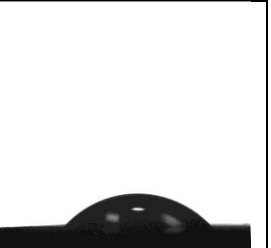




Figure 4.8 : SiO₂ thickness layer growth on flat Si substrates, measurements via ellipsometry, for three different oxidation times (15min, 1:30 hour and 9 hours), in 1000°C, with repetition rate 20°C/min.

C.A. measurements refer to high roughness micro-structured Si substrates (fluence: 0.57J/cm², SF₆:650mbar), which have been fabricated under the same irradiation conditions and oxidized by the same way. Table 4.7 shows the C.A. measurements from both flat (control) and micro-structured Si substrates before and after thermal oxidation in different times. Droplet volume is stable to 3µl and micro-structured substrates' size (5.5x5.5)mm.

Table 4.7: C.A. measurements for different SiO₂ thickness layer on both flat and high roughness micro-structured Si substrates.

<i>Type of roughness</i>	<i>Before thermal oxidation</i>	SiO₂ thickness layer (nm)		
		2.7 ±0.5	100.6±0.5	245.2±0.5
<i>Flat</i>				
	C.A. ± STDEV (°)	75 ± 4.8	46 ± 3.4	54 ± 4.4
<i>High roughness</i>	<i>Super-hydrophobic</i>	<i>Super-hydrophilic</i>		
			C.A. ± STDEV (°)	7 ± 1.2


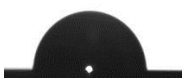

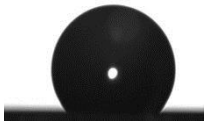
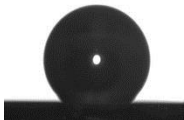
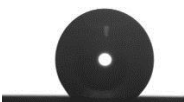
4.2.4 The effect of silane

Silanization process, refers to the binding of a chemical substance, namely MPTMS (section 3.3.3) on microstructured silicon surfaces, for successful binding of gold nanoparticles. MPTMS attach to the surface a negative charge, because of the sulfur cation.

Contact angle measurements, to study the effect of silanization, on flat and microstructured silicon substrates, refer to three micro-roughnes (low, medium and high), which have been fabricated with the same irradiation conditions and different beam intensity, in presence of pressure gas, stable at 650 mbar.

Table 4.8 shows the change of contact angle between silicon substrates without and with, silane. C.A. measurements refer to flat, as well as microstructured silicon substrates for three different micro-topographies.

Table 4.8: C.A. measurements of both flat and micro-structured silicon surfaces (low, medium and high roughness), before and after silanization.

<i>Type of roughness</i>	Before silanization	After silanization
<i>Flat</i>		
C.A. ± STDEV (°)	75±4.8	56±4.5
<i>Low</i>		
C.A. ± STDEV (°)	113±3.7	122±2.8
<i>Medium</i>		
C.A. ± STDEV (°)	127±1.3	133±1.2
<i>High</i>	<i>Super-hydrophobic</i>	<i>Super-hydrophobic</i>
C.A. ± STDEV (°)		

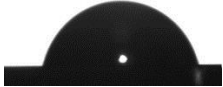
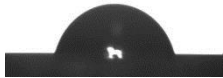
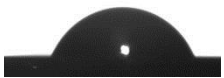


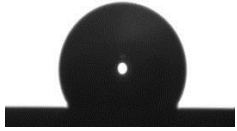
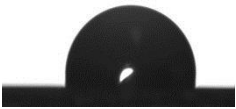
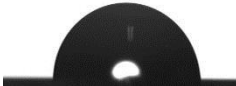


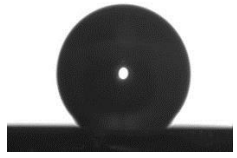





4.2.5 The effect of gold nanoparticles

In this section, we will study the wetting properties, of flat and microstructured silicon surfaces with three roughness (low, medium and high), with deposited gold nanoparticles, in spherical shape, with diameter of 7nm and 13 nm. Each of them, bears a different terminal functional group that imparts a different charge on the respective surface. In general gold nanoparticles, lead to hydrophilic surfaces.

Measurements of contact angle, referred to flat and microstructured silicon substrates fabricated with the same irradiation parameters, with and without gold nanoparticles. The types of gold nanoparticles deposited are: RGD-terminated AuNPs (13nm), DMAP-terminated AuNPs (7nm), Citrate-terminated AuNPs (13nm) and CALNN-terminated AuNPs (13nm), (more details in section 3.2).

Table 4.9 shows C.A. measurements of flat and micro-structured Si surfaces before and after AuNPs evaporation. Micro-structured substrates' size (5.5x5.5)mm, water droplet's volume was stable to 3 μ l and AuNPs drop volume was stable to 50 μ l for all the substrates (flat and micro-structured).

Table 4.9: Comparison of C.A. measurements of both flat and microstructured Si substrates without AuNPs, and with four different types of AuNPs.

<i>Type of roughness</i>	<i>Without AuNPs</i>	Type of AuNPs			
		RGD	CALNN	Citrate	DMAP
Flat					
<i>C.A. ± STDEV</i> (°)	75±4.8	72±3.2	66±2.6	64±2.4	38±1.4
Low					
<i>C.A. ± STDEV</i> (°)	113±3.7	94±3.9	80±2.7	79±2.8	7±1.2
Medium					
<i>C.A. ± STDEV</i> (°)	127±1.3	68±2.8	73±2.6	30±1.9	4±1.1
High	<u><i>Super-hydrophobic</i></u>	<i>Super-hydrophilic</i>		<i>Super-hydrophilic</i>	<i>Super-hydrophilic</i>
<i>C.A. ± STDEV</i> (°)			6±0.7		

Note that the greater C.A. change, refers to DMAP-AuNPs, which convert all the substrates to hydrophilic and more specifically super-hydrophylic.

4.3 Optical properties of micro/nano - patterned substrates

Si is a semiconductor commonly used in optoelectronic devices, such as solar cells and photodetector applications. Furthermore, the crystalline Si band gap (1.1 eV) makes its absorption and photoresponse to abruptly decrease for wavelengths typically above 1100 nm.

In particular, in this chapter we study the optical properties of laser structured Si. Using different beam intensity, we fabricate extended areas of Si spikes, with three different fluencies $0.22\text{J}/\text{cm}^2$, $0.35\text{ J}/\text{cm}^2$ and $0.57\text{J}/\text{cm}^2$ (for low, medium, high roughness substrates respectively), and measure the reflectance as a function of wavelength. Also we study the effect of silicon oxide layer (SiO_2) on the optical reflectance of both flat and fabricated structures, as well as their response to evaporated sphere gold nanoparticles (AuNPs), with diameter 7nm and 13nm.

4.3.1 The effect of roughness

We measure the total hemispherical reflectance (R) of our samples from 250 nm to 2500 nm using the spectrophotometer described in section 3.5.4, equipped with an integrating sphere. The samples fabricated with the same laser pulse duration (180fs), same wavelength (1026nm) and stable SF_6 gas pressure (650 mbar). Figure 4.9 shows the reflectance measurements of three bare Si microstructured substrates with different fluence ($0.22\text{J}/\text{cm}^2$, $0.35\text{ J}/\text{cm}^2$ and $0.57\text{J}/\text{cm}^2$).

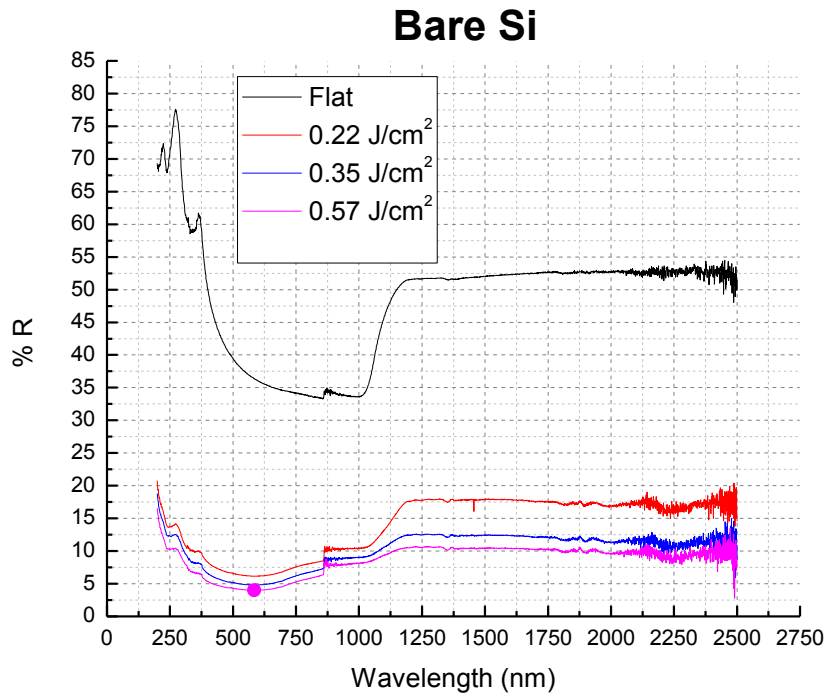


Figure 4.9: Reflectance of bare Si structured using the 180 fs pulse duration at 1026 nm laser source. The same measurements are shown for unstructured (flat), single crystalline Si for reference.

4.3.2 The effect of SiO₂ layer

Through the dry thermal oxidation, a silicon oxide layer (SiO₂ thickness: 100.6nm) grow on Si substrates (flat and micropatterned). Due to the different optical properties of SiO₂ (e.g. permeability, multiple reflections-refractions, low absorption [Ji, Yi-Qin et al., 2014¹¹]), a spectacular change of the reflective spectrum for bare microstructured silicon is observed.

Figure 4.10A shows the reflectance measurements of a flat crystalline Si substrate before (bare) and after (oxidized) dry thermal oxidation.

Figure 4.10B shows the reflectance measurements of a micro-structured Si substrate (low roughness – 0.22J/cm²), before (bare) and after oxidation (oxidized).

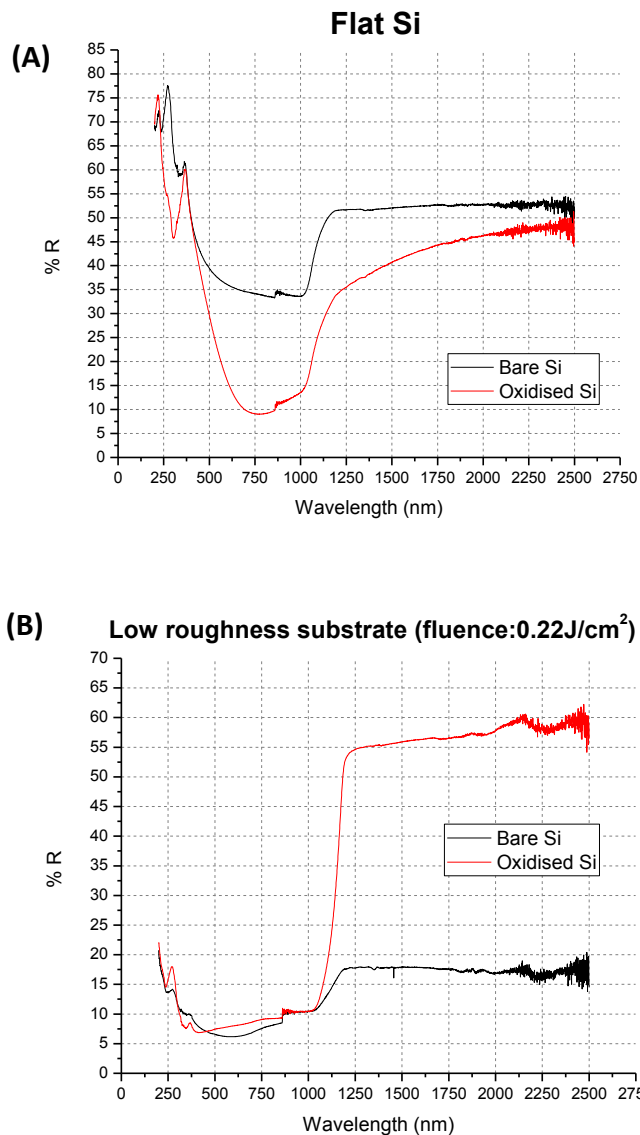


Figure 4.10

Reflectance measurements of non oxidized Si substrates (bare), flat and micro-structured (low and high roughness), in comparison with reflectance measurements of the same substrates after thermal oxidation.

(A) Reflectance measurements between flat bare Si substrate and flat oxidized Si substrate. Reduction (~25%) of reflectivity is observed, for the hole spectrum area.

(B) Reflectance measurements between micro-structured bare Si substrate (low roughness) and low roughness oxidized Si substrate. Phenomenon of reflectivity is reversed, compared to the flat silicon, as there is a tremendous increase of the reflectivity, as for the oxidized silicon (~40%), in the range of IR.

4.3.3 The effect of gold nanoparticles

Because of their unique optical properties, gold nanoparticles are under investigation for many applications. In this section we study the reflectance of a system with many “layers”, to investigate the effect of gold nanoparticles. The system structure is: Silicon (flat and micropatterned-low roughness) – SiO₂ layer growth – spherical AuNPs (13nm and 7nm diameter).

Figure 4.11A shows the effect of gold nanoparticles on reflectance spectrum of flat Si substrate.

Figure 4.11B shows the effect of gold nanoparticles on reflectance spectrum of low roughness micro-structured Si substrate.

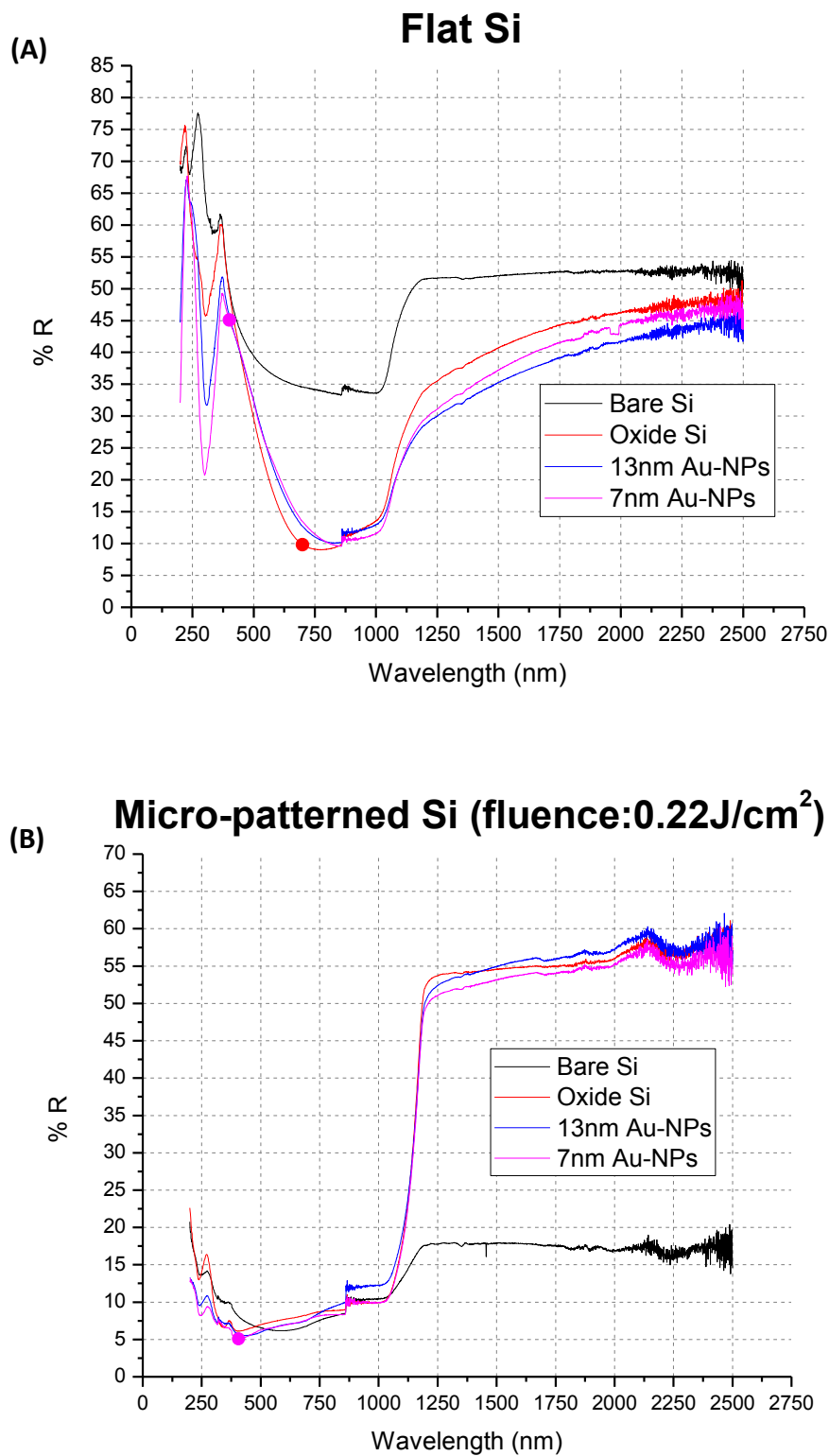


Figure 4.11: Reflectance spectrums on nano-structured Si substrates, via gold nanoparticles (AuNPs). (A) Comparison of reflectance spectrum flat Si substrates, with different surface topography (bare Si, oxidized Si, AuNPs with 7nm (pink line) and 13nm (blue line) diameter). (B) Comparison of reflectance spectrum of micro-structured Si substrates (low roughness), with different surface topography (bare Si, oxidized Si, AuNPs with 7nm (pink line) and 13nm (blue line) diameter).

4.4 NSCs growth and differentiation on the micro/nano patterned surfaces

Hierarchical surface structures have been used as tissue regenerative materials because they prompt an outstanding variety of cellular activities. Surface properties (e.g., surface energy, roughness, and chemical composition) of the tissue-engineered scaffolds are important design parameters because they are closely related to various cellular activities, such as cell adhesion, migration, growth, and differentiation³⁸. In our case, hierarchical surfaces have been assigned via functionalized gold nanoparticles (AuNPs) deposition on micro-structured Si surfaces, because they have been employed as a common platform to construct nonviral vectors in gene delivery. Chemical conjugation of oligonucleotides onto AuNPs increases its cellular stability due to elevated steric inhibition of nuclease digestion, which is a likely cause of tight packing¹²⁷.

In this section, we will study the cellular response of NSCs, on microstructured silicon surfaces (medium roughness), with deposited gold nanoparticles, in spherical shape, with diameter of 7nm and 13 nm. The types of gold nanoparticles deposited are: RGD-terminated AuNPs (13nm), DMAP-terminated AuNPs (7nm) and Citrate-terminated AuNPs (13nm) (more details in section 3.2). RGD-terminated AuNPs shows the greater number of attached NSCs (yellow arrows) (Figure 4.14).

Figure 4.14 shows the cellular response of primary NSCs cultured on medium roughness substrates, with three different functionalized AuNPs on their surfaces, for 5 days.

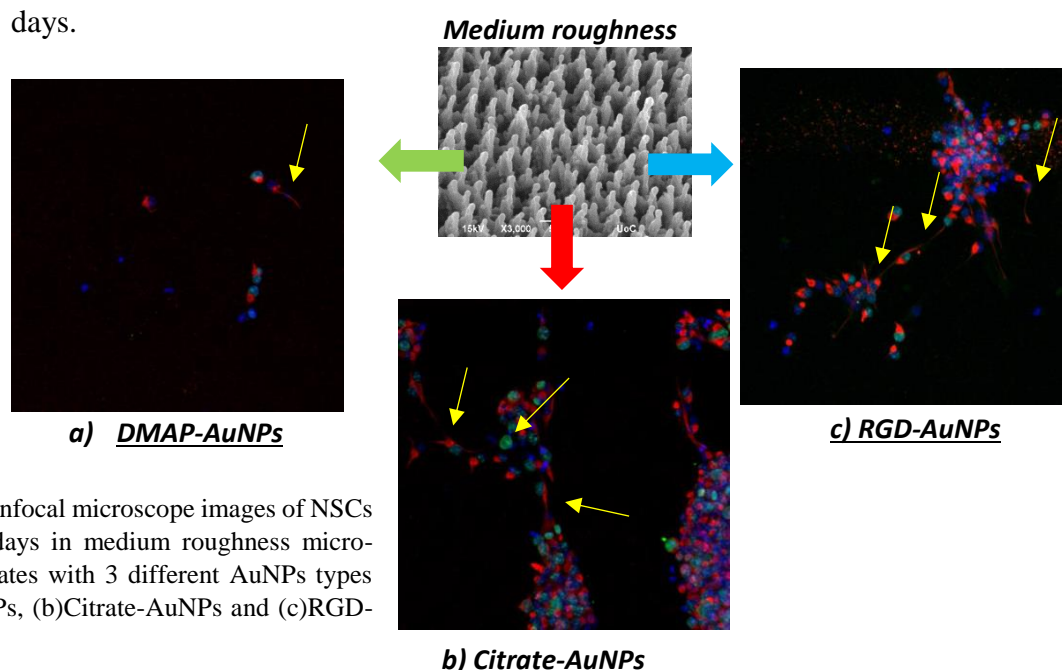


Figure 4.14: Confocal microscope images of NSCs cultured for 5 days in medium roughness micro-patterned substrates with 3 different AuNPs types (a)DMAP-AuNPs, (b)Citrate-AuNPs and (c)RGD-AuNPs.

*The cellular process performed by Post.Doc. Kanelina Karali.

5 Discussion & Conclusions

5.1 Micropatterned Si substrates fabricated via ultrashort-pulsed laser processing as artificial biomimetic surfaces.

The fabrication of biomimetic surfaces constitutes a research area of great interest. The reason is the unique properties of these surfaces, which find numerous applications including nanoscale devices, water repellence, and self-cleaning surfaces, drag reduction in fluid flow, energy conversion and conservation, high adhesion, materials and fibers with high mechanical strength, antireflection and structural coloration [Stratakis, E. I., & Zorba, V., 2010¹].

Various methods have been developed for structuring surfaces and fabrication of micro-nano-patterned and hierarchical surfaces such as electron – beam lithography [E. Martines et al., 2008⁵], photolithography [J.-Y. Shiu et al., 2004⁶], plasma treatments [I. Woodward et al., 200³⁷]. A promising technique for fabrication of micro structures with different scale topographies is irradiation using pulsed laser, with pulse duration lower than a second, i.e. short and ultra-short pulse. With proper setting of the laser parameters (e.g. fluence) and the environment (reactive gas), it is possible the formation of surfaces with different morphologies. The wetting [Hermens, U., 2016³⁰], optical [Rudenko, A et al., 2016¹⁵], microfluidic [Stratakis et al., 2011⁴] and surface properties [Simitzi, C. et al, 2015¹⁴]of micro-structured silicon surfaces, have already studied.

The approach used in the present study involves the fabrication of microconical structured silicon surfaces by ultra-short pulsed laser processing. The aim was to investigate the wetting and optical properties of these surfaces , for different irradiation parameters, surface functionalization via chemical process and via coating of gold nanoparticles. Furthermore , we wanted to see the influence of all the above parameters on neuron cells response.

5.2 Irradiation parameters influence the surface micro-topography

The irradiation of a solid surface via ultra-short fs pulsed laser, lead to microstructures of various morphologies depending on the unique laser-matter interactions. Microstructuring by ultra-short pulsed lasers is an especially attractive approach, because it leads to the formation of arrays of high-aspect ratio microcones

(MCs) on solid surfaces [Stratakis, E.,2012¹⁶]. Proper tuning of the laser (such as laser fluence, repetition rate, etc.) and reactive gas parameters (such as pressure) can lead to the formation of structures with different morphologies [Zorba V. et al., 2006⁷⁶].

In this study we have shown that by keeping constants four experimental parameters, (i.e. wavelength, repetition rate, irradiation environment and pulse duration) and by changing only the beam power, the surface micro-topography can change dramatically in a very controllable manner. Increased beam power (25-65mW) or fluence (0.22-0.57J/cm²) lead to increased, MCs' height (3.21-13.81 μ m) and the structures becoming more pronounced and spatially separated.

Furthermore, irradiation environment is a very important parameter for the topography of the substrates. We have shown that, silicon substrates which have been irradiated in vacuum comprised blunt, irregular and shorter pikes than the ones which have been fabricated in reactive gas (SF₆) environment. In the latter case, spikes were sharp and they exhibited on their surface roughness in the scale of nano-. Furthermore by increasing the ambient gas pressure the formation of second-lengthscale roughness on the surface of the cones is more obvious and in bigger concentration. So, the effect of irradiation environment, plays a distinct role to the nano-scale roughness of the substrate, and hierarchical structures are created.

The surface response to the above parameters has been previously studied [Her, T. H et al., 1998¹⁰;Zorba V.et al, 2008⁹;Stratakis, E et,all 201¹⁴], with the same efficiency.

5.3 The influence of surface micro-topography on its wetting properties.

The control of the wetting properties of surfaces, and particularly the possibility of inducing superhydrophilic and superhydrophobic (the so-called "Lotus effect" [W. Barthlott, C. Neinhuis, 1997¹⁴¹] behavior by micro-nanostructuring is arising an increasing interest for a wide range of applications, such as, self-cleaning surfaces, biological scaffolds, microfluidics, lab-onchip devices, water proof coatings for automotive and aerospace vehicles, textiles [A. Nakajima et al., 1999¹⁴²;Z. Yoshimitsu et al., 2002¹⁴³;N. A. Patankar, 2003¹⁴⁴]. The properties of the lotus leaf have been ascribed to the complex morphology present on its surface, consisting of hierarchical structuring, at two different lengthscales. As a consequence, the main strategy for the

fabrication of any artificial superhydrophobic and water-repellent surface has been to mimic its surface topology.[Zorba V. et al., 2008¹³]. According to this model, we can study the wetting properties of surfaces, e.g. static contact angle measurements, and associate them for microfluidics applications [Stratakis, E et,all 2011⁴].

The shape of the droplet on a flat surface described by Young’s equation (section 3.4.3.1). The effect of the macroscopic surface roughness on the wettability of surfaces has been theoretically approached by two different models. In the Wenzel model [R. N. Wenzel, 1936¹⁴⁰], the liquid is assumed to completely penetrate within the entire rough surface, described as “homogeneous wetting regime” without leaving any air pockets underneath it (Figure 5.1 (a)). This model predicts that the contact angle will decrease / increase with surface roughness for an initially hydrophilic ($\theta_0 < 90^\circ$) / hydrophobic ($\theta_0 > 90^\circ$) surface, since the ratio of the unfolded surface to the apparent area of contact under the droplet (r) is always greater than unity.

In contrast, Cassie and Baxter (CB) model assumes [A. B. D. Cassie, 1944¹⁴⁵] that the liquid does not completely permeate the rough surface because air gets trapped underneath it (“heterogeneous wetting regime”). As a result a droplet will form a composite solid liquid / air –liquid interface with the sample in contact, and the effective surface energy of the scaffold below the water will be dominated by air. As the ratio of the area of the projection surface, which comes into contact with the drop, to the area of the total projected area (f_{is}) is lower than the unity this model always predicts enhancement of hydrophobicity, independently of the value of the initial contact angle θ_0 .

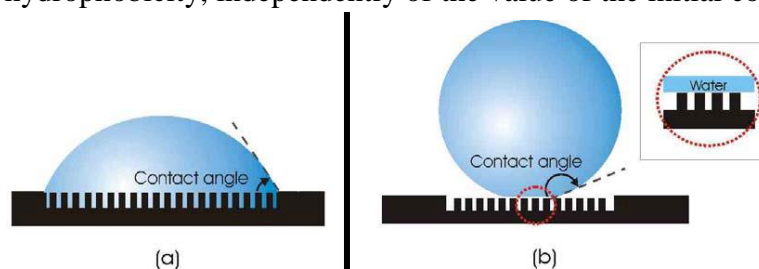


Figure 5.1 (a) : Wenzel model

$$\cos\theta_w = r \cdot \cos\theta_0$$

θ_w : apparent contact angle

$$r < 1$$

* θ_0 is the static contact angle according to Young’s equation

$$\text{In general: } \cos \vartheta_{(CB)} = -1 + f_{is} + r_f f_{is} \cos \vartheta_0$$

$\theta_{(CB)}$: apparent contact angle

r_f : roughness ratio of the wet area

Figure 5.1(b): Cassie-Baxter model

$$r_f = 1 \rightarrow \cos \theta_{(CB)} = -1 + f_{is} (1 + \cos \theta_0)$$

If: $f_{is} < 1 \rightarrow$ Enhancement of hydrophobicity

$\downarrow f_{is} \rightarrow \theta_{(CB)}$ incensement

$f=1$ and $r_f=r \rightarrow$ Wenzel model

Based on the above in this study we have observed that, as the roughness of the surface increased, static contact angle increased also. Furthermore, as the second scale roughness increased, static contact angle increased much more. We suppose that the wetting response of the substrates fabricated via ultra-short pulsed laser in ambient gas can be described by the Cassie-Baxter wettability model. This occurs because the initial contact angle, ie on flat silicon was $< 90^\circ$ (hydrophilic) and after irradiation in gas ambient became hydrophobic ($>90^\circ$) for low laser fluence and super hydrophobic for higher fluence, which opposes to Wenzel theory. Also increased gas pressure (i.e. increased concentration of fluorine radicals on micro-conic structures) leads to more hydrophobic surfaces. This phenomenon, has been studied already [Xia, F., & Jiang, L. 2008²;Stratakis, E. et al.,2012¹²;Zorba V. et al.,2008¹³]with the same efficiency.

5.4 The influence of chemistry on the wetting properties of silane micropatterned surface.

Silanization is the covering of a surface with organofunctional alkoxy silane molecules. Mineral components like glass and metal oxide surfaces can all be silanized, because they contain hydroxyl groups which attack and displace the alkoxy groups on the silane thus forming a covalent -Si-O-Si- bond. The goal of silanization is to form bonds across the interface between mineral components and organic components present in paints, adhesives, etc. Silanization (or siliconization) of glassware increases its hydrophobicity and is used in cell culturing to reduce adherence of cells to flask walls [Brian Seed, 1998¹⁴⁴].

The reason we choose this type of silane is its functional group, because sulfate radicals (S^-) creating strong links with gold (Au). This is something we want to achieve in order to have successful binding of gold nanoparticles on the microstructured silicon substrates.

Based on the above, we deposited MPTMS silane (more details in section 3.3) on oxidized flat and micro-structured silicon substrates. Static contact angle measurements (section 4.2.4) showed that the micro-structured surfaces became more hydrophobic than they used to be before silanisation process. This phenomenon enhanced, as the roughness of the substrates increased.

5.5 The influence of a homogeneous gold nanoparticle layer on the wetting properties of micropatterned silicon.

Inorganic colloidal nanoparticles are very small (usually applies to particles between 1 and 100 nm), nanoscale objects with inorganic cores that are dispersed in a solvent. Prerequisite for every possible application of them, is the proper surface functionalization of such nanoparticles, which determines their interaction with the environment. These interactions ultimately affect the colloidal stability of the particles, and may yield to a controlled assembly or to the delivery of nanoparticles to a target, e.g. by appropriate functional molecules on the particle surface.

Colloidal nanoparticles are dispersed in a solvent that can be either water-based or an organic solvent for hydrophilic or hydrophobic particles, respectively, while amphiphilic nanoparticles can be dispersed in both kinds of solvents. Most commonly, hydrophilic nanoparticles are stabilized by electrostatic repulsion by the equally charged ligand molecules on the particle surface⁸⁸.

In our case, all the types of AuNPs used, are dispersed in a water-based solvent. More specifically, DMAP-AuNPs and RGD-AuNPs bearing a positively charged amino end-group, which is exposed to the surface, CALNN-AuNPs bearing the amino acid of asparagine (N) which is an uncharged, but hydrophilic amino acid, which is exposed to the surface¹²⁸. On the other hand Citrate-AuNPs bearing a negatively charged carboxylate end-group (section 3.2).

Contact angle measurements (Table 4.9), showed an increase of hydrophilicity on the micropatterned silicon surfaces after the deposition of the homogeneous gold nanoparticles layers. This was evident for all the types of AuNPs and was independent of the roughness of the micropatterned substrates. More specifically, as the roughness increased, C.A. decreased respectively. This makes sense if we consider that the surface energy was stable and the interface solid-liquid reduced. Also, as the roughness of the surfaces increased, the number of gold nanoparticles on the micro-cones tops reduced. This affects the wetting of the surfaces, as the surface energy remains the same, while changing the distribution of gold nanoparticles, by leaving exposed to the surface greater silicon oxide area.

5.6 The influence of functionalized gold nanoparticles on NSCs growth.

One of the current challenges in the development of tissue engineered constructs is the lack of a renewable cell source. Embryonic, induced pluripotent and adult stem cells are promising cell sources in therapeutic and regenerative medicine. Due to their ability to self-renew and differentiate into various cell types, these cells could potentially be cultured and harvested for regeneration of damaged injured and aged tissue [Sorensen 2008¹¹², Zipori 2009¹¹³].

In vivo, differentiation and self-renewal of stem cells is dominated by signals from their surrounding microenvironment [Moore and Lemischka, 2006¹¹⁴]. This microenvironment or “niche” is composed of other cell types as well as numerous chemical, mechanical and topographical cues at the micro- and nanoscale, which are believed to serve as signaling mechanisms to control the cell behavior [Place et al., 2009¹¹⁵]. In tissue culture, stem cell differentiation has traditionally been controlled by the addition of soluble factors to the growth media [Pittenger, M.F et al., 1999¹¹⁶]. However, despite much research, most stem cell differentiation protocols yield heterogeneous cell types [Ding, S. et al., 2004¹¹⁷, Hwang, N.S et al., 2008¹¹⁸]. Therefore, it is desirable to use more biomimetic *in vitro* culture conditions to regulate stem cell differentiation and self-renewal. Surface properties (e.g., surface energy, roughness, and chemical composition) of the tissue-engineered scaffolds are important design parameters because they are closely related to various cellular activities, such as cell adhesion, migration, growth, and differentiation [M. M. Stevens and J. H. George, 2005¹¹⁹]. Microstructures also influence basic cellular processes such as adhesion^{14,20}, proliferation [Qi, Lin et al., 2013¹²⁰] and differentiation [Dolatshahi-Pirouuz et al., 2011¹²¹] (Figure 4.12, 4.13).

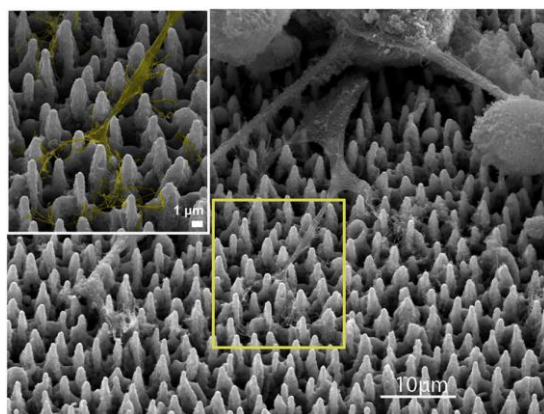


Figure 4.12: ‘Sensing’ substrate roughness: SEM image of differentiated PC12 cells after NGF treatment on laser-patterned Si substrates. Inset is a higher magnification image focusing on sprouting filopodia (pseudocoloured)¹⁴.

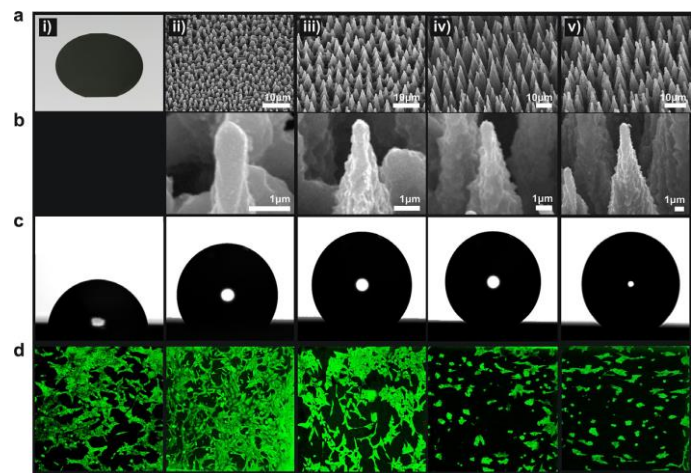


Fig 4.13: (a) Picture of a polished Si wafer (i) and side SEM views of the as-prepared Si spikes surfaces structured at four different laser fluencies (ii) 0.34 J/cm²(A1), (iii) 0.56 J/cm²(A2), (iv) 0.90 J/cm²(A3), and (v) 1.69 J/cm²(A4); (b) high magnification SEM images of the corresponding Si cones obtained; (c) photographs of water droplets on the patterned Si surfaces; and (d) confocal laser microscopy pictures of fibroblast cells cultured for three days on the respective surfaces²⁰.

One of the current challenges in the development of tissue engineered constructs is the lack of a renewable cell source. Embryonic, induced pluripotent and adult stem cells are promising cell sources in therapeutic and regenerative medicine. Due to their ability to self-renew and differentiate into various cell types, these cells could potentially be cultured and harvested for regeneration of damaged injured and aged tissue [Sorensen 2008¹¹² , Zipori 2009¹¹³].

Peptides containing the cell recognition motif RGD. RGD peptides do not only trigger cell adhesion effectively but can also be used to address selectively certain cell lines and elicit specific cell responses. The RGD sequence is by far the most effective and most often employed peptide sequence for stimulated cell adhesion on synthetic surfaces. This is based upon its widespread distribution and use throughout the organism, its ability to address more than one cell adhesion receptor, and its biological impact on cell anchoring, behavior and survival. the RGD sequence is not the “universal cell recognition motif”, but it is nevertheless unique with respect to its broad distribution and usage. The conformation of the RGD containing loop and its flanking amino acids in the respective proteins are mainly responsible for their different integrin affinity¹²⁶. Figure 4.14 showed the best NSCs attachment on medium roughness substrates with RGD-AuNPs deposited.

5.7 The influence of surphase roughness and AuNPs size on surface reflectivity

The optical properties of laser structured Si have been studied [Crouch, C. H. et al.,2004³¹, Crouch, C. H. et al.,2004³²]. The optical properties and intense electromagnetic fields generated by the nanoparticles make these particles very attractive for sensing, diagnostics, and photothermal therapeutic applications in many areas⁹⁶.

For a complete characterization of the optical properties of a surface, we need to measure the respective absorption, transmittance and reflectance. In our case, due to technical problems, measured only the reflectivity of the micro-structured and micro / nano-structured surfaces. The optical properties which we have observed so far, are very interesting, and have enough later study.

6 References

- [1] Stratakis, E. I., & Zorba, V. (2010). Biomimetic Artificial Nanostructured Surfaces. *Nanomaterials for the Life Sciences* (Vol. 7).
- [2] Xia, F., & Jiang, L. (2008). Bio-inspired, smart, multiscale interfacial materials. *Advanced Materials*, 20(15), 2842–2858.
- [3] Alberts B, Johnson A, Lewis J, Raff M, Roberts K, Walter P (eds) (2008) *Molecular biology of the cell*. Garland Science, New York
- [4] Stratakis, E., Ranella, A., & Fotakis, C. (2011). Biomimetic micro/nanostructured functional surfaces for microfluidic and tissue engineering applications. *Biomicrofluidics*, 5(1), 1–31.
- [5] E. Martines, K. Seunarine, H. Morgan, N. Gadegaard, C. D. W. Wilkinson, and M. O. Riehle, *Nano Lett.* 5, 2097 (2005).
- [6] J.-Y. Shiu, C.-W. Kuo, P. Chen, and C.-Y. Mou, *Chem. Mater.* 16, 561 (2004).
- [7] I. Woodward, W. C. E. Schofield, V. Roucoules, and J. P. S. Badyal, *Langmuir* 19, 3432 (2003).
- [8] Bhushan, B., Jung, Y. C., & Koch, K. (2009). Micro-, nano- and hierarchical structures for superhydrophobicity, self-cleaning and low adhesion. *Philosophical Transactions. Series A, Mathematical, Physical, and Engineering Sciences*, 367(1894), 1631–1672.
- [9] Zorba, V., Boukos, N., Zergioti, I., & Fotakis, C. (2008). Ultraviolet femtosecond, picosecond and nanosecond laser microstructuring of silicon: structural and optical properties. *Applied Optics*, 47(11), 1846–1850.
- [10] Her, T. H., Finlay, R. J., Wu, C., Deliwala, S., & Mazur, E. (1998). Microstructuring of silicon with femtosecond laser pulses. *Applied Physics Letters*, 73(12), 1673–1675.
- [11] Zorba, V., Tzanetakis, P., Fotakis, C., Spanakis, E., Stratakis, E., Papazoglou, D. G., & Zergioti, I. (2006). Silicon electron emitters fabricated by ultraviolet laser pulses. *Applied Physics Letters*, 88(8).
- [12] Simitzi, C., Efstathopoulos, P., Kourgiantaki, A., Ranella, A., Charalampopoulos, I., Fotakis, C., Gravanis, A. (2015). Laser fabricated discontinuous anisotropic microconical substrates as a new model scaffold to control the directionality of neuronal network outgrowth. *Biomaterials*, 67, 115–128.
- [13] Zorba, V., Stratakis, E., Barberoglou, M., Spanakis, E., Tzanetakis, P., Anastasiadis, S. H., & Fotakis, C. (2008). Biomimetic artificial surfaces quantitatively reproduce the water repellency of a lotus leaf. *Advanced Materials*, 20(21), 4049–4054.
- [14] Simitzi, C., Stratakis, E., Fotakis, C., Athanassakis, I., & Ranella, A. (2015). Microconical silicon structures influence NGF-induced PC12 cell morphology. *Journal of Tissue Engineering and Regenerative Medicine*, 9(4), 424–434.
- [15] Rudenko, A., Colombier, J., & Itina, T. E. (2016). Influence of Polarization State on Ultrafast Laser-Induced Bulk Nanostructuring. *Journal of Laser Micro/Nanoengineering*, 11(3), 304–311.
- [16] Stratakis, E. (2012). *Nanomaterials by Ultrafast Laser Processing of Surfaces*, 4, 407–431.
- [17] Whitesides, G. M. (2006). The origins and the future of microfluidics. *Nature*, 442(7101), 368–73.

- [18] Koch, K., Bhushan, B., & Barthlott, W. (2008). Diversity of structure, morphology and wetting of plant surfaces. *Soft Matter*, 4(10), 1943.
- [19] Guo, Z., Liu, W., & Su, B. L. (2011). Superhydrophobic surfaces: From natural to biomimetic to functional. *Journal of Colloid and Interface Science*, 353(2), 335–355.
- [20] Ranella, A., Barberoglou, M., Bakogianni, S., Fotakis, C., & Stratakis, E. (2010). Tuning cell adhesion by controlling the roughness and wettability of 3D micro/nano silicon structures. *Acta Biomaterialia*, 6(7), 2711–2720.
- [21] Karthick, B., & Maheshwari, R. (2008). Lotus-inspired nanotechnology applications. *Resonance*, 13(12), 1141–1145.
- [22] Bonse, J. et al. Femtosecond laser-induced periodic surface structures on steel and titanium alloy for tribological applications. *Appl. Phys. A* 117, 103–110 (2014) .
- [23] Vukusic, P., & Sambles, J. R. (2003). Photonic structures in biology. *Nature*, 424(6950), 852–5.
- [24] Rossiter, J., Yap, B., & Conn, A. (2012). Biomimetic chromatophores for camouflage and soft active surfaces. *Bioinspir Biomim*, 7(3), 36009.
- [25] Morhard, C., Pacholski, C., Lehr, D., Brunner, R., Helgert, M., Sundermann, M., & Spatz, J. P. (2010). Tailored antireflective biomimetic nanostructures for UV applications. *Nanotechnology*, 21(42), 425301.
- [26] Stuart A. Boden and Darren M. Bagnall, Natural Moth-eye. “Moth-Eye Antireflective Structures,” 2015.
- [27] Boden, Stuart A, and Darren M Bagnall. “Nanostructured Biomimetic Moth-Eye Arrays in Silicon by Nanoimprint Lithography.” In *Proc. SPIE7401 J*, edited by Raul J. Martin-Palma and Akhlesh Lakhtakia, 74010:74010J, 2009.
- [28] Siddique, Radwanul Hasan, Guillaume Gomar, and Hendrik Hölscher. “The Role of Random Nanostructures for the Omnidirectional Anti-Reflection Properties of the Glasswing Butterfly.” *Nature Communications* 6, no. November (2015).
- [29] Watanabe, Keiichiro, Takayuki Hoshino, Kazuhiro Kanda, Yuichi Haruyama, and Shinji Matsui. “Brilliant Blue Observation from a Morpho-Butterfly-Scale Quasi-Structure.” *Japanese Journal of Applied Physics, Part 2: Letters* 44, no. 1–7 (2005).
- [30] Hermens, U., S.V. Kirner, C. Emons, P. Comanns, E. Skoulas, A. Mimidis, H. Mescheder, et al. “Mimicking Lizard-like Surface Structures upon Ultrashort Laser Pulse Irradiation of Inorganic Materials.” *Applied Surface Science*, 2016.
- [31] Crouch, C. H., J. E. Carey, J. M. Warrender, M. J. Aziz, E. Mazur, and F. Y. Génin. “Comparison of Structure and Properties of Femtosecond and Nanosecond Laser-Structured Silicon.” *Applied Physics Letters* 84, no. 11 (2004): 1850–52.
- [32] Crouch, C. H., J. E. Carey, M. Shen, E. Mazur, and F. Y. Génin. “Infrared Absorption by Sulfur-Doped Silicon Formed by Femtosecond Laser Irradiation.” *Applied Physics A: Materials Science and Processing* 79, no. 7 (2004): 1635–41.
- [33] C. Frantz, K.M. Stewart, V.M. Weaver, The extracellularmatrix at a glance, *J. Cell Sci.*123 (2010) 4195–4200.
- [34] K.C. Clause, T.H. Barker, Extracellularmatrix signaling in morphogenesis and repair, *Curr. Opin. Biotechnol.* 24 (2013) 830–833.

- [35] A.D. Theocharis, C. Gialeli, V.C. Hascall, N.K. Karamanos, Extracellular matrix: a functional scaffold, in: N.K. Karamanos (Ed.), *Extracellular Matrix: Pathobiology and Signaling*, Walter de Gruyter GmbH & Co. KG, Berlin/Boston 2012, pp. 3–20.
- [36] Theocharis , Achilleas D., Spyros S. Skandalis, Chrysostomi Gialeli, and Nikos K. Karamanos. “Extracellular Matrix Structure.” *Advanced Drug Delivery Reviews* 97 (2016): 4–27.
- [37] Liu, Xiaomei, Jung Yul Lim, Henry J. Donahue, Ravi Dhurjati, Andrea M. Mastro, and Erwin A. Vogler. “Influence of Substratum Surface Chemistry/energy and Topography on the Human Fetal Osteoblastic Cell Line hFOB 1.19: Phenotypic and Genotypic Responses Observed in Vitro.” *Biomaterials* 28, no. 31 (2007): 4535–50.
- [38] Lee, Jae Yoon, Hyeongjin Lee, Yong Bok Kim, and Geun Hyung Kim. “Fabrication of a Biomimetic Hierarchical Surface Replicated from a Lotus Leaf and in Vitro Cellular Activities.” *Plasma Processes and Polymers* 12, no. 2 (2015): 141–52.
- [39] Papadopoulou EL, Samara A, Barberoglou M et al. 2010; Silicon scaffolds promoting three-dimensional neuronal web of cytoplasmic processes. *Tissue Eng C Methods* 16: 497–502.
- [40] Birnbaum, Milton. “Semiconductor Surface Damage Produced by Ruby Lasers.” *Journal of Applied Physics* 36, no. 11 (1965): 3688–89.
- [41] Janzén, E., R. Stedman, G. Grossmann, and H. G. Grimmeiss. “High-Resolution Studies of Sulfur- and Selenium-Related Donor Centers in Silicon.” *Physical Review B* 29, no. 4 (1984): 1907–18.
- [42] Nolte, S, C Momma, H Jacobs, A Tu, B N Chichkov, B Wellegehausen, and H Welling. “Ablation of Metals by Ultrashort Laser Pulses.” *Journal of the Optical Society of America B* 14, no. 10 (1997): 2716–22.
- [43] Jost, D., W. Lüthy, H. P. Weber, and R. P. Salathé. “Laser Pulse Width Dependent Surface Ripples on Silicon.” *Applied Physics Letters* 49, no. 11 (1986): 625–27.
- [44] Henyk, M., N. Vogel, D. Wolfframm, A. Tempel, and J. Reif. “Femtosecond Laser Ablation from Dielectric Materials: Comparison to Arc Discharge Erosion.” *Applied Physics A: Materials Science and Processing* 69, no. 7 (1999): 355–58.
- [45] Barberoglou, M., G. D. Tsibidis, D. Gray, E. Magoulakis, C. Fotakis, E. Stratakis, and P. A. Loukakos. “The Influence of Ultra-Fast Temporal Energy Regulation on the Morphology of Si Surfaces through Femtosecond Double Pulse Laser Irradiation.” *Applied Physics A: Materials Science and Processing* 113, no. 2 (2013): 273–83.
- [46] Jing-tao , Z H U, Zhao Ming, Y I N Gang, Zhao Li, and Chen De-ying. “Silicon Micro-Structuring Using Ultra-Short Laser Pulses” 5629 (n.d.): 11–14.
- [47] Sukumar Basu , *Crystalline Silicon – Properties and Uses*, 2011
- [48] Voldman J, Gray ML, Schmidt MA, 1999, *Microfabrication in biology and medicine*, *Annu Rev Biomed Eng*, 1:401.
- [49] Sievila P, 2013, *Microfabrication technologies for single-crystal sensors*, PhD thesis, Aalto University
- [50] Pearce TM, Williams JC, 2007, *Microtechnology: Meet neurobiology, Lab on a Chip*, 7:30.
- [51] Stratakis, E. “Nanomaterials by Ultrafast Laser Processing of Surfaces.” *Science of Advanced Materials* 4 (2012): 407–31.

- [52] Hunt LP, 1990, Silicon Precursors: Their Manufacture and Properties In Handbook of semiconductor silicon technology, ed. WC O'Mara, RB Herring, LP Hunt, Noyes Publications
- [53] B.G. Streetman, Solid State Electronics, Third Edition, Chapter 1, Prentice Hall, 1990
- [54] Brown, P. J. "The Crystal Structure of Solids." Physics Today 27 (1974): 50.
- [55] Logofatu, C., C. C. Negri, R. V. Ghita, F. Ungureanu, C. Cotirlan, C. G. Adrian Lazarescu, M. Stefan, and M. Florin. Study of SiO₂/Si Interface by Surface Techniques. Crystalline Silicon - Properties and Uses, 2011.
- [56] F. J. Himpsel, F.R.Mc Feely, A.Taleb-Ibrahimi and J.A.Yarmoff, Physical Review B, Vol.38, No.9, pp.6084-6095 (1988)
- [57] M. Razeghi Technology of Quantum Devices pp.42 LLC (2010), Springer, ISBN 978-1-4419-1055-4
- [58] B.E. Deal and A.S. Grove, "General Relationship for the Thermal Oxidation of Silicon," J. Appl. Physics., 36 , 3770 (1965).
- [59] Weast, R.C. (1968). editor of Handbook of Chemistry and Physics, the 48-th edition, The Chemical Rubber Publishing Co., F149.
- [60] G. S. Henderson, D. R. Baker, (eds. . Synchrotron, Earth. Radiation, Environmental, Sciences. Material, Short. Applications, Series. 3. Course, Association. Mineralogical, Canada. of, (2002)159-178. Henderson G. S., The Geochemical News, 113 113 October (2002), 13
- [61] Carrier, P.; Lewis, L.J. & Dharma-Wardana, M.W.C. (2002). Optical properties of structurally relaxed Si/SiO₂ superlattices: The role of bonding at interfaces, Phys. Rev. B65, pp.165339-165350
- [62] Morita, M., T. Ohmi, E. Hasegawa, M. Kawakami, and M. Ohwada. "Growth of Native Oxide on a Silicon Surface." Journal of Applied Physics 68, no. 3 (1990): 1272–81.
- [63] Hierlemann A, Thermal Oxidation of Silicon, Microtechnology and microelectronics
- [64] Sze SM, 2002, Semiconductor Devices, Physics and Technology, Wiley
- [65] E. Magoulakis, E. L. Papadopoulou, E. Stratakis, C. Fotakis, and P. A. Loukakos, Appl.Phys. A. 98, 701 (2010).
- [66] A.C. Tien, S. Backus, H. Kapteyn, M. Mourane, G. Mourou, Phys. Rev. Lett. 82, 3883 (1999).
- [67] Sundaram, S K, and E Mazur. "Inducing and Probing Non-Thermal Transitions in Semiconductors Using Femtosecond Laser Pulses." Nature Materials 1, no. 4 (2002): 217–24.
- [68] Lucas, L. and J. Zhang, Femtosecond laser micromachining: a back-to-basics primer. 2012
- [69] Y.C. Koji Sugioka, Ultrafast Laser Processing: From Micro- to Nanoscale, 2013.
- [70] J.F.Young, J.E. Sipe, H.M. van Driel, Phys. Rev. B 30(4) , 2001 (1984).
- [71] Tsibidis, George D., Evangelos Skoulas, Antonis Papadopoulos, and Emmanuel Stratakis. "Convection Roll-Driven Generation of Supra-Wavelength Periodic Surface Structures on Dielectrics upon Irradiation with Femtosecond Pulsed Lasers." Physical Review B - Condensed Matter and Materials Physics 94, no. 8 (2016): 2–6.

- [72] Tsibidis, George D., C. Fotakis, and E. Stratakis. "From Ripples to Spikes: A Hydrodynamical Mechanism to Interpret Femtosecond Laser-Induced Self-Assembled Structures." *Physical Review B* 92, no. 4 (July 9, 2015): 41405.
- [73] S. Sakabe, M. Hashida, S. Tokita, S. Namba, and K. Okamuro, *Phys. Rev. B* 79, 033409 (2009).
- [74] Pedraza AJ, Fowlkes JD, Lowndes DH, 1999, Silicon microcolumn arrays grown by nanosecond pulsed-excimer laser irradiation, *Phys. Lett.* , 74:2322
- [75] Dolgaev SI, Lavrishev SV, Lyalin AA, Simakin AV, Voronov VV, Shafeev GA, 2001, Formation of conical microstructures upon laser evaporation of solids, *Applied Physics A: Materials Science & Processing*, 73:177.
- [76] Zorba V, Persano L, Pisignano D, Athanassiou A, Stratakis E, et al, 2006, Making silicon hydrophobic: wettability control by two-lengthscale simultaneous patterning with femtosecond laser irradiation, *Nanotechnology*, 17:3234.
- [77] T.-H. Her, R. J. Finlay, C. Wu, S. Deliwala, E. Mazur, *Appl. Phys. Lett.* 1998, 73, 1673.
- [78] Bates Robert L, P L Stephan Thamban, Matthew J Goeckner, and Lawrence J Overzet. "Silicon Etch Using SF₆/C₄F₈/Ar Gas Mixtures," 2014, 0–11.
- [79] D. Bäuerle, *Laser Processing and Chemistry*, Third Edition, Springer-Verlag Berlin Heidelberg New York (2000).
- [80] Lii, Y.-J., J. Jorné, K.-C. Cadien, and J.-E. Schoenholtz Jr. "Plasma Etching of Silicon in SF₆." *J. Electrochem. Soc.* 137, no. 11 (1990): 3633.
- [81] J.D.Fowlkes, A.J.Pedraza, D.H.Lowndes, *Appl. Phys. Lett.* 77, 1629 (2000).
- [82] D. Bäuerle, *Chemical processing with lasers*, Springer-Verlag Berlin Heidelberg New York (1986).
- [83] Salata OV . 2004. Applications of nanoparticles in biology and medicine . *J Nanobiotechnol.* 2 : 3.
- [84] Thakkar KN ., Mhatre SS , and Parikh RY . 2010. Biological synthesis of metallic nanoparticles . *Nanomedicine.* 6 : 257 – 262
- [85] Mody VV , Siwale R, Singh A , Mody HR . 2010. Introduction to metallic nanoparticles . *J Pharm Bioall Sci.* 2: 282– 9
- [86] Vollath, D. "Introduction to Nanoparticles and Nanomaterials," 2013, 1–24.
- [87] Zhou, Jingfang, John Ralston, Rossen Sedev, and David A. Beattie. "Functionalized Gold Nanoparticles: Synthesis, Structure and Colloid Stability." *Journal of Colloid and Interface Science* 331, no. 2 (2009): 251–62.
- [88] Sperling R. and W. J. Parak. "Surface Modification, Functionalization and Bioconjugation of Colloidal Inorganic Nanoparticles." *Philosophical Transactions. Series A, Mathematical, Physical, and Engineering Sciences* 368, no. 1915 (2010)
- [89] Verma HN , Singh P , Chavan RM . 2014. Gold nanoparticle: synthesis and characterization . *Vet World.* 7 : 72 – 77 .
- [90] Hu M , Chen J , Li ZY , Au L , Hartland GV , Li X , et al . 2006 . Gold nanostructures: engineering their plasmonic properties for biomedical applications . *Chem Soc Rev.* 35: 1084– 1094.

- [91] Jain PK , Lee KS , El-Sayed IH , El-Sayed MA . 2006 . Calculated absorption and scattering properties of gold nanoparticles of different size shape, and composition: applications in biological imaging and biomedicine . *J Phys Chem B*. 110: 7238– 7248.
- [92] Shah M, V Badwaik, Y Kherde, H K Waghvani, T Modi, Z P Aguilar, H Rodgers, et al. “Gold Nanoparticles: Various Methods of Synthesis and Antibacterial Applications.” *Front Biosci (Landmark Ed)* 19, no. May 2015 (2014): 1320–44.
- [93] Yeh, Yi-Cheun, Brian Creran, and Vincent M Rotello. “Gold Nanoparticles: Preparation, Properties, and Applications in Bionanotechnology.” *Nanoscale* 4, no. 6 (2012): 1871–80.
- [94] Majidi, Sima, Fatemeh Zeinali Sehrig, Samad Mussa Farkhani, Mehdi Soleymani Goloujeh, and Abolfazl Akbarzadeh. “Current Methods for Synthesis of Magnetic Nanoparticles.” *Artificial Cells, Nanomedicine, and Biotechnology* 44, no. 2 (2016): 722–34.
- [95] Tiwari PM, Vig K , Dennis VA , Singh SR . 2011. Functionalized gold nanoparticles and their biomedical applications . *Nanomaterials*. 1 : 31 – 63 .
- [96] Eustis Susie, and Mostafa El-Sayed. “Why Gold Nanoparticles Are More Precious than Pretty Gold: Noble Metal Surface Plasmon Resonance and Its Enhancement of the Radiative and Nonradiative Properties of Nanocrystals of Different Shapes.” *Chemical Society Reviews* 35, no. 3 (2006): 209–17.
- [97] Pong, Boon Kin, Hendry I. Elim, Jian Xiong Chong, Wei Ji, Bernhardt L. Trout, and Jim Yang Lee. “New Insights on the Nanoparticle Growth Mechanism in the Citrate Reduction of gold(III) Salt: Formation of the Au Nanowire Intermediate and Its Nonlinear Optical Properties.” *Journal of Physical Chemistry C* 111, no. 17 (2007): 6281–87.
- [98] Turkevich, John. “Colloidal Gold. Part I.” *Gold Bulletin* 18, no. 4 (1985): 125–31.
- [99] Hubert, C., L. Billot, P. M. Adam, R. Bachelot, P. Royer, J. Grand, D. Gindre, K. D. Dorkenoo, and A. Fort. “Role of Surface Plasmon in Second Harmonic Generation from Gold Nanorods.” *Applied Physics Letters* 90, no. 18 (2007): 89–92.
- [100] Kumar, S, K S Gandhi, and R Kumar. “Modeling of Formation of Gold Nanoparticles by Citrate Method.” *Industrial & Engineering Chemistry Research* 46, no. 10 (2007): 3128–36.
- [101] Turkevich, J.; Stevenson, P.; Hillier, J. A Study of the Nucleation and Growth Process in the Synthesis of Colloidal Gold. *Discuss. Faraday Soc.* 1951, 11, 55.
- [102] Muhlfordt, H. The Preparation of Colloidal Gold Particles Using Tannic Acid as an Additional Reducing Agent. *Experientia* 1982, 38, 1127.
- [103] Brust, M.; Walker, M.; Bethell, D.; Schiffrin, D. J.; Whyman, R. Synthesis of Thiol-Derivatised Gold Nanoparticles in a Two-Phase Liquid-Liquid System. *Chem. Commun.* 1994, 801.
- [104] Reetz MT , Helbig W , Quaiser SA , Stimming U , Breuer N , Vogel R . 1995 . Visualization of surfactants on nanostructured palladium clusters by a combination of STM and high-resolution TEM . *Science*. 267 : 367 – 369 .
- [105] Reetz MT , Helbig W . 1994. Size-selective synthesis of nanostructured transition metal clusters . *J Am Chem Soc.* 116: 7401– 7402.
- [106] Jana NR, Gearheart L , Murphy CJ . 2001. Seeding growth for size control of 5 – 40 nm diameter gold nanoparticles . *Langmuir*. 17 : 6782 – 6786

- [107] Das RK , Gogoi N , Bora U . 2011 . Green synthesis of gold nanoparticles using *Nyctanthes arbortristis* flower extract . *Bioprocess Biosyst Eng.* 34 : 615 – 619 .
- [108] Smitha SL , Philip D , Gopchandran KG . 2009 . Green synthesis of gold nanoparticles using *Cinnamomum zeylanicum* leaf broth . *Spectrochim Acta A Mol Biomol Spectrosc.* 74 : 735 – 739 .
- [109] Itoh H, Naka K , Chujo Y . 2004. Synthesis of gold nanoparticles modified with ionic liquid based on the imidazolium cation . *J Am Chem Soc.* 126: 3026– 3027.
- [110] U. Drechsler, N. O. Fischer, B. L. Frankamp and V. M. Rotello, *Adv. Mater.*, 2004, 16, 271–274.
- [111] Ji, Yi-Qin, Yu-Gang Jiang, Hua-Song Liu, Li-Shuan Wang, Dan-Dan Liu, Cheng-Hui Jiang, Rong-Wei Fan, and De-Ying Chen. “Optical Constants of SiO₂ Films Deposited on Si Substrates.” *Chinese Physics Letters* 31, no. 4 (2014): 46401.
- [112] Sorensen, M.L. *Stem Cell Applications in Diseases*; Nova Biomedical Books: New York, NY, USA, 2008.
- [113] Zipori, D. *Biology of Stem Cells and the Molecular Basis of the Stem State (Stem Cell Biology and Regenerative Medicine)*; Humana Press: New York, NY, USA, 2009.
- [114] Moore, K.A.; Lemischka, I.R. Stem cells and their niches. *Science* 2006, 311, 1880-1885.
- [115] Place, E.S.; Evans, N.D.; Stevens, M.M. Complexity in biomaterials for tissue engineering. *Nat. Mater.* 2009, 8, 457-470.
- [116] Pittenger, M.F.; Mackay, A.M.; Beck, S.C.; Jaiswal, R.K.; Douglas, R.; Mosca, J.D.; Moorman, M.A.; Simonetti, D.W.; Craig, S.; Marshak, D.R. Multilineage potential of adult human mesenchymal stem cells. *Science* 1999, 284, 143-147.
- [117] Ding, S.; Schultz, P.G. A role for chemistry in stem cell biology. *Nat. Biotechnol.* 2004, 22, 833-840.
- [118] Hwang, N.S.; Varghese, S.; Elisseeff, J. Controlled differentiation of stem cells. *Adv. Drug Delivery Rev.* 2008, 60, 199-214.
- [119] M. M. Stevens, J. H. George, *Science* 2005, 310, 1135.
- [120] Qi, Lin, Ning Li, Rong Huang, Qin Song, Long Wang, Qi Zhang, Ruigong Su, Tao Kong, Mingliang Tang, and Guosheng Cheng. “The Effects of Topographical Patterns and Sizes on Neural Stem Cell Behavior.” *PLoS ONE* 8, no. 3 (2013): 2–9.
- [121] Dolatshahi-Pirouz, Alireza, Mehdi Nikkhal, Kristian Kolind, Mehmet R. Dokmeci, and Ali Khademhosseini. “Micro- and Nanoengineering Approaches to Control Stem Cell-Biomaterial Interactions.” *Journal of Functional Biomaterials* 2, no. 4 (2011): 88–106.
- [122] Dalby, Matthew J, Nikolaj Gadegaard, and Richard O C Oreffo. “Harnessing Nanotopography and Integrin-Matrix Interactions to Influence Stem Cell Fate.” *Nature Materials* 13, no. 6 (2014): 558–69.
- [123] Kulangara, Caroline, Andrey V. Kajava, Giampietro Corradin, and Ingrid Felger. “Sequence Conservation in *Plasmodium Falciparum* Cysteine-Rich Helical Coiled Coil Domains Proposed for Vaccine Development.” *PLoS ONE* 4, no. 5 (2009): 1–11.

- [124] Ratner, B.D. *Biomaterials Science: An Introduction to Materials in Medicine*, 2nd ed.; Elsevier Academic Press: Amsterdam, The Netherlands, 2004.
- [125] Biver, T., A. Corti, N. Eltugral, E. Lorenzini, M. Masini, A. Paolicchi, A. Pucci, G. Ruggeri, F. Secco, and M. Venturini. "Analysis of 4-Dimethylaminopyridine (DMAP)-Gold Nanoparticles Behaviour in Solution and of Their Interaction with Calf Thymus DNA and Living Cells." *Journal of Nanoparticle Research* 14, no. 2 (2012).
- [126] Hersel, Ulrich, Claudia Dahmen, and Horst Kessler. "RGD Modified Polymers: Biomaterials for Stimulated Cell Adhesion and beyond." *Biomaterials* 24, no. 24 (2003): 4385–4415.
- [127] Remant Bahadur, K. C., Bindu Thapa, and Narayan Bhattarai. "Gold Nanoparticle-Based Gene Delivery: Promises and Challenges." *Nanotechnology Reviews* 3, no. 3 (2014): 269–80.
- [128] Lévy, Raphaël, Nguyen T K Thanh, R. Christopher Doty, Irshad Hussain, Richard J. Nichols, David J. Schiffrin, Mathias Brust, and David G. Fernig. "Rational and Combinatorial Design of Peptide Capping Ligands for Gold Nanoparticles." *Journal of the American Chemical Society* 126, no. 32 (2004): 10076–84.
- [129] E.H. Nicollins and J.R. Brews, *MOS Physics and Technology*. New York: Wiley, 1952.
- [130] Hermanson Gerg T., *Bioconjugate techniques*, 2nd edition
- [131] Cortadellas N, Fernández E, Garcia A. 2012. *Biomedical and Biological Applications of Scanning Electron Microscopy. Handbook of instrumental techniques*. Scientific and Technological Centers of the University of Barcelona.
- [132] John Wiley & Sons Ltd, *Energy dispersive spectroscopy*, Second edition 2015, The Atrium, Southern Gate, Chichester, West Sussex, PO19 8SQ
- [133] Zorba V, 2007, *Study of electron and ion emission mechanisms from micro/nano-structured Si surfaces using ultrashort laser pulses*, PhD thesis, University of Crete, Heraklion
- [134] By, Published. "World βETM S Largest Science , Technology & Medicine Open Access Book Publisher Infrared Spectroscopic Ellipsometry for Ion-Implanted Silicon Wafers," n.d.
- [135] Débora Gonçalves and Eugene A. Irene, *FUNDAMENTALS AND APPLICATIONS OF SPECTROSCOPIC ELLIPSOMETRY*, Quím. Nova vol.25 no.5 São Paulo Sept./Oct. 2002
- [136] R.M.A. Azzam, N.M. Bashara "Ellipsometry and polarized light", North Holland , Amsteram, 1977
- [137] Chauhan, Sourabh Singh. "Ellipsometry for Measuring the Thickness of Thin Films," n.d.,2014
- [138] Ghiran, Ionita C. "Introduction to Fluorescence Microscopy." *Methods in Molecular Biology* (Clifton, N.J.) 689 (2011): 93–136.
- [139] Semwogerere, Denis, and Eric R Weeks. "Confocal Microscopy." *Encyclopedia of Biomaterials and Biomedical Engineering*, 2005, 1–10.
- [140] R. N. Wenzel, *Ind. Eng. Chem.* **28**, 988 (1936).
- [141] W. Barthlott, C. Neinhuis, *Planta* **202**, 1 (1997).
- [142] A. Nakajima, A. Fujishima, K. Hashimoto, T. Watanabe, *Adv. Mater.* **11**, 1365 (1999).

- [143] Z. Yoshimitsu, A. Nanajima, T. Watanabe, K. Hashimoto, *Langmuir* **18**, 5818 (2002).
- [144] N. A. Patankar *Langmuir* **19**, 1249 (2003).
- [145] A. B. D. Cassie, S. Baxter, *Trans. Faraday. Soc.*, **40**, 546 (1944).
- [144] Brian Seed, *Current Protocols in Cell Biology*. "Silanizing Glassware." Protein Science, 1998, 2–3.

Webpages

<http://www.virginiasemi.com/pdf/BasicCrystallographicPropertiesofSi.pdf>

<http://www.cem.msu.edu/~cem924sg/Topic03.pdf>

<http://www.elementalmatter.info/silicon-properties.htm>

<http://web.ift.uib.no/AMOS/PHYS208/larsP-N/p-n-slide-lars.pdf>

https://people.eecs.berkeley.edu/~hu/Chenming-Hu_ch1.pdf

<http://www.iue.tuwien.ac.at/phd/filipovic/node26.html>

<http://www.geo.arizona.edu/xtal/nats101/s04-19.html>

<http://www.cmxr.com/Education/Short.html>

<http://www.cmxr.com/Education/Long.html>